The Pennsylvania State University
The Graduate School
Department of Electrical Engineering

PURE ROTATIONAL RAMAN LIDAR FOR TEMPERATURE MEASUREMENTS IN THE LOWER TROPOSPHERE

A Thesis in
Electrical Engineering

by
Paul A.T. Haris

Submitted in Partial Fulfillment
of the Requirements
for the Degree of

Doctor of Philosophy

August 1995

We approve the thesis of Paul A. T Haris.

Date of Signature

_____ _____

Charles R. Philbrick
Professor of Electrical Engineering
Thesis Advisor and Chair of Committee

_____ _____

Timothy J. Kane
Assistant Professor of Electrical Engineering

_____ _____

Ian-Choon Khoo
Professor of Electrical Engineering

_____ _____

Christopher S. Ruf
Assistant Professor of Electrical Engineering

_____ _____

Richard Stern
Professor of Engineering Sciences and Mechanics

_____ _____

Larry C. Burton
Professor of Electrical Engineering
Head of the Department of Electrical Engineering

ABSTRACT

An examination into the use of the pure rotational Raman spectrum for lidar measurements of lower tropospheric thermal structure has been made. This technique was chosen because it showed potential for making measurements on short spacial and temporal scales. To determine if the rotational Raman technique may be extended down through the boundary layer, it was necessary to calculate the absolute intensities of water vapor's pure rotational Raman quantum lines, to establish design configurations for an ideal optical detector, to parameterize different analysis techniques for obtaining temperature versus lidar rotational ratio conversion curves, and to evaluate possible means of filtering lidar temperature data. Results showed that for an atmosphere containing 3 % water vapor at 320 K, and a detector system using a 0.2 nm bandwidth filter, water vapor contributed less than 0.1 % (~ 0.2 K error) of the total backscattered signal for filter placements less than 163.9 cm^{-1} from the primary laser frequency. For filters with 3 nm bandwidths, filter placements need to be less than 224.2 cm^{-1}. Ideal filter configurations were calculated to reside at 30.1 cm^{-1} with a 17.7 cm^{-1} bandwidth and at 140.6 cm^{-1} with a 75.3 cm^{-1} bandwidth. Filtering temperature profiles using an optimal estimation algorithm, based on balloon climatology data, was shown to work as well as, if not better, than general weighted average filters. The filtered data show temperature standard deviations less than 0.8 K at altitudes below 7 km with a minimum of 0.3 K at 1 km. It was determined that the rotational Raman technique provides a useful and powerful method to measure profiles of atmospheric temperature in the lower troposphere, even in the presence of light to moderate backgrounds of haze, fog, and clouds.

TABLE OF CONTENTS

LIST OF FIGURES

LIST OF TABLES

ACKNOWLEDGMENTS

I have found that life is not just about achieving goals and milestones, but experiencing journeys which are shared with others. In my research at Penn State University I have traveled, met, and collaborated with people all over the world. I have had the opportunity to travel from Norway to Antarctica, which included two months on board the German research vessel RV Polarstern, and from Germany to California in order that I may try and add a new piece of knowledge to the human endeavor. For these experiences, I am forever greatful to my advisor, C. Russell Philbrick. His clarity of purpose and wisdom ensured the successful completion of my journey through graduate school while helping me prepare for the journeys to come.

My committee members, Richard Stern, Christopher Ruf, Iam-Choon Khoo, and Timothy Kane provided the ongoing consultation essential for keeping me focussed. With all those at the Applied Research Laboratory, the Department of Electrical Engineering, and the long conversations with Dannial Lysak, the successful completion of my research was unstoppable.

I have had the privilege of developing friendships with the international community and benefitting from their experiences and knowledge. Special thanks need to be given to William F. Murphy, in Ottawa Canada, who helped me increase my understanding of the rotational Raman spectrum of water vapor. His patience, guidance and friendship were invaluable and will always be cherished.

To my family, Mom, Dad, Alexandra, and Robi, and to my friends, my life's journeys would have lost a great deal of meaning without all of you. Your support during the tough times, and your sharing during my many joys will never be forgotten. I look forward to sharing with all of you the adventures to come.

I would like to thank all those who have supported my graduate work: the Applied Research Laboratory for the Exploratory and Foundational Grant, the Office of Naval Research for the Research Assistantship, the Aerospace Education Foundation for the

Theodore von Karman Scholarship, and the United State Air Force who allowed me to pursue my graduate work immediately after my undergraduate studies.

The effort to prepare the LAMP instrument has been supported by the National Science Foundation, the U.S. Navy's SPAWAR PMW-175 Environmental Systems Program Office, the Penn State Applied Research Laboratory, the College of Engineering, and the Department of Electrical Engineering. I am indebted to these institutions. Their support is greatfully acknowledged.

Chapter 1

INTRODUCTION

The objective of this research is to provided an examination into the use of the pure rotational Raman spectrum for temperature measurements in the lower troposphere where aerosol scattering dominates and water vapor molecules are a possible source of interference. To achieve this objective, it was necessary to calculate the absolute intensities of the pure rotational Raman spectrum of water vapor and determine if it contributes to the received lidar signals, to establish design configurations for an ideal optical detector, to parameterize different analysis techniques for obtaining temperature versus ratio conversion curves, and to present a possible means of filtering the resulting lidar data to obtain true temperatures.

Temperature is a principle state variable which helps to describe the condition of the atmosphere at any point in time. Instantaneous vertical profiles and time series plots of temperature can give information concerning the dynamics of the atmosphere which in turn can be used to make forecasts of the meteorological conditions.

1.1 Importance of Temperature Measurements in the Atmosphere

Describing here all of the theoretical and practical uses of temperature profiles in meteorology would be impractical and beyond the scope of this paper. Only one of the most common and important uses for vertical temperature profiles will be briefly mentioned, that is, conditions for atmospheric stability. One measure of atmospheric stability comes from the calculation of the environmental lapse rate from vertical temperature profiles. The environmental lapse rate is the rate at which the temperature of the environment changes with altitude. By comparing this environmental lapse rate at each altitude with the dry and moist adiabatic lapse rates, one can estimate whether

possible conditions for convection exists. The dry and moist adiabatic lapse rates are models of the maximum rate of temperature change that a parcel of air will undergo as a function of a change in altitude, assuming that their is no exchange of heat between the environment and the parcel of air, and assuming that there is no environmental turbulence. The dry adiabatic lapse rate has a constant value of approximately -9.8 °C/km. However, if the parcel of air is saturated, then the effects of heating from condensation must be included in the lapse rate, and thus is called the moist adiabatic lapse rate. This heating effect causes the maximum adiabatic lapse rate to drop off slower than the dry adiabatic lapse rate (approximately -6 °C/km) and at a non-constant value with altitude.

Determining the stability of the atmosphere is important because it helps to predict how the environment may behave under certain environmental conditions. For example, if the atmospheric conditions allow a parcel of air to rise, it will expand and cool because the pressure of the atmosphere is decreasing with altitude. As the parcel of air cools, its temperature falls and eventually reaches the saturation temperature, or dew point temperature, which is the temperature at which water vapor molecules begin to condense to form water droplets. This is the beginning of the formation of clouds. If the lifting of air is strong enough and contains a large amount of water vapor, then there is the possibility for severe weather.

1.2 History of Temperature Measuring Techniques in the Atmosphere

Vertical temperature profiles of the Earth's atmosphere were first obtained in 1749 in Glasgow when a thermometer was placed on a kite. These measurements were crude because they did not have a recording device. With the development of the balloon in 1783, measurements could be recorded in situ by hand as the balloon ascended. The limitation was the survival limit of the human body with altitude. In the 1890's automatic recording devices were invented so balloons could ascend up to 18 km without humans. The only problem was that retrieval of the balloon took time. The introduction of the airplane provided new capabilities for investigations, but it had an altitude limit of about 4

km. In 1927 the first radiosonde was launched, which had the capability of transmitting data back to the ground as it ascended by using radio waves. The radiosonde is a small package that is tethered on the end of a balloon which today has the capability to measure temperature, pressure, relative humidity, and wind. The radiosonde balloon is one of the primary meteorological data sources for weather forecasting and synoptic meteorology.

However, for modern meteorological applications, balloons have become ineffective for mesoscale model descriptions and smaller scale meteorology, for two reasons. First, balloons do not take a vertical profile over the sight in question since they are subject to horizontal winds which take it off course. Second, balloons can take hours to ascend to high altitudes. By the time the upper altitude measurements are taken, the lower altitudes may have already changed, and thus, high temporal resolution is not possible. New measuring techniques were needed to profile temperature in the troposphere and stratosphere.

RASS (Radio Acoustic Sounding System) was first proposed by Marshall in 1972. RASS uses a combination of acoustic and radio waves to obtain atmospheric temperature. The most recent RASS technique sends an acoustical pulse out into the atmosphere and uses a coherent detection radar to track the density wave which the acoustical pulse creates. The technique measures the scattering of the electromagnetic wave from the density perturbations, and determines the speed of sound from the acoustical movement [May, 1990]. Since the speed of sound is related to virtual temperature, an atmospheric temperature profile can be obtained. The range of RASS is restricted to the lower troposphere because of acoustical signal attenuation. If atmospheric conditions were just right, May et al. [1990] were able to obtain temperature measurements up to 9 km, using an acoustical frequency of 110 Hz. Before these measurements, most RASS systems were limited to a 1 km range because they utilized acoustical frequencies that were strongly attenuated in the atmosphere, such as 1 kHz or higher. A large source of error for the RASS measurements is atmospheric turbulence and contributions from vertical and horizontal winds. These factors cause the acoustic pulse to be distorted as it propagates through the atmosphere which in turn causes error in the received signal. This technique

can only be used in calm weather when convective cells are not present in the atmosphere.

Lidar (Light detection and Ranging) using elastic scattering was first used by Elterman [1953] with a spotlight illuminating the sky, and an off axis telescope receiving the scattered signal. Elastic scattering occurs when a photon of light interacts with a molecule to excite it to a virtual energy level by inducing a dipole moment. The molecule scatters the light at the same frequency as the incident photon, thereby maintaining its same energy, only slightly modified by Doppler broadening. The received profile is a relative density profile of the atmosphere where the scattering is due only to molecular species. Temperature profiles from the elastic scattered lidar signal can be obtained by integrating down the relative density profiles using the hydrostatic equation and the ideal gas law [Philbrick, 1985]. This technique has been used by a number of groups over the years [Chanin et al.,1984; Hauchecorne et al.,1980; Philbrick et al.,1985]. Measurements taken by the Penn State lidar of elastic temperature profiles will be discussed in Section 1.3.

This process of integrating down the density profiles to obtain temperature assumes that there are no aerosols in the atmosphere to contaminate the signal. Aerosol scattering can have cross sections which are 18 or more orders of magnitude greater than the elastic scattering cross section. Since the particle scattering line overlays the elastic scattering line, only a few particles in the air can be enough to cause the lidar signal to be considerably modified relative to the molecular profile. Since temperature is derived from the gradient of the signal, the temperature profile would be distorted by the presence of particle scatterers. It turns out that the only region in the atmosphere that is essentially free of particles is above the tropopause at approximately 8 - 15 km depending on latitude. This altitude range assumes that there has not been any recent volcanic eruptions to send particles into the stratosphere. If there have been some eruptions, the particle free region may be pushed up to as high as 35 km as was seen when the Pinatubo volcano erupted in 1991 [Stevens et al.,1993].

Even if there were no particles in the atmosphere other than molecules, obtaining temperature measurements using elastic scattering in the troposphere would be difficult in

regions of storm activity. The hydrostatic equation assumes that there is no net force acting on a parcel of air. The parcel of air is in equilibrium with its surroundings when the downward force of gravity exactly balances the upward pressure gradient force. Regions of storm activity contain cells of turbulent motion which cause conditions in which the hydrostatic equation is not valid. This in turn causes the method of obtaining temperature using the hydrostatic assumption from the profile of molecular scattering to break down.

DIAL (DIfferential Absorption Lidar) techniques have been used to measure atmospheric temperature by examining the temperature dependence of the oxygen absorption lines. The DIAL technique utilizes two laser wavelengths, one on an absorption line and one just off the absorption line. Temperature measurements from DIAL require the calculation of the absorption coefficient from the measured signals while assuming that particle scattering is the same for the closely chosen wavelengths [Theopold,1993]. The relation of the measured absorption coefficient to temperature can be obtained from the results of an iterative calculation which models such a relationship. In order to perform this iterative calculation a pressure must be assumed. Because measurements are performed on specific lines of oxygen, which are very narrow in bandwidths, the technical demands on the stability of the lidar system are great. Theopold et al [1993] were able to measure temperature up to 2.2 km with 82 m resolution averaged over 30 minutes. This gave them a temperature accuracy of 4 K. This was the second time that temperature measurements have been obtained since the introduction of the DIAL temperature technique. A major problem with the technique is that of potential particle scattering contamination. Unless the contribution of this scattering is known precisely, temperature measurements using DIAL are not possible (Theopold, 1993).

Lidar using vibrational Raman scattering to obtain a molecular profile was first used by Leonard [1967]. He used a lidar to measure the nitrogen concentration in the atmosphere to 1.2 km by monitoring the nitrogen's first Stoke's vibrational level at 365.8 nm excited by a nitrogen laser whose primary wavelength was 337.1 nm. Vibrational Raman scattering occurs when a photon of light interacts with a molecule to excite it to a virtual energy level as in the case of molecular scattering, but unlike molecular scattering,

the molecule relaxes to a vibrational energy state that produces a photon with either greater or lesser energy than the incident photon. If the scattered photon contains more energy than the incident photon, the anti-Stoke's region, then the molecule's original energy level was already in a vibrationally excited level. In this case, when it relaxes from the virtual level to the ground state level, the molecule produces a photon of higher energy than the incident photon. Stoke's vibrational scattering occurs when the molecule is originally in the ground state before being excited to a virtual level. The molecule may then relax into a vibrational state that is higher than the ground state, producing a photon whose energy is less than the incident photon. Since at ordinary temperatures, the probability of normal atmospheric molecules being in their vibrational states is extremely small, anti-Stoke's vibrational scattering occurs rarely, while Stoke's vibrational scattering occurs readily. In fact, at 300 K, the ratio of the number of molecules in the first vibrational level to that of the zeroth vibrational level for N_2 is 1.4×10^{-5}. Since it is already difficult to measure the signal scattered from the first Stoke's vibrational line in the atmosphere using today's technology, it would be extremely difficult to measure a signal five orders of magnitude less. The vibrational states of a molecule are quantized and are due to very specific properties of the molecule being excited. This results in the wavelength of the emitted photon being characteristic of the molecular species causing the scattering. Since the received molecular signal is proportional to density, temperature is obtained from using the same technique used for Rayleigh scattering. The only error in the signal, aside from the possible break down of the hydrostatic equation, would be due to extinction of the laser beam as it moved though the aerosols in the atmosphere. It has been shown that correction of the molecular profile for extinction is generally not possible in the strong aerosol layers typically found in the troposphere [Rau, 1993].

1.3 Instrumentation used in the Thesis

Two lidars have been developed at Penn State and used in the formulation of this thesis. Of primary use was the Penn State LAMP lidar, which has been developed over the past five years, and its successor, the LAPS lidar which has been developed over the past 3 years from lessons learned from the LAMP lidar. Comparisons of the data retrieved from these instruments were made against meteorological balloons, to determine the validity and stability of the LAMP system.

1.3.1 The Penn State LAMP Lidar

The LAMP lidar was first completed in the Summer of 1991 at Penn State University. It consists of five primary subsystems: transmitter, receiver, detector, data collector, and safety system [Stevens, 1992]. The transmitter is a Nd:YAG laser with output wavelengths at 532 nm and either 355 nm or 266 nm. The laser operates at a pulse repetition rate of 20 Hz, emitting 7 nsec long pulses with energies of 400 mJ, 250 mJ, and 85 mJ at the respective wavelengths. The laser pulses are directed off of three hard coated mirrors before entering into the atmosphere in a monostatic arrangement with the receiver. The lidar configuration is shown in Figure 1.1. The backscattered light is directed by an optical flat into a 16" classical Cassigrain telescope. It is then coupled into a one millimeter diameter fiber optic which directs the signal into one of two detector boxes.

The first detector box was originally designed to allow for measurements between the ground and 70 kilometers. Because the measurements obtained by this box come from the high altitude regions, only the 532 nm and 355 nm wavelengths are emitted from the laser. The detector box utilizes a unique shuttering system and six separate detector channels to detect both high and low altitude elastic scattering data and low altitude nitrogen and water vapor Raman data. The high altitude signal paths are shuttered over the first 15 km to prevent saturation of the photon counting photomultiplier tubes. In the photon counting mode, the data collection units consist of amplifier, discriminator,

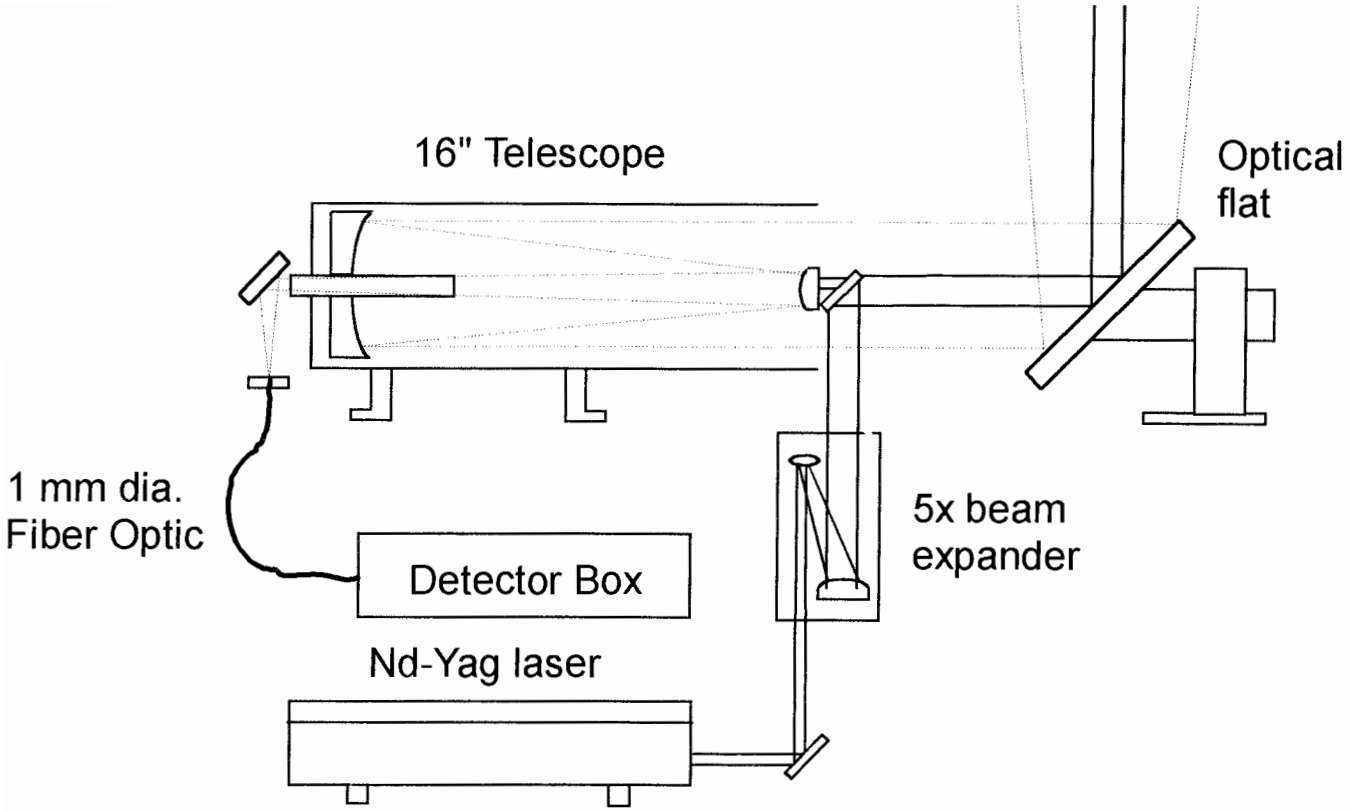

Figure 1.1. Schematic diagram of the Penn State LAMP lidar

counter, and accumulator. The photon counting data is binned with 75 m height resolution and integrated in one minute durations. In the analog mode, the data collection units consists of amplifier, digitizer, and average. The analog signal is also averaged in one minute intervals but with height resolution of 15 m.

The second detector box was designed in 1992 for low altitude measurements and to incorporate rotational Raman temperature measurement capabilities for the first time at Penn State. The detector box measures signals derived from the 532 nm wavelength and either the 355 nm or 266 nm wavelengths. The scattering from the 532 nm laser photons provide information on temperature, water vapor concentration , nitrogen concentration, molecular density, and aerosol backscattering. With the 355 nm crystal installed in the laser, the same information as that obtained by the 532 nm wavelength is obtained except for temperature. If the 266 nm crystal is installed in the laser, then information about ozone density, nitrogen density, oxygen density, and water vapor concentration can be obtained. Also because it is in the solar blind region, signals from the 266 nm wavelength can be measured during the day. Figure 1.2 is the schematic diagram for the LAMP low altitude detector box and the corresponding optical components are given in Appendix A. The filters used for measuring sections of the rotational spectrum are shown in Figure 2.1b. The filters are centered at 528.4 nm (FWHM = 1.1 nm) and 530.2 nm (FWHM = 0.6 nm) and are thermally stabilized at 35 °C. Great care was needed to insure that the filters and beam spitters for the temperature channels were thermally stabilized, because it was shown that this was necessary in order to prevent system drift, and thus, subsequent temperature errors [Nedelijkovic et al., 1993].

1.3.2 The Penn State LAPS Lidar

The Penn State LAPS lidar has been developed with improvements based upon the result of tests and lessons learned from the LAMP lidar. It is fully automated in operation and deployable in any environment. It is housed in two separate units. The first unit consists of the detector and receiver systems and the second unit consists of the detector

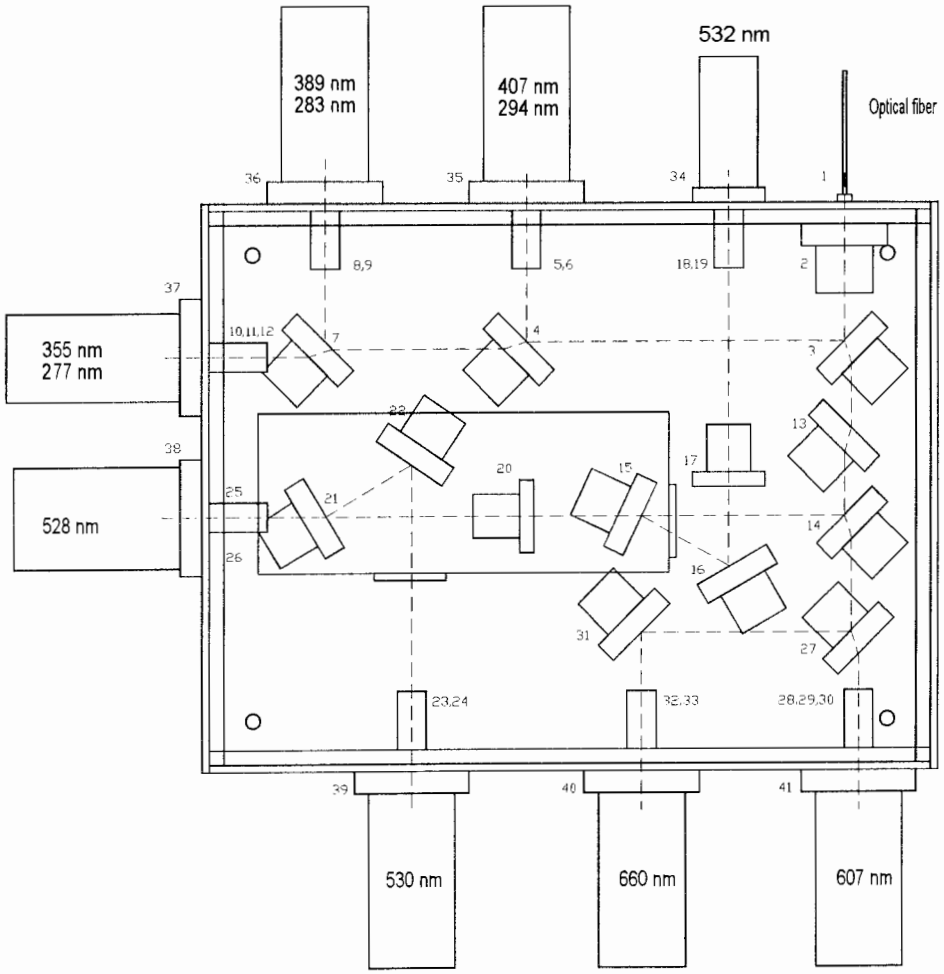

Figure 1.2. LAMP low altitude detector box

and data collection systems. The two units are connected by fiber optic cables. The specifications for the LAPS system are shown in Table 1.1.

Table 1.1. LAPS system characteristics

Transmitter: Continuum Powerlite 90-30, Nd:YAG		
Wavelength	532.1 nm	266.1 nm
Pulse Energy	0.42 J	0.12 J
Pulse Rate	30 Hz	
Receiver: f/2.5 Prime Focus telescope		
Focal Length	1.53 m	
Diameter	0.61 m	

LAPS is capable of measuring water vapor, nitrogen, and temperature from scattering off of the 532 nm laser signal, and water vapor, nitrogen, and oxygen off of the 266 nm laser signal. It is capable of operating at night and during the day. By using a field stop at the focal point of the receiver, the intensity of the day sky background can be reduced far enough to allow for daytime temperature measurements. Because of its large receiver and high transmitting power, LAPS is capable of making statistically sound measurements on short time scales.

1.3.3 Meteorological Balloons

The meteorological balloons used for weather sounding, which measure temperature, humidity, and pressure, are the Vaisala RS 80-15N. Wind speeds and directions are obtained by using the OMEGA tracking system, which triangulates the coordinates of the rising balloon from transmitting stations placed around the United States. The data collection and processing unit used is the Vaisala MARWIN portable rawinsonde set. Table 1.2 lists the manufacturers specifications on the radiosonde balloon

system.

Table 1.2. Meteorological balloon specifications and accuracies

Instrument	Range	Precision
RS 80-15N		
Temperature	+60 °C to -90 °C	0.1 °C
Pressure	1060 mb to 3 mb	0.1 mb
Humidity	0 to 100 % RH	2 %
MARWIN (OMEGA)		
Wind Speed	0 to 180 m/s	
Wind Direction	0 to 359°	
Wind Vector		1 m/s

1.3.4 Ground Based Weather Monitor

The ground base weather station being used is the Davis Weather Monitor II. It has the capabilities to monitor temperature, pressure, relative humidity, wind speed, wind direction, and rain fall amount. Data is averaged every minute. A list of the specifications is shown in Table 1.3.

Table 1.3. Davis Weather Station specifications and accuracies

Parameter	Range	Precision
Temperature	-45°C to 60°C	±0.5°C
Pressure	880.0 mb to 1080 mb	±1.7 mb
Relative Humidity	0 to 100 %	2 %
Wind Speed	0 knots to 152 knots	±5 %
Wind Direction	0 to 360°	22.5° increment
Rain Fall Amount	0 to 999.8 mm	0.2 mm resolution

1.4 Rayleigh Temperature Measurements from the Penn State LAMP Lidar

One of the original purposes of the Penn State LAMP lidar was to take temperature measurements in the stratosphere and mesosphere above the stratospheric particle layer [Haris et al.,1993; Philbrick et al., 1992]. Temperature was obtained using the elastic scattering technique described in Section 1.1.

The most intensive measuring campaign for the LAMP lidar, in which high altitude temperature measurements were sought, was during the LADIMAS (LAtitudinal Distribution of Middle Atmospheric Structure) campaign which took place between September 1991 and January 1992 [Philbrick et al., 1992] . The goal of the campaign was to measure atmospheric density, temperature, dynamics, and trace constituents from the ground to 120 km across a global distribution of latitudes. The LAMP lidar was deployed on the German research ship, RV Polarstern, as it made its voyage from Bremerhaven, Germany to Antarctica. During the voyage, and weather permitting, the LAMP lidar collected profiles of upper atmospheric density and lower atmospheric nitrogen and water vapor. The voyage marked the first latitudinal measurement of temperature from a ground based instrument [Haris et al., 1993]. Figure 1.3 shows a comparison of the temperature obtained from the 355 nm and 532 nm lidar wavelengths to the CIRA 1988 Model, and Figure 1.4 shows a comparison with a falling sphere from a meteorological rocket. The lidar data definitely shows good agreement with both model and rocket. However the CIRA model falls short in accounting for the wave motions of the atmosphere.

Prior to the LADIMAS campaign, the LAMP lidar was operated at the Andoya Rocket Range, Norway where it took measurements during the METALs campaign [Alpers et al.,1994]. One of the primary measuring instruments during the campaign was falling spheres which were launched on meteorological rockets. Since the instruments take measurements from 100 km to approximately 30 km, the rockets provided an opportunity to compare data to the LAMP lidar temperature data [Haris et al., 1993]. There have been previous studies [Philbrick et al., 1987] between rockets and lidars that

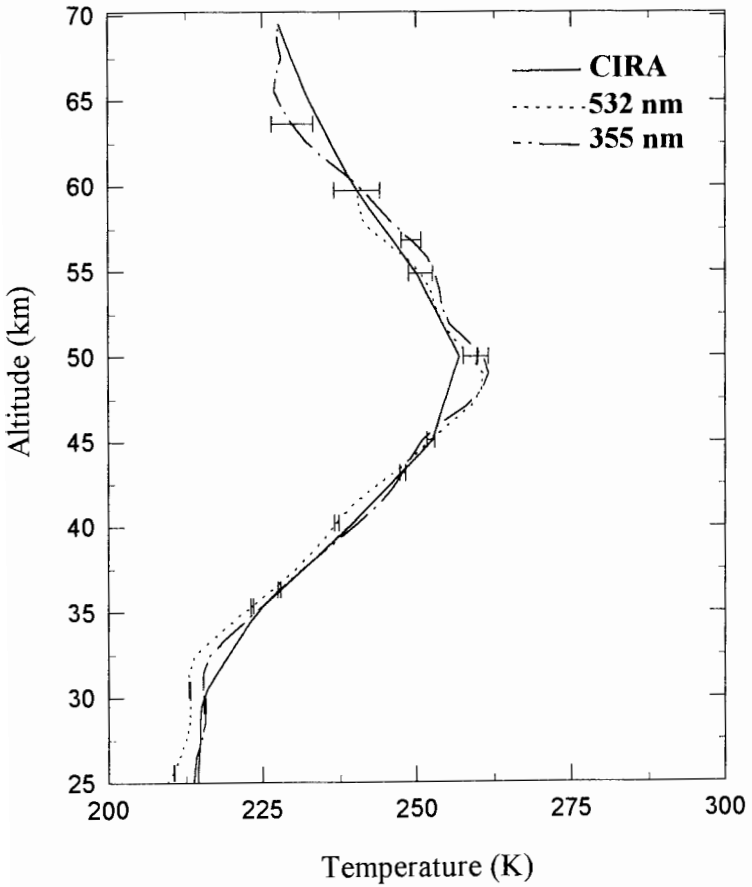

Figure 1.3: Comparison between CIRA: 1986 Atm. model and LAMP lidar data. Obtained on 11/10/91 1712 -1817 UT 60 minute average. [Haris et al., 1994]

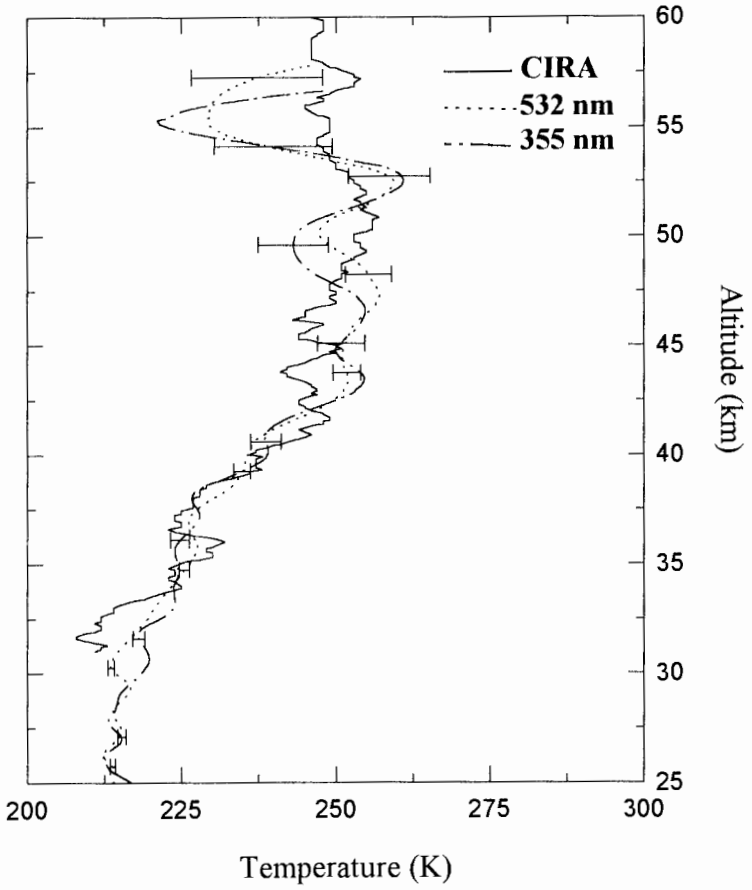

Figure 1.4: Comparison of rocket and LAMP lidar data using 532 nm and 355 nm wavelengths. Data obtained on 11/04/91 0039 UT 30 minute average. [Haris et al.,1994]

have shown good agreement between the two techniques. This was also the case for the measurements in Norway. Figure 4 shows a sample data plot of the rocket temperature data and the temperature data obtained from the 355 nm and 532 nm wavelengths of the LAMP lidar. This figure shows good agreement between the two measuring techniques.

The next logical step in the development of the LAMP lidar was to extend temperature measurements down to the ground. The possibility of using N_2 vibrational Raman and two-wavelength lidar to extend the measurements into the troposphere was explored and shown to be severely limited in its usefulness [Rau,1994]. The rotational Raman technique was therefore chosen because it appeared to be the most promising of all the other techniques.

The rotational Raman technique has been incorporated into the LAMP lidar since 1993. Tests have been conducted to determine the effects of system drift on lidar temperature measurements so that future systems could be designed to produce accurate temperature profiles. A number of preliminary atmospheric temperature measurements have been made using the LAMP lidar. Two examples are shown in Figure 1.5a and 1.5b taken on 07/26/94 and 09/11/94, respectively. The reason for the lack of data below 2.2 km in the 09/11/94 profile is due to the data collection units' limited dynamic range. By adding neutral density filters in the optical paths of the lidar, the intense backscatter signal can be reduced in order to bring the profile down to the ground.

Since lidar data can be taken continuously, individual profiles can be grouped on one plot to give a time series account of how the atmosphere behaves in the zenith. An example of this is shown in Figure 1.6 for data taken on 09/11/94. The figure consists of seven successive 30 minute integrated data profiles with temporal smoothing a product of the plotting program. Results, such as those shown in Figures 1.5 and 1.6 indicate that the rotational technique for obtaining temperature measurements using lidar should be explored further.

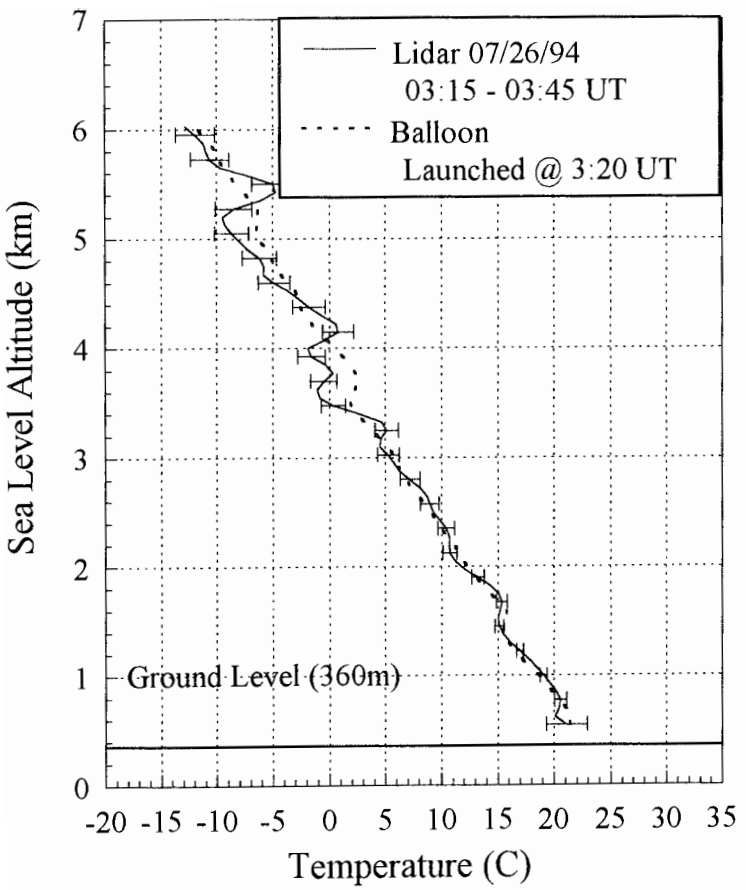

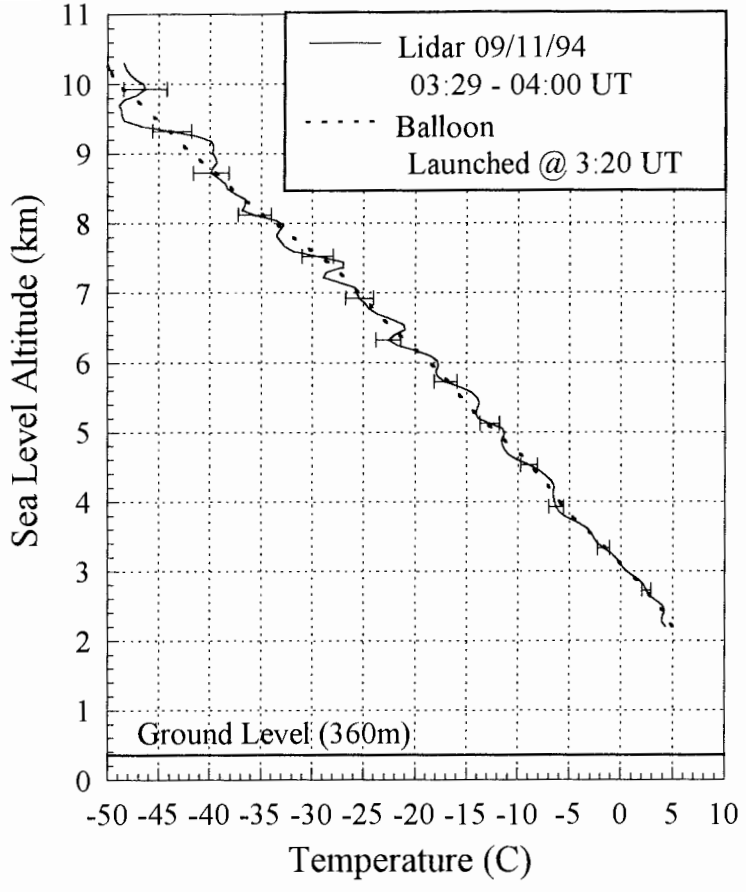

Figure 1.5. LAMP lidar rotational Raman temperature profiles taken on 07/26/94 at 03:15 - 03:45 GMT (**a**) and 09/11/94 at 03:29 - 04:00 GMT (**b**). One sigma error bars are based on the number of counts recieved by the lidar.

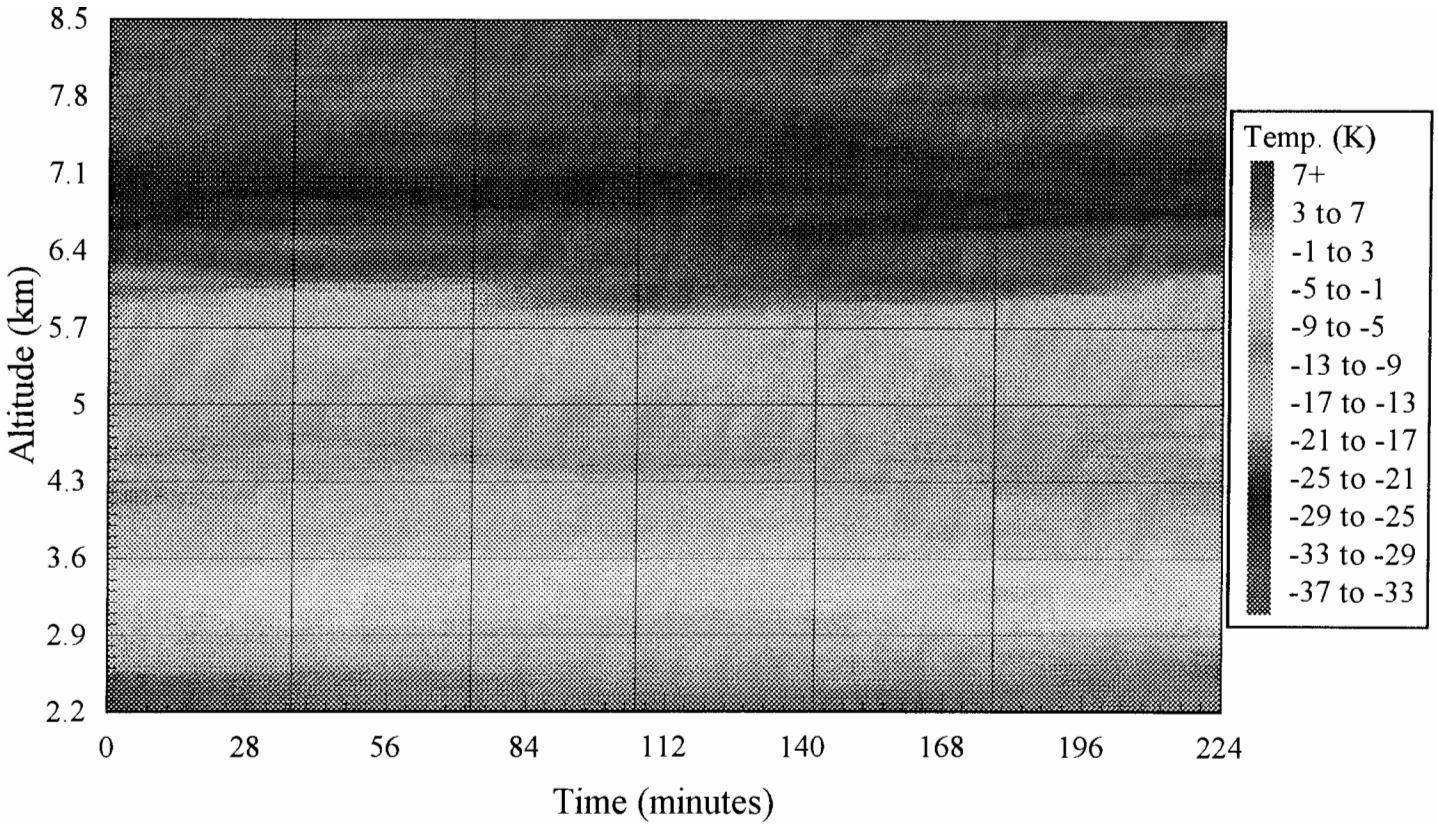

Figure 1.6 LAMP lidar rotational Raman temperature data measured on 09/11/94 at 02:16 - 06:30 GMT. Plot consists of seven successive 30 minute average lidar runs. Temporal smoothing is a product of the plotting program.

Chapter 2

PURE ROTATIONAL RAMAN TEMPERATURE MEASUREMENT THEORY

Because of the strengths of the spectral rotational Raman components, which for N_2 and O_2 are about two orders of magnitude greater than their corresponding vibrational states, and because the technique is independent of aerosol extinction and scattering (limited only by laser strength), the use of the pure rotational Raman spectrum was the only laser remote sensing technique expected to be able to measure the temperature through the aerosol rich lower troposphere. The large return obtained from the pure rotational Raman spectrum allows the statistics of the temperature measurements to be limited to the linearity of today's detector systems. Rotational Raman temperature is obtained from the ratio of two spectrally close signals. The difference in the extinction between the two signals is small, and thus can be neglected in theoretical calculations. The development of the pure rotational Raman temperature technique assumes that the only backscattered lines, which contribute to the received lidar signals, come from molecules that have density concentrations which are constant relative to each other at all temperatures and altitudes. The only two molecules which behave according to these assumptions, and have high enough concentrations and backscatter cross sections to give a strong enough signal, are molecular nitrogen (N_2) and molecular oxygen (O_2). Since the pure rotational Raman temperature technique is based on the scattering from N_2 and O_2 , and since both molecules are linear, the rotational quantum theory used to describe the molecules is relatively straight forward. This theory will be discussed later in this chapter.

The only other molecule which may have an impact on rotational temperature measurements is water vapor. However, the effects of the water vapor molecule on the rotational temperature measurements has not been explored in the past. Even though the basic rotational lidar equation remains the same for water vapor, the formulation of the rotational energy intensities and quantum line spacings becomes extremely complicated

due to the fact that water vapor is an asymmetric molecule. Because the concentration of water vapor changes with space and time, the effects of water vapor on the temperature measurements cannot be determined without correlative water vapor measurements. Thus, water vapor effects have to be considered as an error in the measurements. Chapter 3 will address the theory of the spectrum of water vapor and also explore whether high concentrations of the molecule will effect the temperature measurements. With the determination of the effect of water vapor on temperature measurements, considerations into the optimal design of the optical detector can be examined (see Chapter 4.)

2.1 The Pure Rotational Raman Spectrum and the Temperature Measurement Technique

In elastic scattering, an incident photon will cause an induced dipole moment on a molecule which varies with the frequency of the incident photon. The excited molecule will act like a dipole radiator, emitting a photon which has the same frequency as the incident photon. If the molecule is rotating, and its polarizability is isotopic, then like elastic scattering, a photon will be emitted without a change in frequency. Pure rotational Raman scattering occurs if a molecule is anisotropically polarizable. This anisotopy causes the molecule to be distorted depending on the direction of the induced electric field. This change in the induced dipole moment will cause the emission of a photon with a different frequency from the incident photon. The change in the frequency is dependent on the initial energy state of the molecule, which is in turn, dependent on the rotational speed. The rotational speed causes the molecules to reside at energy levels above the ground state. If an incident photon interacts with the rotating molecule, exciting it to an even higher virtual energy state, the molecule may relax to an energy level which is either greater than (anti-Stoke's region) or less than (Stoke's region) the energy of the incident photon. This is in contrast with vibrational scattering, which for most molecules, have only Stoke's shifts because only the ground vibrational state is effectively populated. In order for vibrational anti-Stoke's scattering to occur, the molecule must initially reside in an excited vibrational state before it is excited by an incident photon. The probability of

this level of excitation at typical atmospheric temperatures is small. This is in contrast with the pure rotational energy levels which may be populated at normal atmospheric temperatures

The rotational Raman spectrum, not only resides around the primary laser frequency, but also around each vibrational state. However, the pure rotational Raman spectrum is used instead of the rotational spectra off of the vibrational states because its intensity is about four orders of magnitude greater than the vibro-rotational intensities.

The pure rotational Raman temperature technique is based on measuring the number of photons backscattered from a parcel of air. The expected number of backscattered photons by a lidar system is given by,

$$N_{rot}(z) = \frac{E_L}{E_{p_L}} \Delta z \frac{A_o}{4\pi z^2} T^2_{atm}(z) n(z) \xi(z) \eta_{opt} F(J,T) \qquad 2.1$$

where,

E_L	: laser energy per pulse
Ep_L	: energy of photon at laser wavelength
Δz	: altitude increment
A_o	: receiver area
z	: altitude
$T_{atm}^2(z)$	: atmospheric transmission
n(z)	: number density
η_{opt}	: optical efficiency of the system
$\xi(z)$	: telescope form factor
J	: quantum number

and,

$$F(J,T) = \sum_J A(J,T) filt(J) \sigma_{J \to J'} \qquad 2.2$$

F(J,T) is the probability that a molecule will be in an initial quantum state within the filter spectrum, filt(J), and will backscatter, $\sigma_{J \to J'}$, to the observer. The thermal population

distribution of the rotational states, A(J,T), is given by,

$$A(J,T) = \frac{g(J)}{Q(T)}(2J+1)\exp\left[-\frac{E_J}{kT}\right] \qquad 2.3$$

g(J) : nuclear spin statistical weight factor
Q(T) : rotational partition function
E_J : energy in the Jth quantum state

The rotational partition function ensures that the sum of all quantum states in the population distribution is equal to one. It is important to note that the number of molecules backscattered is a function of only molecular properties and temperature. The key to calculating the expected return is being able to calculate the rotational energy levels and the backscatter cross sections for the distribution of allowed quantum transitions.

The possible energy levels, due to rotation, to which a molecule may be excited are quantized. These energy levels can be calculated by solving the Schrodinger equation given by,

$$\left[-\frac{h}{2cm}\frac{d^2}{dx^2} + V(x)\right]\Psi = E\Psi \qquad 2.4$$

The wave function, Ψ, describes all there is to know about the location and motion of the particle in question. The left side of the equation which operates on the wave function is the Hamiltonian operator which will be of importance in Chapter 3 when the calculation of the water vapor rotational spectrum is needed. The allowed rotational energy states are the eigenvalue solutions to the Schrodinger equation which are single valued, finite, and continuous.

Temperature measurements using the rotational Raman scattering principle were first proposed based upon preliminary estimates by Cooney [1972]. Cooney used the rotational Raman spectrum from the vibrational nitrogen line to model temperature profiles from the ground to 2 km with 100 m resolution. He measured in the Stoke's band

of the rotational states of the nitrogen molecule. Since that time, several refinements of the rotational Raman technique have been made [Armstrong,1975; Arshmov et al.,1983; Salzman,1974]. Nedeljkovic et al. [1993] were the first to propose that the anti-Stokes rotational spectrum should be used in order to avoid possible contamination from fluorescence. The experimental technique consists of placing two narrow band filters, Figure 2.1b, in one of the bands of the rotational spectrum, Figure 2.1a. Figure 2.1a shows that the effect of having a high temperatures is to widen the rotational spectrum and increase the line intensities at the higher quantum numbers. Since the rotational spectrum changes with changing temperature, the ratio of the two signals can produce a temperature profile,

$$R(T) = \frac{\sum_{S}\sum_{J}(N_S * A_S(J,T) * filt2_S(J)}{\sum_{S}\sum_{J}(N_S * A_S(J,T) * filt1_S(J)} = \frac{N2}{N1} \qquad 2.5$$

where,

S	: molecular species
N_S	: fraction of species in the atmosphere
N1	: signal from the first filter channel
N2	: signal from the second filter channel

Figure 2.2 is the theoretically calculated ratio versus temperature curve for the LAMP lidar. An important point to note is that since the signal is a ratio, all of the system parameters except filter functions drop out, and thus, measurements can be obtained through the entire range of the telescope form factor. Also, because the spectrum is narrow, the difference in the extinction value of the two signals is small and can be neglected [Nedeljkovic et al., 1993]. The rotational spectrum's shape is slightly modified by the effects of pressure broadening. However, Nedeljkovic et al. [1993] have shown that since the range of the atmosphere which is typically measured is small, and thus so is the range of pressures, pressure broadening does not produce a significant effect on temperature measurements.

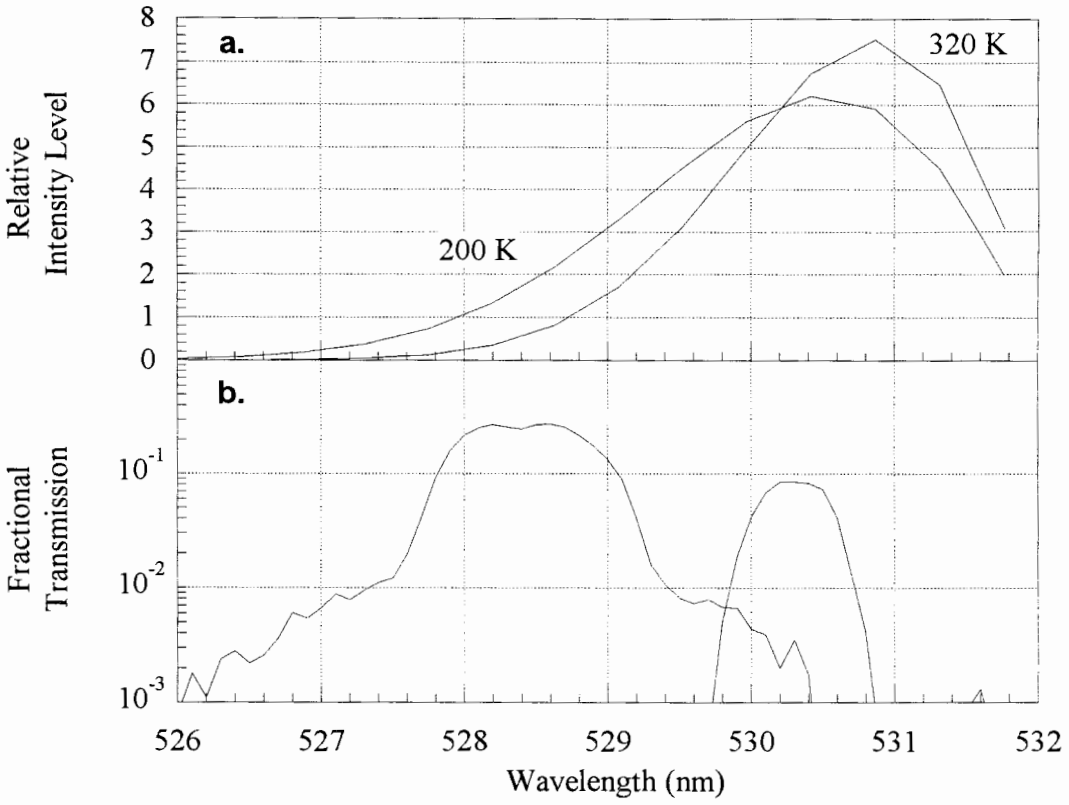

Figure 2.1. a. Temperature dependance of the rotational Raman spectra for N2 at 190 K and 320 K. **b.** LAMP filter functions for the temperature channels measured using a Hitachi U-4001 spectrophotometer.

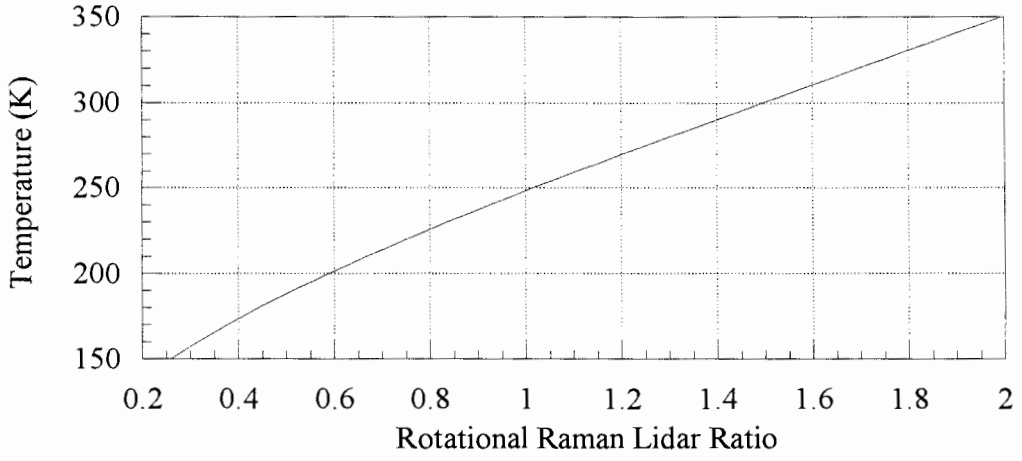

Figure 2.2. The theoretically calculated temperature versus ratio curve for the LAMP lidar.

2.2 The Pure Rotational Raman Spectrum of Linear Molecules

Linear molecules can be considered point masses with rotation occurring perpendicular to the line of the atoms. In this simplification, two of the moments of inertia (I) are equal to zero. This makes the solution to the Schrodinger equation relatively straight forward. The resulting quantized energy values can be calculated using,

$$E_J = \frac{h^2 J(J+1)}{8\pi^2 I} = Bhc J(J+1) \qquad 2.6$$

where B is the rotational constant for a particular linear molecule. From the calculated energy levels, the transition spacing between quantum lines can be calculated using the selection rules designated for linear molecules: $\Delta J = 0, \pm 2$. For the Stoke's spectrum,

$$\Delta\omega_{J\to J'} = -2B(2J+3) + D(8J^3 + 36J^2 + 60J + 36) \qquad 2.7$$

and for the anti-Stoke's spectrum,

$$\Delta\omega_{J\to J'} = 2B(2J-1) + D(8J^3 - 12J^2 + 12J - 4) \qquad 2.8$$

The last terms in each equation allow for the centripetal distortions of the atomic separation at high J values. With the derivation of the frequency spacings of the quantum lines, the backscattering cross sections of each of the lines can be determined by,

$$\sigma_\pi = \frac{32\pi^4}{15} b(J)(\omega_o + \Delta\omega_{J\to J'})^4 \gamma^2 \qquad 2.9$$

where γ is the anisotropic invariant of the polarizability tensor and b(J) is the Placzek-Teller coefficient. For linear molecules, b(J) is given by,

$$b(J) = \frac{3(J+1)(J+2)}{2(2J+1)(2J+3)} \qquad 2.10$$

for Stoke's scattering and,

$$b(J) = \frac{3J(J-1)}{2(2J+1)(2J-1)} \qquad 2.11$$

for anti-Stoke's scattering.

Penney et al [1974] reviewed the absolute rotational cross sections of N_2, O_2, and CO_2. The backscattering intensities can now be calculated with the molecular coefficients given in Table 2.1. Figure 2.3 shows the calculated Stoke's and anti-Stoke's population distribution for both N_2 and O_2 at 310 K. Included in the figure are the respective fraction of the atmospheric number density for each of the molecules (0.78 for N_2 and 0.21 for O_2). A note of interest is that even though the concentration of nitrogen is almost four times that of oxygen, both molecules have the almost the same relative backscattering intensities due to oxygen's higher anisotropic coefficient.

Table 2.1. Molecular rotational Raman coefficients for N_2 and O_2

Coefficient	**N_2**	**O_2**
B	1.9895 ± 0.00002	1.43768 ± 0.00001
g(J) even J	6	0
odd J	3	1
γ^2	0.518×10^{-48} ± 8%	1.35×10^{-48} ± 10%

The ability to calculate the spectrum of N_2 and O_2 permits for the design of an optimized optical detector system. The calculation of the rotational Raman spectrum of water vapor is much more involved than that for linear molecules, and thus will be discussed latter in Chapter 3.

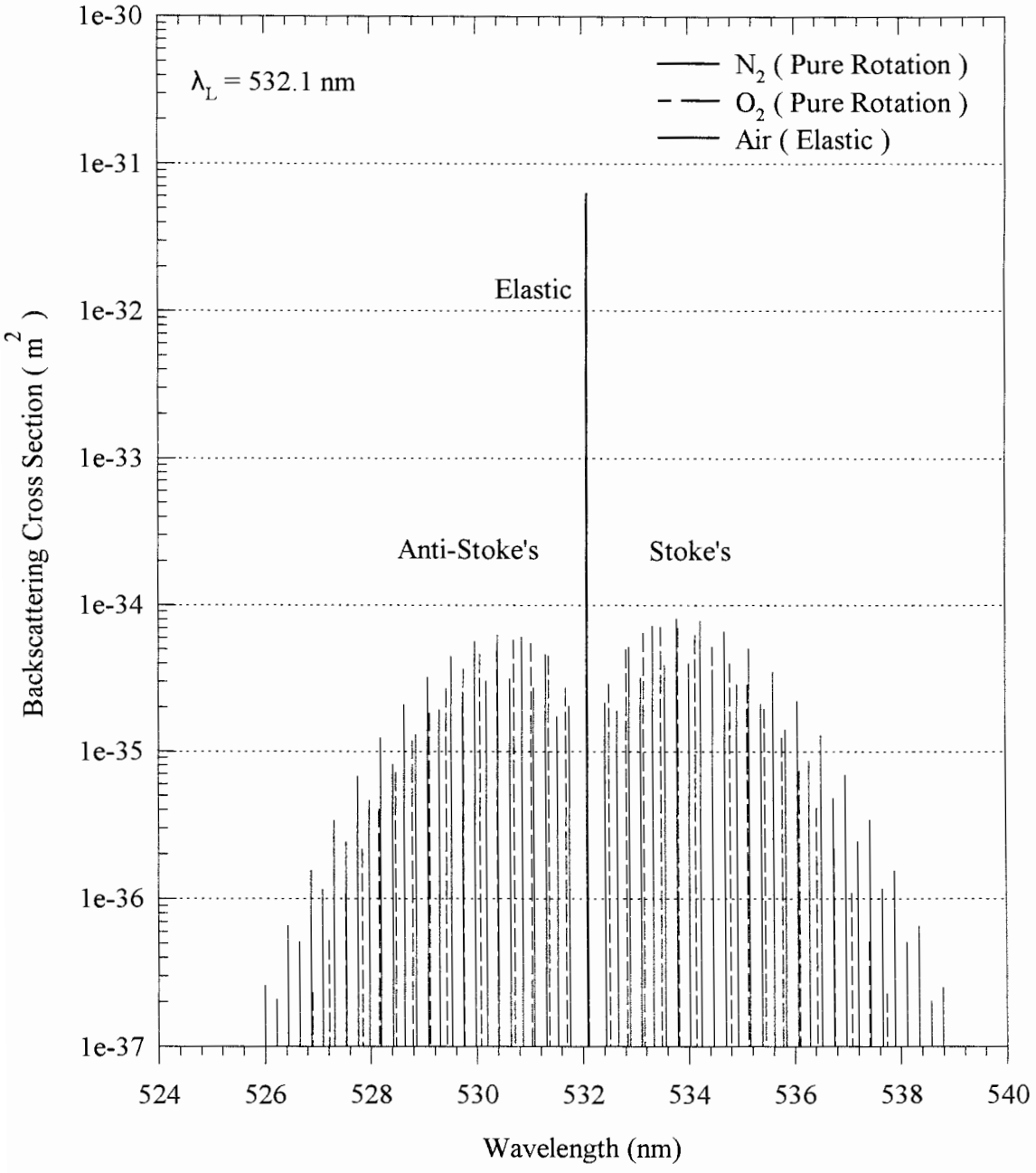

Figure 2.3. Calculated quantum rotational line intensities for N_2 and O_2 at 310 K, along with the elastic backscatter cross section of air. Rotational intensities include species' fraction of air.

Chapter 3

WATER VAPOR EFFECTS ON PURE ROTATIONAL RAMAN TEMPERATURE MEASUREMENTS

The theory and modeling of atmospheric temperature measurements using the rotational Raman scattering technique have been concentrated on how the spectra of the rotational states of diatomic nitrogen and diatomic oxygen molecules affect the intensities measured in each of the lidar passband filters. It has been shown that other minor species, such as CO_2, are of little consequence because their densities are very low in the atmosphere compared to that of N_2 and O_2. However, in the lower troposphere, extreme values of the volume percent of atmospheric water vapor have been recorded as high as 5% in some areas of the world [USSA, 1976]. This concentration equates to approximately 6 % that of the N_2 density and 25 % that of the O_2 density. If the backscatter cross section of water vapor is sufficiently large, then water vapor will cause contamination in temperature measurements of the lower troposphere. The objective then in this chapter is to calculate the influences that water vapor may have on the rotational Raman temperature measurements in the boundary layer.

3.1 Water Vapor in the Atmosphere

Like temperature, water vapor concentration is a fundamental property of the atmosphere which goes into predicting the weather. The amount of water in the atmosphere is a product of both the different water sources available and the current atmospheric temperature. What is important to lidar measurements is the water vapor content which crosses the path of the laser beam. The sources of the water vapor can come from either evaporation of cloud droplets and ground water, or from entrainment, or from both. However, the amount of water vapor that is present in a parcel of air is

determined ultimately by the temperature. The approximate limit of the water vapor concentration in air is called the saturation point, and it increases with increasing temperature. If saturation is approached, then the probability for condensation is high. Calculation of water density (ρ_w) at the saturation points with temperature is given by,

$$\rho_w = \frac{e_s}{R_w T} \qquad 3.1$$

where, R_w is the ideal gas constant for water, T (◦C) is temperature, and $e_{s\,(mb)}$ is the saturation pressure given by,

$$e_s \approx 6.112\exp\left(\frac{17.67T}{T + 243.5}\right) \qquad 3.2$$

for the temperature range -30 °C ≤ T ≤ 35 °C. In the absence of aerosol particles, the water vapor content may exceed slightly that given by Equation 3.1.

The amount of water vapor in the atmosphere has been documented by a large number of groups over the past century, especially in the last 50 years. These measurements have been the basis of a number of atmospheric calculations and models. The US Standard Atmospheric model, 1976, gives the average atmosphere for the mid-latitude region over all seasons. It also provides the measured extreme water vapor concentrations that have been recorded on the Earth up until the time of the making of the model. Table 3.1 shows these average and extreme values. The average values in the mid-latitudes contain both high and low fractional percents. Thus, at any one time, the fractional value of water vapor can be much higher than the average value. From the extreme values, the water vapor concentration can be as high as 5.3% of the atmospheric density. Figure 3.1 also shows average water vapor mixing ratios, but over all latitudes [Ahrens,1994]. Even at the peak of this average curve, the fractional percentage of the air due to water vapor can be 2.7%.

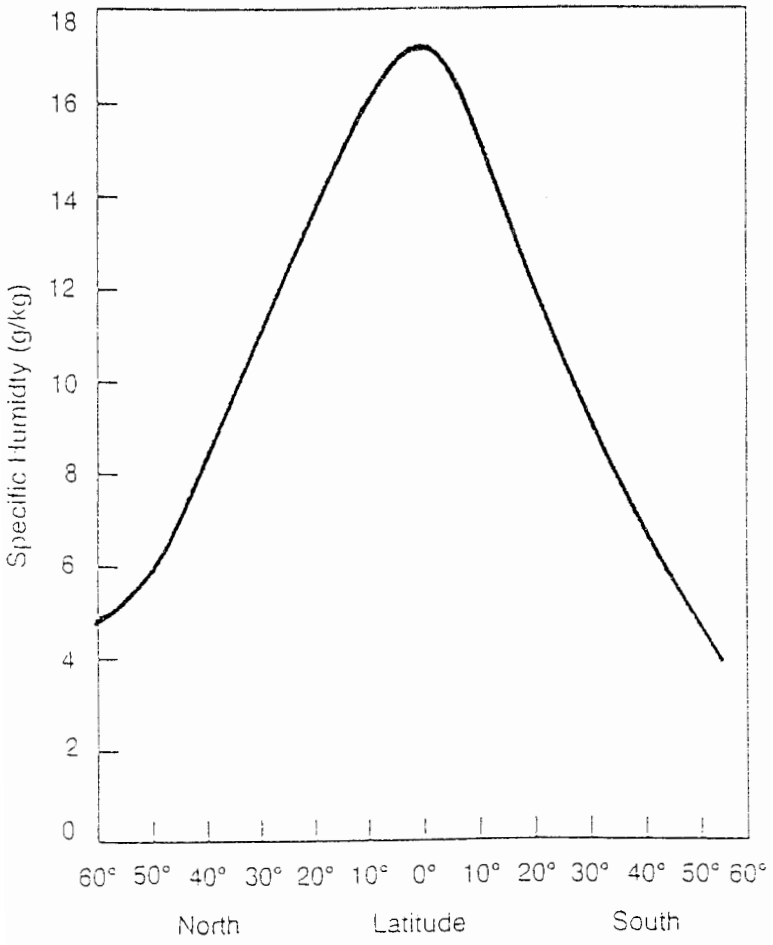

Figure 3.1. The average specific humidity for each latitude. The highest average values observed in the tropics and the lowest values in polar regions [Ahrens,1994]

Table 3.1: Fractional volume concentration of air for some atmospheric constituents calculated from values found in USSA, 1976.

	Average Mid-Latitude				Measured Global Extreme Values		
Altitude	N_2	O_2	H_2O		N_2	O_2	H_2O
Surface	0.775	0.208	0.007		0.740	0.198	0.053
1	0.776	0.208	0.006		0.744	0.200	0.047
2	0.778	0.209	0.005		0.747	0.201	0.043
4	0.780	0.209	0.002		0.754	0.202	0.034
6	0.780	0.209	0.001		0.770	0.207	0.014

3.2 Theory and Computer Program for the Pure Rotational Raman Spectrum of Water Vapor

Asymmetric-top molecules (i.e. water vapor) are molecules which have three different principle moments of inertia. If it is assumed that they behave like rigid rotators, then the rotational energy levels of asymmetric-top molecules can be calculated by beginning with the classical expression for the energy of a rotating body and then applying quantum mechanical principles. The energy of any rigid rotor can be expressed as the summation of the kinetic energies about each of the rotating axis. These kinetic energies are a product of the moment of inertia (I) about each axis times the square of the angular velocity (ω),

$$E = \tfrac{1}{2} I_x \omega_x^2 + \tfrac{1}{2} I_y \omega_y^2 + \tfrac{1}{2} I_z \omega_z^2 \qquad 3.3$$

or in terms of angular momentum (P),

$$E = \frac{1}{2}\left[\frac{P_x^2}{I_x} + \frac{P_y^2}{I_y} + \frac{P_z^2}{I_z}\right] \qquad 3.4$$

Solving the equation in terms of quantum mechanics, Ray [1932] as corrected by King, Hainer, and Cross [1943] has shown that for an asymmetric top rotor, Equation 3.4 is equivalent to,

$$F(J,\tau) = \frac{E(J,\tau)}{hc} = \frac{1}{2}(A+C)J(J+1) + \frac{1}{2}(A-C)E_{\tau} \qquad 3.5$$

where $F(J,\tau)$ is the energy in wave numbers, A, B, and C, are the principle moments of inertia, and E_{τ} are the $2J + 1$ roots of a secular determinant of degree $2J + 1$ for each J [Hertzberg, 1989]. Equation 3.5 shows that the calculations needed for each energy level quickly increases as J increases. When comparing the results to measured spectra, Equation 3.5 does not accurately describe the energy levels of an asymmetric top molecule, because as J increases, distortion coefficients become important. Even in the case of linear molecules, there are higher order distortion terms (see Equations 2.7 and 2.8). However, because these distortion coefficient are small, they can be neglected for small J.

Since direct calculations of the rotational spectrum from initial electronic conditions are impractical, an indirect method had to be developed. Watson [1967] showed that the molecular Hamiltonian, which is expansionistic in nature, could be reduced by applying a unitary transformation. This transformation reduced the number of coefficients in the equation while maintaining the same eigenvalues. By then fitting this reduced Hamiltonian to a measured spectrum, the coefficients could be determined [Murphy, 1977]. The corresponding eigenvectors can thus be calculated by solving the Hamiltonian. Since the molecular Hamiltonian was reduced while maintaining the same eigenvalues, the eigenvectors are changed and must be corrected by applying the same unitary transformation [Watson, 1967]. However, for the spectral range considered in this thesis, the error caused by the unitary transformation on the eigenvectors is negligible as will be seen by comparing the calculated and measured water vapor spectrums shown later in this chapter.

Johns [1985] showed that a tenth order reduced Hamiltonian with one twelfth order coefficient was sufficient to calculate the energies of the water vapor pure rotational Raman spectrum for J ≤ 14 and K ≤ 7 and is given by,

$$\begin{aligned} H_W = [A &- \tfrac{1}{2}(B+C)J_z^2 + \tfrac{1}{2}(B+C)J^2 + \tfrac{1}{2}(B-C)J_{xy}^2 \\ &- \Delta_K J_z^4 - \Delta_{JK} J_z^2 J^2 - \Delta_J J^4 - \delta_K (J_z^2 J_{xy}^2 + J_{xy}^2 J_z^2) - 2\delta_J J_{xy}^2 J^2 \\ &+ H_K J_z^6 + H_{KJ} J_z^4 J^2 + H_{JK} J_z^2 J^4 + H_J J^6 \\ &+ h_K (J_z^4 J_{xy}^2 + J_{xy}^2 J_z^4) + h_{JK} (J_z^2 J_{xy}^2 + J_{xy}^2 J_z^2) + 2h_J J_{xy}^2 J^4 \\ &+ L_K J_z^8 + L_{KKJ} J_z^6 J^2 + L_{JK} J_z^4 J^4 + l_K (J_z^6 J_{xy}^2 + J_{xy}^2 J_z^6) \\ &+ P_K J_z^{10} + p_K (J_z^8 J_{xy}^2 + J_{xy}^2 J_z^8) \\ &+ T_K J_z^{12} \end{aligned} \qquad 3.6$$

where J_x, J_y, and J_z are the components of the angular momentum (P) and are given by,

$$J_x = \frac{P_x}{h} \quad , \quad J_y = \frac{P_y}{h} \quad , \quad J_z = \frac{P_z}{h} \qquad 3.7$$

with,

$$J_{xy}^2 = J_z^2 - J_y^2 \qquad 3.8$$

The resulting coefficients calculated by Johns are given in Table 3.2. If it is necessary, Equation 3.6 can be expanded to any number of orders to account for higher order distortions.

The intensities of the quantum transitions can be calculated if the eigenvalues, eigenvectors, principle polarizability tensor components, and the nuclear spin statistical weight factor are known. If the principle polarizability coefficients are not known, then like that for the calculation of the energies, the quantum line intensities have to be determined indirectly. The calculation can be made by noting that the relative intensities of the quantum lines are proportional to the ratio (R_{20}) of the invariant polarizability components [Murphy, 1977],

Table 3.2. Coefficients used in the reduced Hamiltonian to calculate the energy levels of the pure rotational Raman spectrum of water vapor for $J \leq 14$ and $K \leq 7$.

Effective Principle Rotational Constants		Fourth Order Distortion Coefficients		Sixth Order Distortion Coefficients	
A	835839.672	Δ_K	974.444	H_K	3.8620
B	435346.828	Δ_{JK}	-173.3183	H_{KJ}	-5.203×10^{-1}
C	278140.312	Δ_J	37.5917	H_{JK}	-5.720×10^{-2}
		δ_K	39.603	H_J	1.6515×10^{-2}
		δ_J	15.22164	h_K	0.9305
				h_{JK}	-2.623×10^{-2}
				h_J	8.1761×10^{-3}

Eighth Order Distortion Coefficients		Tenth Order Distortion Coefficients		Twelth Order Distortion Coefficients	
L_K	-2.650×10^{-2}	P_K	17.92×10^{-5}	T_K	-56.70×10^{-8}
L_{KKJ}	7.73×10^{-3}	P_{KKJ}	-65.2×10^{-6}		
L_{JK}	$-2.070 \times 103^{-}$	P_{KJ}	26.3×10^{-6}		
L_{JJK}	13.15×10^{-5}	P_{JK}	-0.134×10^{-5}		
L_J	-11.07×10^{-6}	P_{JJK}	-2.94×10^{-7}		
l_K	-10.35×10^{-3}	P_J	0.329×10^{-8}		
l_{KJ}	5.77×10^{-4}	p_K	5.90×10^{-5}		
l_{JK}	1.60×10^{-5}	p_{KKJ}	-0.960×10^{-5}		
l_J	-4.751×10^{-6}	p_{KJ}	-		
		p_{KJJ}	-1.50×10^{-7}		
		p_J	-		

$$R_{20} = \frac{\alpha_2^2 + \alpha_{-2}^2}{\alpha_0^2} \qquad 3.9$$

The intensities can be calculated by varying R_{20}, so that the intensity levels fit that of the measured spectrum. This calculation was performed by Murphy for the water vapor molecule. The results of Murphy's calculations are shown in Figure 3.2a and 3.2b. Figure 3.2a is the measured pure rotational Raman spectrum of water vapor and 3.2b is the calculated spectrum assuming a filter bandpass of 2.2 cm^{-1} for the spectrometer. The bias in the measured spectrum of Figure 3.2a has been attributed to Raman scattering from the walls of the silica cell. The extra bands in the measured spectrum at 27, 44, and 84 cm^{-1} are due to scattering from trace impurities. By performing the fit, Murphy was also able to determine that the anisotropic coefficient (γ) was equal to 9.792×10^{-26}.

With a knowledge of all of the components needed for the calculation of the rotational Raman spectrum, Murphy's energy and intensity programs can be used to calculate the spectrum at any temperature. These programs were written for the NRCC TSS computer [Murphy, 1977]. The code for the calculation was separated into two programs. The first program, now referred to as the energy program, calculates the energies and eigenvectors using the reduced Hamiltonian, and stores the results in a file according to J value and the energy symmetry classifications (E^+, E^-, O^+, and O^-). These symmetries come from the ability to factor the polarizability tensor. The second program, now referred to as the intensity program, inputs both the file with the energies and eigenvectors and the file which contains the non-vanishing irreducible spherical tensor components (mean polarizability and anisotropy), and computes the allowed frequencies and intensities of all of the rotational quantum shifts for a certain J and K range and temperature. The allowed energy transitions for asymmetric top molecules are given by,

$$\begin{aligned} \Delta J = \pm 1 \qquad & E^{\pm} \rightarrow E^{\mp} \;, \quad O^{\pm} \rightarrow O^{\mp} \\ \Delta J = \pm 2 \qquad & E^{\pm} \rightarrow E^{\pm} \;, \quad O^{\pm} \rightarrow O^{\pm} \end{aligned} \qquad 3.10$$

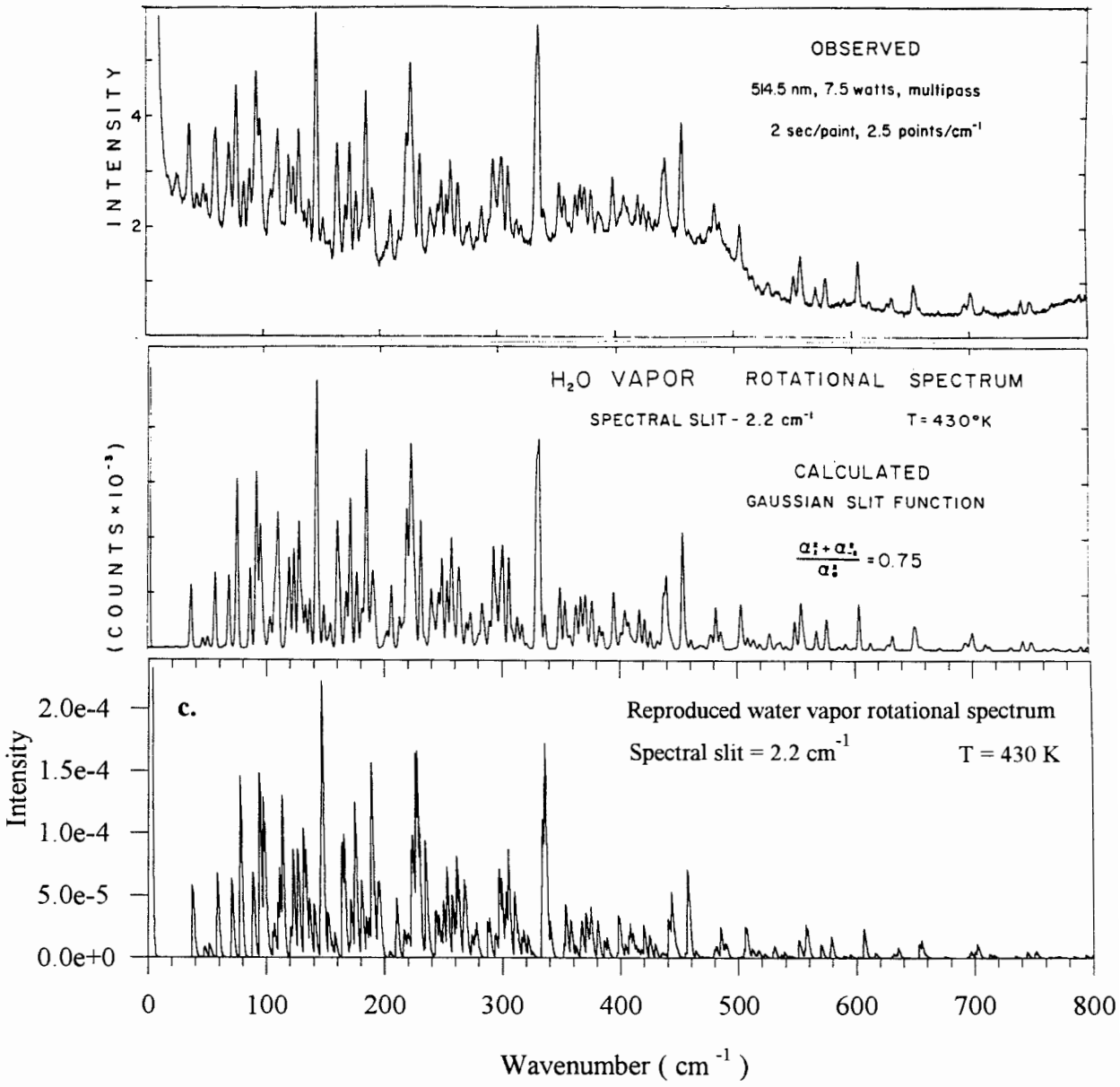

Figure 3.2. The pure rotational Raman spectrum of water vapor. **a**. Spectrum measured by Murphy [1977]. **b**. Calculated spectrum by Murphy assuming a 2.2 cm-1 Gaussian filter function. **c**. Reproduction of Murphy's calculations.

Since its development, Murphy's asymmetric top programs have been used to calculate the spectra of other asymmetric top molecules [Murphy, 1977, 1981; Fernandez-Sanchez et al., 1979]. Because the programs were written for a different machine and in a different version of Fortran than was available for this thesis, Murphy's programs where adapted to operate on a PC using Microsoft Fortran. The modifications included a number of input and output routines which were necessary for calculations described latter in this chapter. Murphy's modified energy program is given in Appendix B, and that for the intensity program in Appendix C.

Before the results of the modified programs could be used, it was necessary to prove that Murphy's previous work could be duplicated [Murphy, 1977]. The stick spectrum for water vapor at 430 K was calculated with each line the summation of all the quantum lines which fill a 0.25 cm^{-1} interval. The Fourier transform was taken of the stick spectrum and multiplied with the Fourier transform of a Gaussian filter function with a FWHM bandwidth of 2.2 cm^{-1}. The results are shown in Figure 3.2c. It is quite apparent that the output of these modified programs are producing the correct results.

3.3 Absolute Rotational Raman Line Intensities

The energy program was run to calculate the energies and eigenvectors in the spectral range of -500 $cm^{-1} \leq \omega \leq 500$ cm^{-1}. The energies are listed in Appendix D. This spectral range was chosen because beyond 500 cm^{-1}, the intensities of the N_2 and O_2 rotational quantum lines become exceedingly small. The intensity program was then run to calculate the pure rotational Raman line intensities at various temperatures, the values of which are given in Appendix E. The calculated intensities are only relative measurements to the actual line strengths. The line intensities include the nuclear spin statistical weight factor, the partition function, part of the anisotropic coefficient, and the Boltzman factor. In order to make them absolute, the line intensities must be multiplied by,

$$\frac{32\pi^4}{15}(\omega_o + \Delta\omega_{J\to J'})^4 \frac{3\gamma_e}{2} \qquad 2.11$$

where $\gamma_e = 10^{-48}$. Figures 3.3a and 3.3b show the calculated backscatter cross section multiplied by the thermal distribution of quantum lines for water vapor at 200 K and 320 K, respectively. Because of the broad width of the spectrum and because of the complexity of the quantum lines, the cross over between the intensity envelopes at the two different temperatures for water vapor occurs much further out than in the envelope for N_2 and O_2. Figure 3.4 shows the superposition of the anti-Stoke's water vapor spectra at 200 K and 320 K. The quantum lines in the 320 K spectrum do not dominate over the quantum lines in the 200 K spectrum until about 163 cm^{-1}, where as for N_2, this occurs at 67 cm^{-1}.

The differences in the spectral width of the anti-Stoke's pure rotational spectrum of H_2O, N_2, and O_2 at 320 K are shown in Figure 3.5a and 3.5b. The line intensities include the backscatter cross sections and the thermal distribution of the quantum envelope while ignoring the atmospheric percentages of each species. When compared to the scattering intensities of N_2 and O_2 at the peak of its spectrum, the H_2O intensity is approximately 0.5% of that for O_2 and 1.1% of that for N_2.

3.4 Effects of Water Vapor on Rotational Raman Temperature Measurements

The determination of any possible errors in temperature measurements caused by water vapor, requires a knowledge of the concentrations of each constituent at a particular temperature and a knowledge of the filter functions used in receiving the lidar signal. Since the saturation limit of water vapor in a parcel of air is primarily determined by temperature, a high temperature of 320 K was chosen for the model. The fractional percentage of water vapor in the air was chosen to be 3% after considerations of the latitudinal averages and the global extremes given in Figure 3.1 and Table 3.1. The corresponding N_2 and O_2 concentrations calculate to 76% and 20%, respectively.

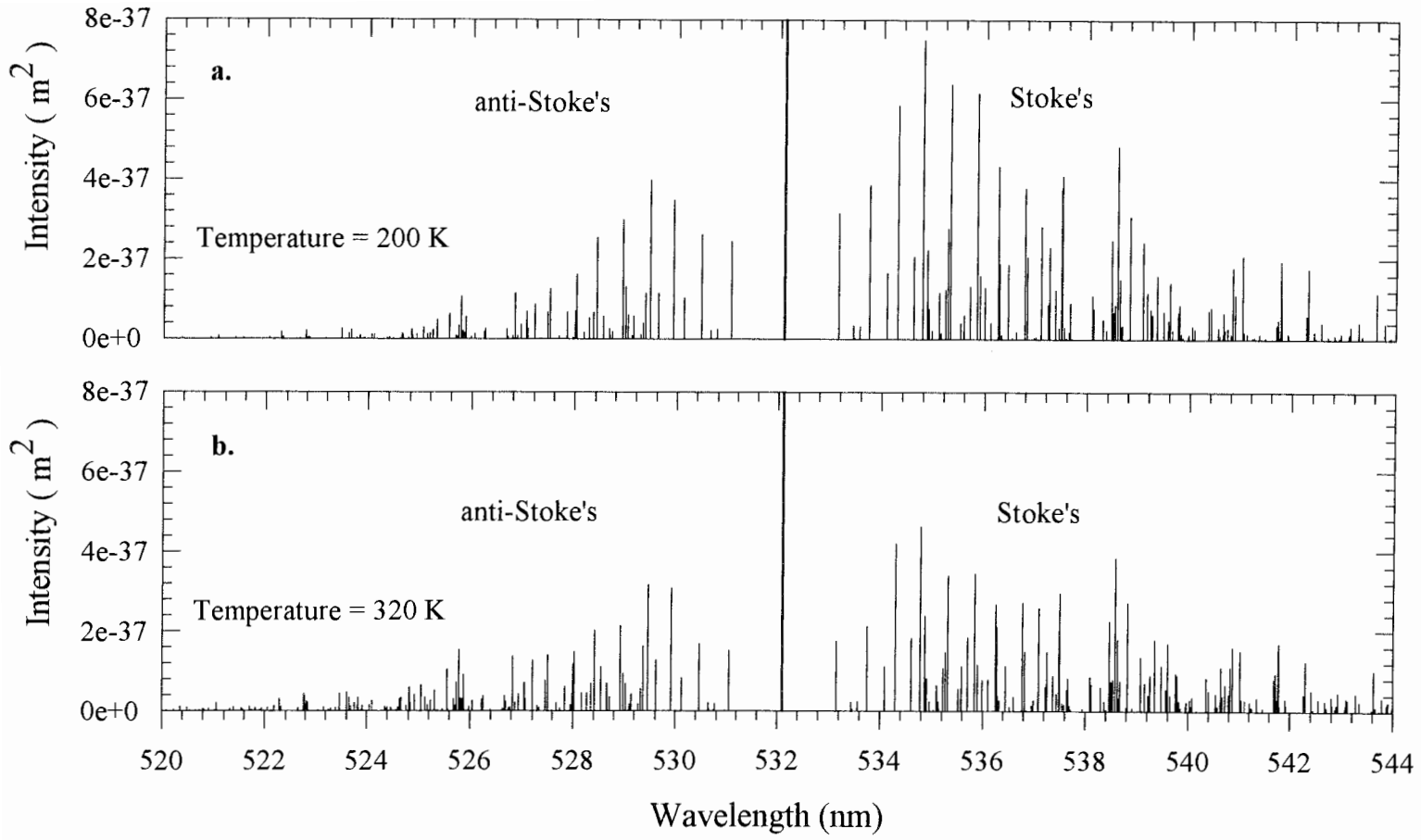

Figure 3.3. Pure rotational Raman spectra of water vapor at 200K (**a**.) and 320 K (**b**.). Intensities include the backscatter cross section for each quantum line and the thermal distribution of all the quantum lines at the particular temperature.

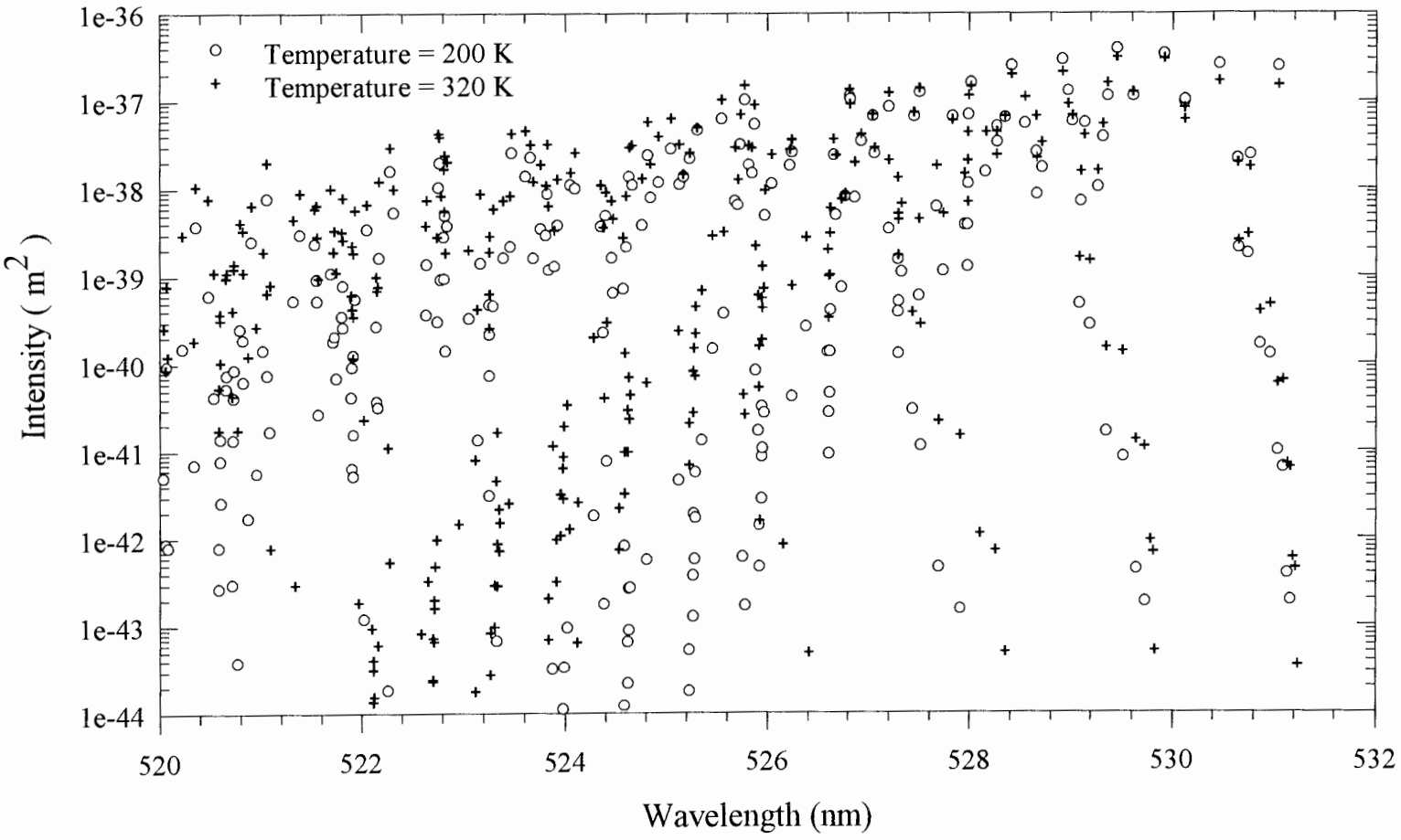

Figure 3.4. Combined pure rotational anti-Stoke's Raman spectra of water vapor at 200K and 320 K. Intensities include the backscatter cross section for each quantum line and the thermal distribution of all the quantum lines at the particular temperature.

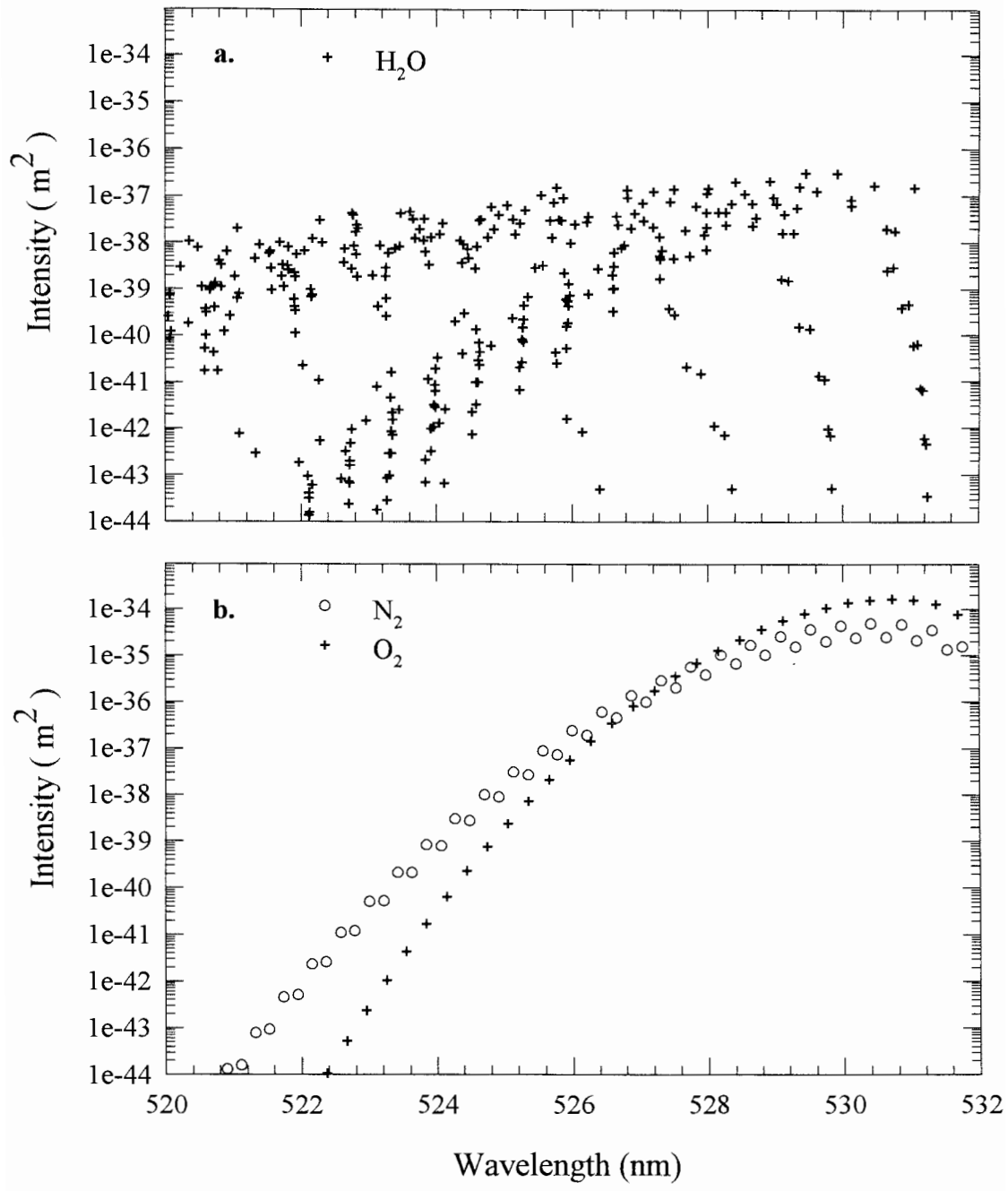

Figure 3.5. Comparison of the Pure rotational Raman spectra of water vapor at 320 K (**a.**) to the spectra of N_2 and O_2 (**b.**). Intensities include the backscatter cross section for each quantum line and the thermal distribution of all the quantum lines at the particular temperature while excluding the fractional percent of each constituent in the atmosphere.

Because it is impossible to determine the temperature error caused by water vapor unless both filter configurations are set, only the error in the received signal from a single filter will be considered. For sake of space, only three filter bandwidths were chosen (FWHM = 0.2 nm, 1.4 nm, 3.0 nm). The filter functions were convolved with the spectra of N_2, O_2, and H_2O. The results of the H_2O intensities were then divided by the sum of the N_2 and O_2 intensities. This provided a spectral plot of the fractional percent of error caused by H_2O with filters located at each point in the spectral range. Figure 3.6a, 3.6b, and 3.6c show the results of the calculations at the 0.2 nm, 1.4 nm, and 3.0 nm FWHM bandwidths, respectively. Figure 3.6 does not include the fractional percent of each constituent in the atmosphere so that the line intensities of each molecule could be compared. Figure 3.7 shows the same results as Figure 3.6 except that the fractional percentage of each constituent is factored into the calculation. Figure 3.6 and 3.7 show that as the filter bandwidths decrease, the potential for water vapor contamination can either increase or decrease dramatically depending on the filter placement. This is because the number of quantum lines per unit wave number for the H_2O spectrum is much larger than that of N_2 and O_2. Figure 3.7 indicates that the error in the received lidar signal due to water vapor does not need to be considered above approximately 527.5 nm (163.9 cm^{-1}) for a 0.2 nm FWHM filter, or above approximately 525.8 nm (225.2 cm^{-1}) for a 3.0 nm FWHM filter. These values were the points at which an error in the signal was less than 0.1%. If the LAMP theoretical temperature versus ratio curve is considered, then this 0.1% error in the signal would equate to about 0.2 K error in the temperature profile. These limits are in the range of filter functions used in most practical rotational Raman temperature measurement configurations. Therefore, it is concluded that the contributed water vapor error in rotational Raman temperature measurements is negligible when appropriate design considerations are followed.

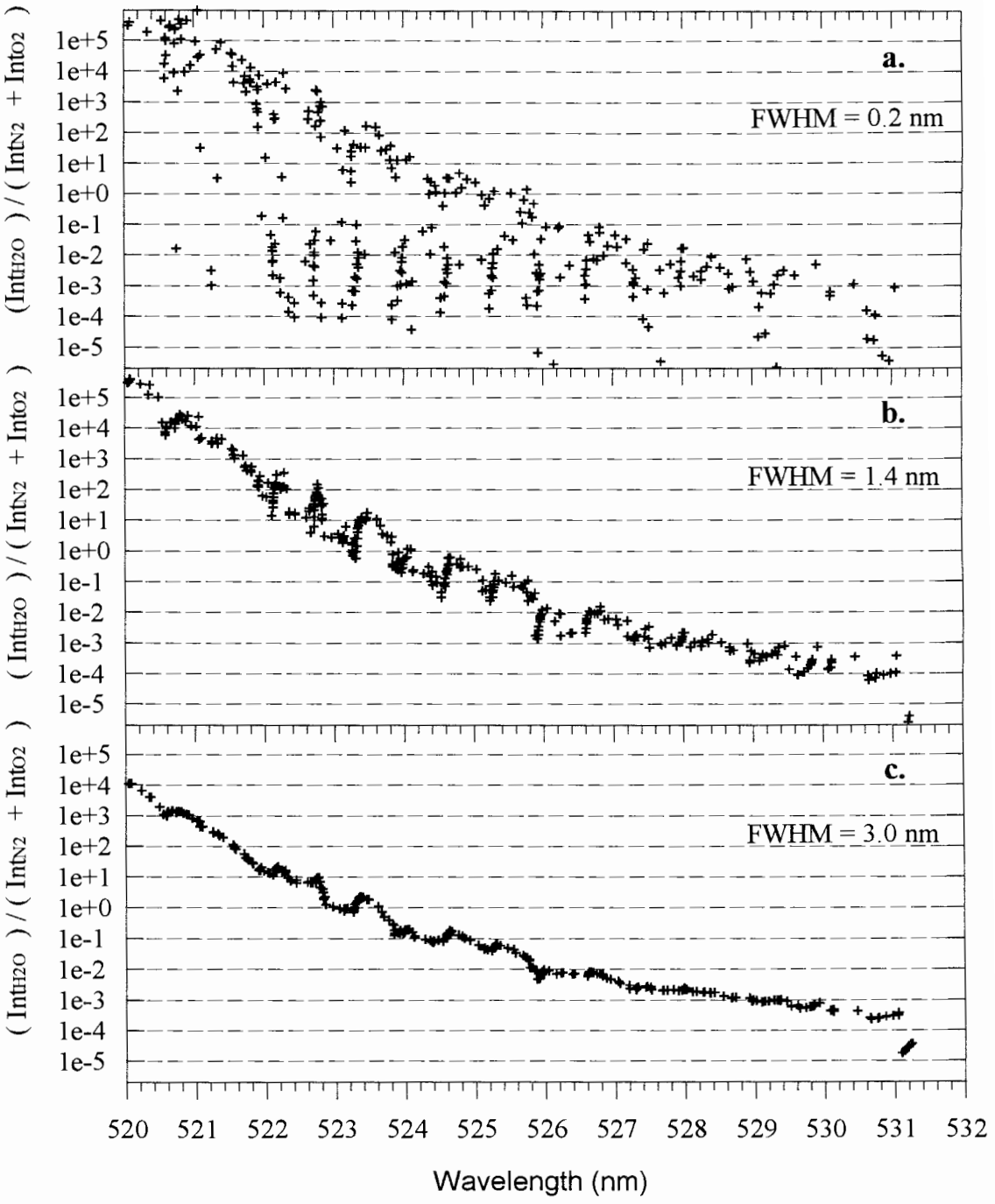

Figure 3.6. Comparison of the water vapor intensity to the sum of N_2 and O_2 intensities at 320 K with filter FWHM of 0.2 nm (**a**.), 1.4 nm (**b**.), and 3.0 nm (**c**.) Intensities do not contain the fractional percent of each constituent in the atmosphere

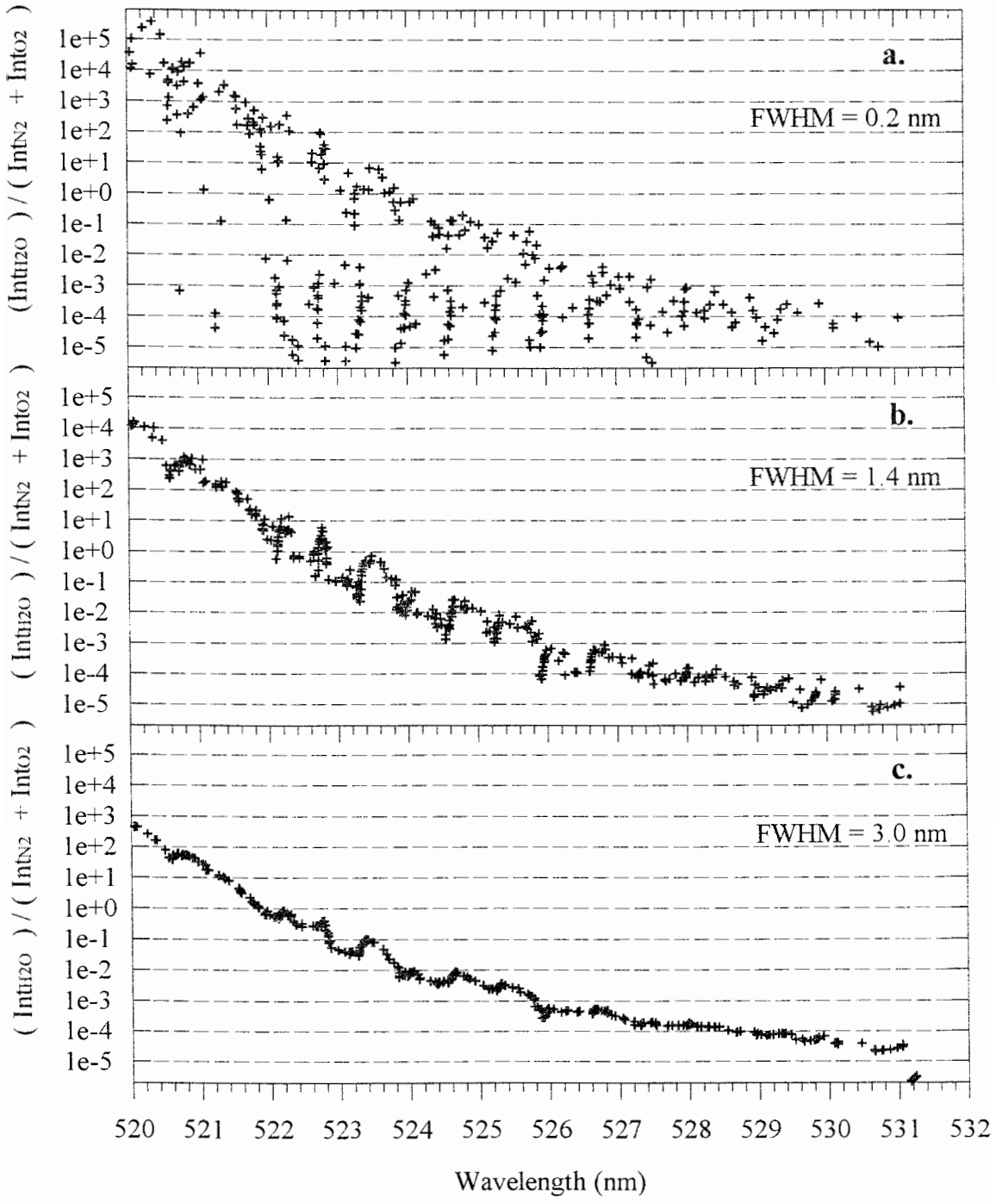

Figure 3.7. Comparison of the water vapor intensity to the sum of N_2 and O_2 intensities at 320 K with filter FWHM of 0.2 nm (**a**.), 1.4 nm (**b**.), and 3.0 nm (**c**.) It is assumed that the fractional percentage of each constituent is $H_2O = 0.03$, $N_2 = 0.76$, and $O_2 = 0.20$.

Chapter 4

IDEAL OPTICAL FILTER CONFIGURATION

In order to measure atmospheric temperatures effectively using the rotational Raman technique, filter functions in the detector system need to be chosen in order to minimize errors. The ideal optical filter setting is a trade off between the signal strength and the sensitivity between lidar ratios and temperatures. The larger the filter separation in the rotational spectrum, the larger the dynamic range (see Figure 4.1). However, if the filter, which is placed furthest from the elastic line, is placed too far into the rotational spectrum, then the number of counts received by the detector will be low and the statistical error will increase. Figure 2.3 shows where the line strengths drop off exponentially. The filters must also have a large enough blocking power at the laser line to remove any contamination that may result from elastic molecular and particle scattering. Because the elastic line strength is two orders of magnitude larger than the rotational lines, and because particle scattering strengths can be as large as five orders of magnitude more than the elastic line, as measured using the LAMP lidar, filter functions are required to reduce the fundamental frequency by nine orders of magnitude or more.

Though the optimization performed in this chapter was based on the 532 nm laser wavelength, the results can be used for any laser wavelength. The reason is that the shift in the wavelengths of the quantum lines are originally calculated in wave numbers which are independent of incident wavelengths. To convert to other wavelengths the following equation can be used,

$$\lambda_J = \frac{1}{\frac{1}{\lambda_L} + \Delta\omega_{J\to J'}} \qquad 4.1$$

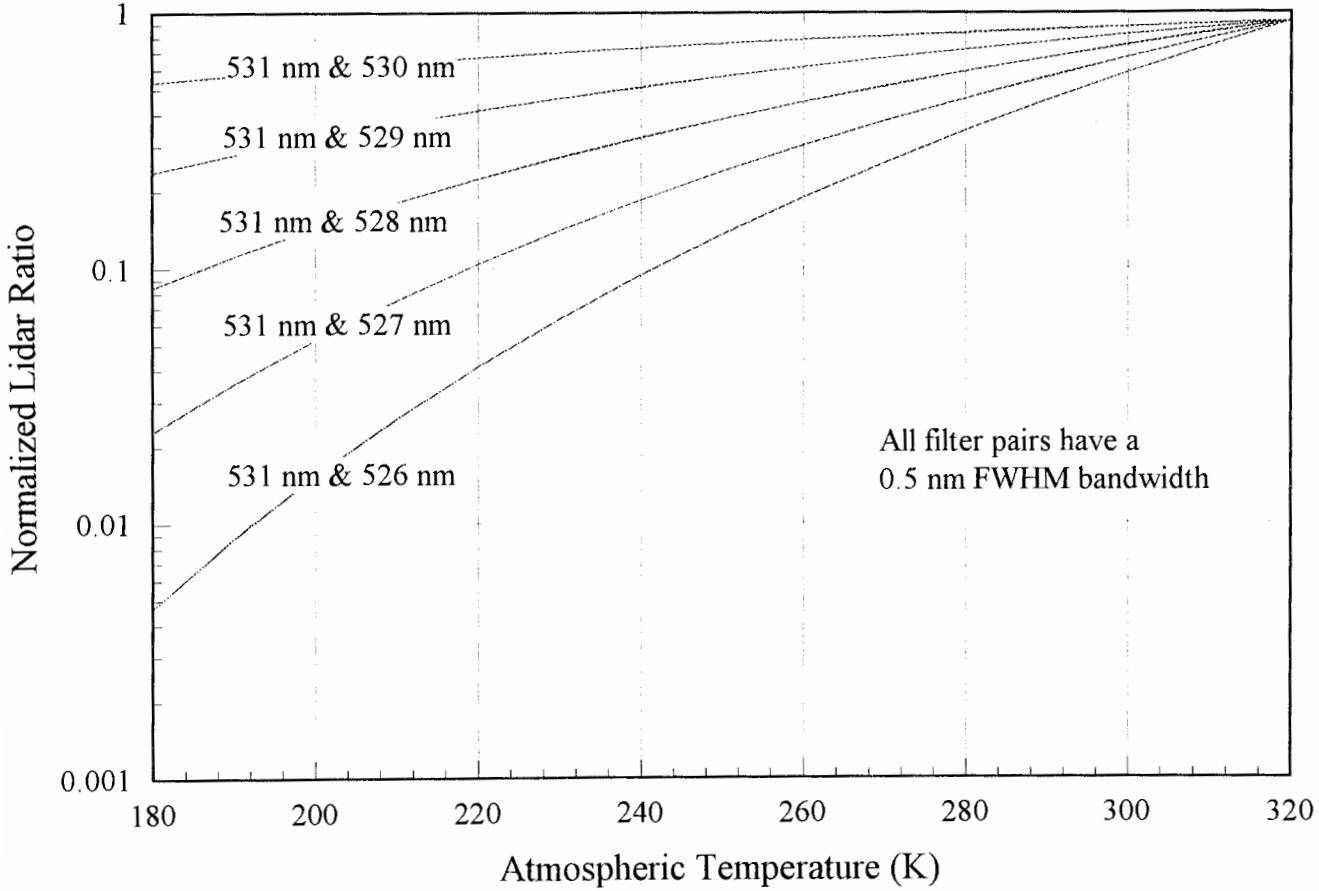

Figure 4.1. Comparison of the dynamic range between lidar ratio and atmospheric temperature for filter function seperation distance. Each filter has a 0.5 nm FWHM.

where λ_L is the wavelength of the incident photon and $\Delta\omega_{J-J'}$ is the shift in the scattered photon. Going to shorter laser wavelengths results in the quantum lines being bunched up closer to the elastic line. This can be seen in Figure 4.2, where Figure 3.3 has been calculated for the 355 nm and 532 nm laser wavelengths. The differences in the intensities are due to the $1/\lambda^4$ factor in Equation 2.9.

The delta functions representing the quantum lines in Figures 2.3 and 4.2 do not show the fact that the lines actually have a spectral width. The broadening of the lines come from four sources: natural broadening, pressure broadening, Doppler broadening, and broadening because of the finite spectral width of the incident laser [Measures, 1984].

Natural broadening arises from the fact that an excited molecule has a natural mean radiative lifetime associated with it. From the Heisenberg uncertainty principle $\Delta E \Delta t \sim h/2\pi$, this finite lifetime in the time domain leads to a finite spectral width in the frequency domain. The resulting line shape distribution from this type of broadening is Lorentzian.

Collisional (pressure) broadening occurs because of elastic or inelastic collisions between molecules. Collisions reduce the lifetime of an excited state or perturb the energy widths of the two quantum states. A reduction of the lifetime in the time domain equates to a broadening of the spectral width in the frequency domain. Collisional broadening also contributes to a Lorentzian profile.

The FWHM of the Lorentzian profile can be shown to be,

$$\Delta\nu = \frac{1}{2\pi\tau} \qquad 4.2$$

where τ is the radiative lifetime of the molecule and $\Delta\nu$ is the frequency broadening. For natural broadening, a typical lifetime is approximately 10 nsec which equates to a spectral width of 1.50×10^{-5} nm at a frequency of 532 nm.

Doppler broadening occurs because molecules have a random thermal velocity associated with them. The Maxwellian distribution of the velocities of the molecules at a certain temperature gives the radiating molecules a Gaussian spectral profile. The FWHM

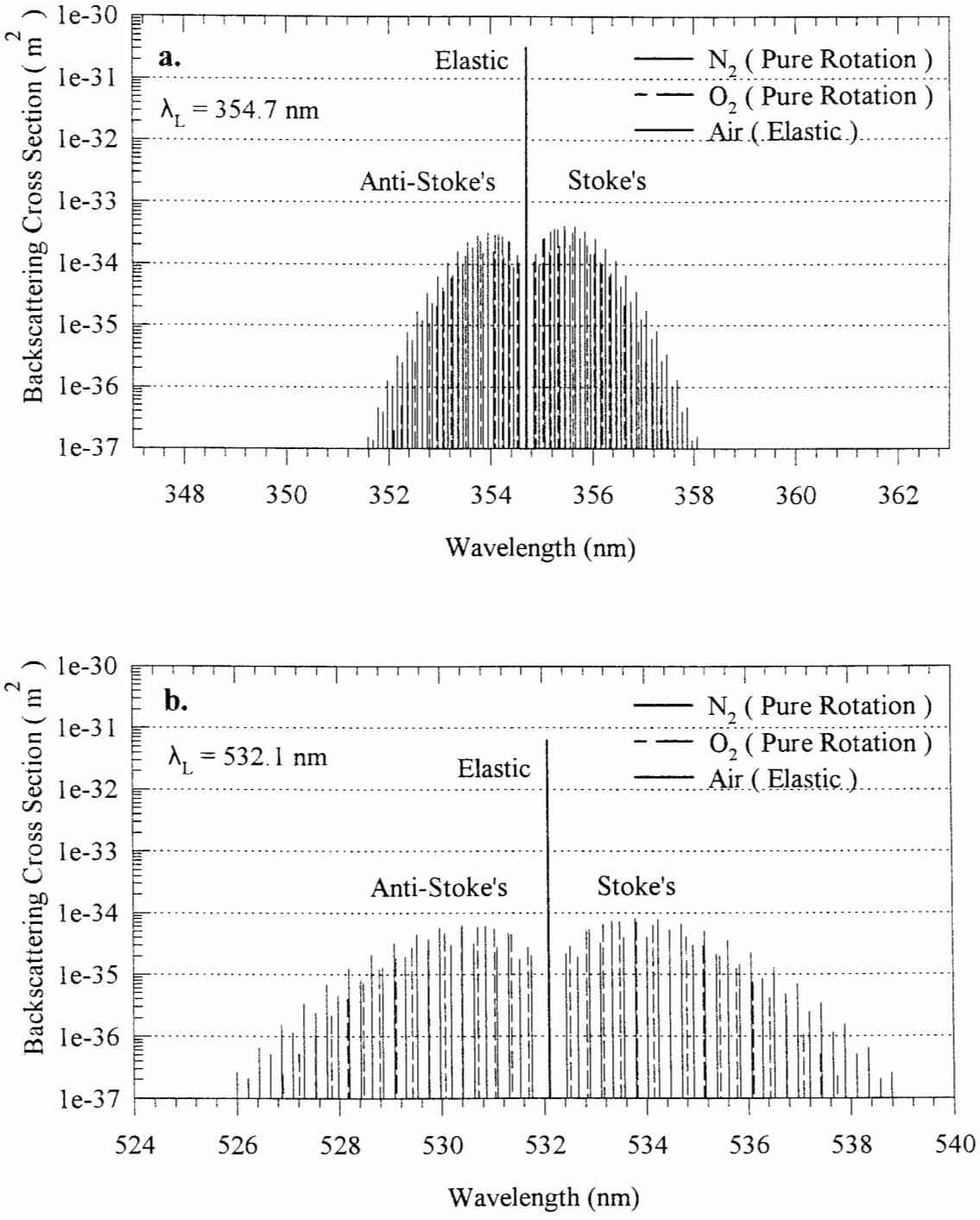

Figure 4.2. Calculated quantum rotational line intensities for N_2 and O_2 at 354.7 nm central line position (**a**) and at 532.1 nm central line position (**b**) at 310 K, along with the elastic backscatter cross section of air. Rotational intensities include species' fraction of air.

of the Doppler shape can be shown to be,

$$\Delta\omega = \left[\frac{2kT\omega_o^2}{mc^2}\right]^{1/2} (ln2)^{1/2} \qquad 4.3$$

where T is temperature, m is the mass of the molecule, and ω_0 is the line position being broadened.

The broadening effects mentioned above can be modeled by convolving the Gaussian and Lorentzian profiles to obtain the Voigt profile, which is represented as,

$$V(u) = \frac{a}{\beta\pi^{3/2}}\int_{-\infty}^{\infty}\frac{e^{-y^2}dy}{(u-y)^2+a^2} \qquad 4.4$$

Finally, each of the lines can be broadened because of the fact that the laser has a finite spectral width. This width equates to the molecules being excited by a range of frequencies. Thus a larger frequency width of the laser will contribute to a larger rotational quantum line width. The broadening effect is proportional to the spectral width. The width of the Nd:YAG laser at 532.1 nm used in the experiments is 2.8×10^{-2} nm (30 GHz).

Since they have been shown to be less than five orders of magnitude less than the expected filter bandwidths, the broadening effects due to Doppler, radiative lifetime, and laser width can be neglected from the model. Also, Nedeljkovic et al. [1993] have shown that the effects of pressure broadening over the range of pressures typical of the atmosphere, can be neglected in the error calculations.

A limited optimization was performed by Cohen et al. [1976] assuming 1 nm FWHM filter bandwidths, a single average temperature for the atmosphere, and a laser output frequency of 694.3 nm. In the model developed in this thesis, his method was broadened to include all ranges of filter bandwidths and to include temperature ranges instead of a single temperature, because there is an ideal filter configuration for every temperature. For this reason, temperature errors calculated in the model for each filter

choice were integrated over a range of temperatures. These temperature ranges are taken from the US Standard Atmosphere 1976 model, in three regions of the atmosphere; entire troposphere (200K - 320K), cirrus cloud region (200K - 280K), and the boundary layer (240K - 320K).

A program was written to calculate the optimum filter configurations based on filter bandwidth, center wavelength, and minimization of temperature error over a temperature range. The filter functions used in the model were calculated with a modified Gausian function given by,

$$L_{MG}(\omega) = \exp\left[-\left[\frac{(\omega - \omega_o)^2 * \ln 2}{\Delta\omega^2 * \ln 2^{(1-1/x)}}\right]^x\right] \qquad 4.5$$

where ω is the wave number, ω_o is the center wave number, and x is a modifier set equal to 1.4. This function best fit the double filter functions which were already installed in the LAMP lidar.

4.1 Modeled Rotational Raman Lidar Temperature Statistics

The statistics used in the optimization algorithm are based solely on the number of counts received in both the signal and the background. As was mentioned previously, the data needed to obtain temperature is the ratio of the lidar signals from two filter bandwidths in the rotational spectrum minus any background noise,

$$R = \frac{N2}{N1} = \frac{C2 - B2}{C1 - B1} \qquad 4.6$$

where N's are the rotational signal from each of the bandwidths, C's are the received signals from the lidar, and B's are the measured backgrounds. If background is included in the model (daytime measurements), then it must be added to the signal in order to calculate the correct statistical error. In general, background can be sampled n number of

times more than the signal. This leads to an n factor reduction of the standard deviation of the background average. The resulting ratio fractional error is given by,

$$\frac{\sigma_R}{R} = \left[\frac{N1 + B1 + \frac{B1}{n}}{N1^2} + \frac{N2 + B2 + \frac{B2}{n}}{N2^2} \right]^{1/2} \qquad 4.7$$

The number of lidar counts were calculated using Equation 2.1. The background was calculated using system parameters and values from the LOWTRAN model to calculate the solar radiance given a particular solar zenith angle. The corresponding temperature fractional error is given by,

$$\frac{\sigma_T}{T} = \frac{R(\sigma_R/R)}{T(dR/dT)} \qquad 4.8$$

where,

$$\frac{dR}{dT} = R\left| \frac{1}{N1}\frac{dN1}{dT} - \frac{1}{N2}\frac{dN2}{dT} \right| \qquad 4.9$$

4.2 Night-time Instrument Optimization

If it is assumed that the background is negligible at night, all system and atmospheric characteristics drop out of the statistics in the form of a constant. The computer code, written in Microsoft Fortran, used for calculating the optimal filter settings for lidar night-time operation is given in Appendix F. Figure 4.3 shows the results of the model for the temperature range of the entire troposphere (200 K - 320 K). The top graph gives the inverse of the relative integrated temperature fractional error that would be obtained given the corresponding filter center wavelengths. The values corresponding to the center wavelengths in the figure are the best values for all choices of filter bandwidths. The optimal filter bandwidths for the center wavelengths in the top figure are given in the bottom two graphs.

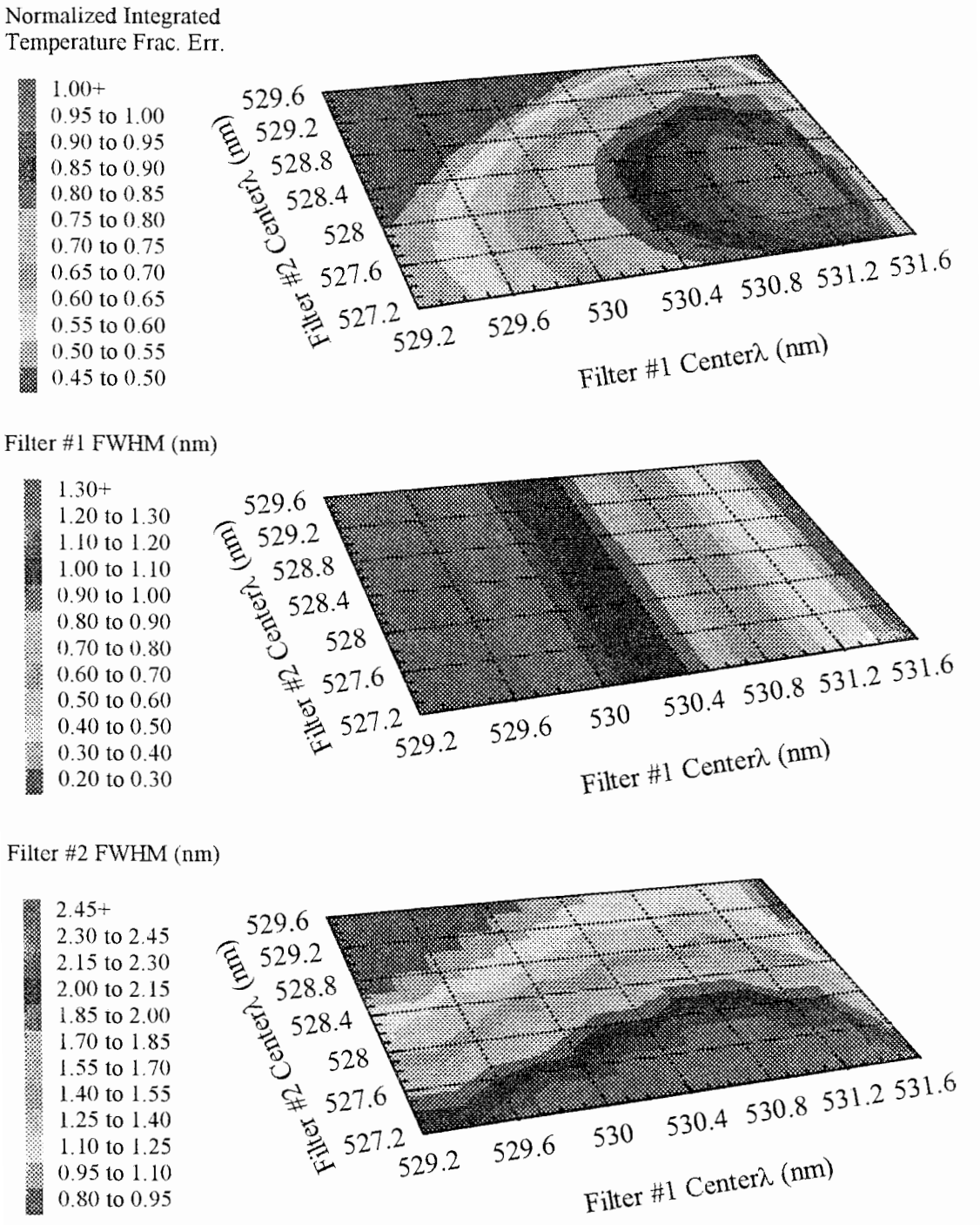

Figure 4.3. Optimum Filter Configurations for Rotational Raman Temperature Measurements with Primary Laser Wavelength of 532.1 nm over the Temperature Range of 200K - 320K assuming Zero Background Noise

Since the optimal filter settings correspond to a specific temperature range, several ranges were chosen for optimization. The results are given in Table 4.1.

Table 4.1. Ideal optical filter settings for various temperature ranges in the atmosphere

Temperature Range	Optimum Filter Settings		
		Filter #1	Filter #2
200 K - 270 K (cirrus cloud region)	Center λ	30.069 cm^{-1}	133.388 cm^{-1}
	FWHM	17.716 cm^{-1}	71.645 cm^{-1}
200 K - 320 K (troposphere)	Center λ	30.069 cm^{-1}	140.555 cm^{-1}
	FWHM	17.716 cm^{-1}	75.284 cm^{-1}
240 K - 320 K (boundary layer)	Center λ	33.613 cm^{-1}	147.728 cm^{-1}
	FWHM	19.495 cm^{-1}	78.929 cm^{-1}

The values in Table 4.1 are relative to the laser line and are thus given in wave numbers so that they can be translated to any wavelength. The corresponding filter positions and widths for the 532 nm and 355 nm wavelengths are given in Table 4.2. These tables shows that the ideal optical filter positions do not vary much from the three different temperature ranges. Table 4.3 gives the percent improvement of using the tropospheric filter choices at various temperatures over those of the other temperature region filter choices.

Table 4.2. Ideal optical filter settings with a laser wavelength of 532 nm and 355 nm for various temperature ranges in the atmosphere

Temperature Range		Optimum Filter Settings			
		532.1 nm Laser		354.7 nm laser	
		Filter #1 (nm)	Filter #2 (nm)	Filter #1 (nm)	Filter #2 (nm)
200 K - 270 K (cirrus cloud region)	Center λ	531.25	528.35	354.32	353.03
	FWHM	0.50	2.00	0.22	0.89
200 K - 320 K (troposphere)	Center λ	531.25	528.15	354.32	352.94
	FWHM	0.50	2.01	0.22	0.93
240 K - 320 K (boundary layer)	Center λ	531.15	527.95	354.28	352.85
	FWHM	0.55	2.20	0.24	0.98

Table 4.3. Comparison of the ideal filter configurations for the three temperature regions at various temperatures.

Measured Temperature	**Percent improvement in temperature fractional error in going from the below listed filter configurations to the optimal filter configuration for the troposphere temperature range.**	
	Boundary Layer Region	**Cirrus Cloud Region**
200 K	5 %	(-3 %)
240K	2 %	0 %
280K	(-1 %)	2 %
320 K	(-3 %)	3 %

Table 4.3 shows that the differences in the temperature fractional error are minimal over the entire temperature range. Thus using the tropospheric filter choice is the probably the

best overall choice.

Since the rotational spectrum is narrower at lower incident laser wavelengths, and thus the filters are closer to the elastic line, it becomes more difficult to block out the center wavelength. Tables 4.4, 4.5, and 4.6 explore how moving the ideal filter configurations affects the overall performance of taking temperature measurements. In these tables, the position of the filter closest to the elastic line was moved further into the spectrum and the corresponding optimized filter settings were calculated. The increase in the integrated temperature fractional error from that of the original configuration was calculated.

Table 4.4. Calculation of the decrease in optimization for the cirrus cloud temperature region by moving the filters further away from the elastic line.

Cirrus Cloud Temperature Region (200 K - 270 K)				
Filter #1	New Ideal Filter Parameters			
	Filter #1	Filter #2		Percent down from Ideal
Center λ	FWHM	Center λ	FWHM	
531.25	0.50	528.35	2.00	0 %
531.00	0.65	528.35	2.00	3 %
530.70	0.80	528.30	1.95	10 %
530.40	1.00	528.20	1.90	19 %
530.10	1.10	528.10	1.85	29 %

Table 4.5. Calculation of the decrease in optimization for the tropospheric temperature region by moving the moving the filters further away from the elastic line.

Troposphere Temperature Region (200 K - 320 K)				
Filter #1	New Ideal Filter Parameters			
	Filter #1	Filter #2		Percent down from Ideal
Center λ	FWHM	Center λ	FWHM	
531.25	0.50	528.15	2.10	0 %
531.00	0.60	528.15	2.10	2 %
530.70	0.80	528.10	2.10	8 %
530.40	0.95	528.05	2.05	17 %
530.10	1.10	528.00	1.90	26 %

Table 4.6. Calculation of the decrease in optimization for the boundary layer temperature region by moving the moving the filters further away from the elastic line.

Boundary Layer Temperature Region (240 K - 320 K)				
Filter #1	New Ideal Filter Parameters			
	Filter #1	Filter #2		Percent down from Ideal
Center λ	FWHM	Center λ	FWHM	
531.15	0.55	527.95	2.20	0 %
531.00	0.60	527.95	2.20	2 %
530.70	0.80	527.95	2.15	7 %
530.40	0.95	527.90	2.10	15 %
530.10	1.15	527.80	2.05	23 %

The loss in statistics from the ideal setting, can generally be made up for by using high powered lasers and medium sized telescopes. For the LAMP and LAPS lidars, the filter

configurations are set at positions that are at least 50 % below the ideal settings given in Table 4.1. However, because of the lasers and telescopes used, the backscattered signals for temperature measurements still have to be attenuated by an order of magnitude in LAMP lidar in order that the data system is not forced into non linearity. Because it incorporates a faster data system, LAPS only has to attenuate the signals by half.

3.4 Daytime Optimization Considerations

Because daytime background can be larger than the received lidar signal, the general optimization formula used for night-time operation could not be used to determine the optical configuration in the daytime without considering system parameters and atmospheric characteristics. The theoretical background, calculated from the radiance results obtained from the LOWTRAN model is given by [Machuga,1993],

$$N_{Back} = \frac{A_o \xi_{opt} T_D 2\Delta z}{c} \int_{\lambda_2}^{\lambda_1} \frac{L(\lambda) filt(\lambda)}{E_p(\lambda)} \, d\lambda \qquad 4.10$$

where,

$$T_D = \pi \sin^2\left(\frac{FS}{2FL}\right) \qquad 4.11$$

and,

$L(\lambda)$: radiance
$E_p(\lambda)$: energy of a photon at λ
FS : field stop diameter
FL : focal length of the telescope

Since it is possible to obtain data when the signal to noise ratio (S/N) is much smaller than one, the limitation to daytime measurements is the speed of the detectors and data collection system. Large number of counts hitting the detector system cause it to perform non-linearly. Thus, if the background is too large compared to the signal then measurements cannot be made.

If the optimization is performed at a particular altitude, it can be seen from

Equations 4.10 and 2.1 that the system parameters which can change the signal to noise ratio are the laser energy and wavelength, the ratio of the telescope field stop to focal length, and the filter bandwidths,

$$\frac{N_{laser}(z)}{N_{background}} = \frac{\frac{E_L}{E_{p_L}} \frac{1}{4\pi z^2} T_{atm}^2(z) F(J,T)}{\frac{2T_D}{c} \int_{\lambda_1}^{\lambda_2} \frac{L(\lambda) filt(\lambda)}{E_p(\lambda)} d\lambda} \qquad 4.12$$

When operating with high powered lasers it is much more effective, in both cost and technical simplicity, to design a certain telescope than it is to try and build a more powerful laser. Simply narrowing the field stop or obtaining a telescope with a longer focal length can reduce the background intensity much more quickly than increasing laser power.

The narrowing of the filter bandwidths is essential for reducing the day-sky background. The degree of narrowing depends on the operating wavelength of the laser. The quantum lines are 55.4 % closer together at 355 nm than at 532 nm. The smaller the wavelength, the closer the rotational lines, the larger the number of quantum lines captured by the filter per filter bandwidth, and thus, the greater the signal to noise ratio. Also, going to shorter wavelengths increases the received signal by $1/\lambda^4$.

If it is desired to center narrow band filters on single quantum lines, it was determined that it was much better to center narrow band filters (< 0.2 nm FWHM filters at 532 nm laser wavelength) over the N_2 rotational quantum lines than the O_2 quantum lines in order to obtain the greatest signal to noise ratio. In this case, the ideal quantum lines to center on are located at 11.94 cm^{-1} and 107.32 cm^{-1}

It is impossible to come up with one ideal filter configuration for daytime operation without prior knowledge of system characteristics and atmospheric conditions. For this reason it is left to the reader to determine their own filter choices based on trade-offs of system design.

Chapter 5

REGRESSION TECHNIQUES FOR PROCESSING LIDAR TEMPERATURE DATA

To properly calculate a temperature profile of the atmosphere from the ratio of two rotational Raman lidar signals, a temperature versus ratio curve for the lidar system must be determined that expresses such a relationship. The theoretical expression can be calculated using Equation 2.5 and is shown graphically in Figure 2.2. However, due to the difficulty in measuring parameters, such as, optical efficiencies, quantum efficiencies of photomultiplier tubes, and physical molecular constants, which are critical to its calculation, an accurate theoretical temperature versus ratio curve is usually not practical using Equation 2.5. Vaughan et al. [1993] attempted to do this by designing a receiver and detector system that was capable of using the theoretical temperature versus ratio curve directly. They used a monochromator to determine the spectral curves of their optical systems. The final result was a temperature error of ~ 2.5 K. Of that error, they calculated that at least 1 K was due to uncertainties in the molecular parameters. However, they also suggested that further system modifications could improve the overall accuracy.

Because it is very difficult to calculate an accurate theoretical temperature versus ratio curve for a specific lidar system, another method was needed. Nedeljkovic et al. [1993] proposed that by applying a least squares fit of lidar rotational ratio data to balloon temperature data, one could obtain a temperature versus ratio curve that could be used to convert future lidar profiles to temperature. Figure 5.1 demonstrates this procedure using data obtained from the LAMP lidar with the assumption that a second order polynomial model relates the balloon temperatures (T) to the lidar ratios (R), and is given by,

$$T = C_0 + C_1 R + C_2 R^2 \qquad 5.1$$

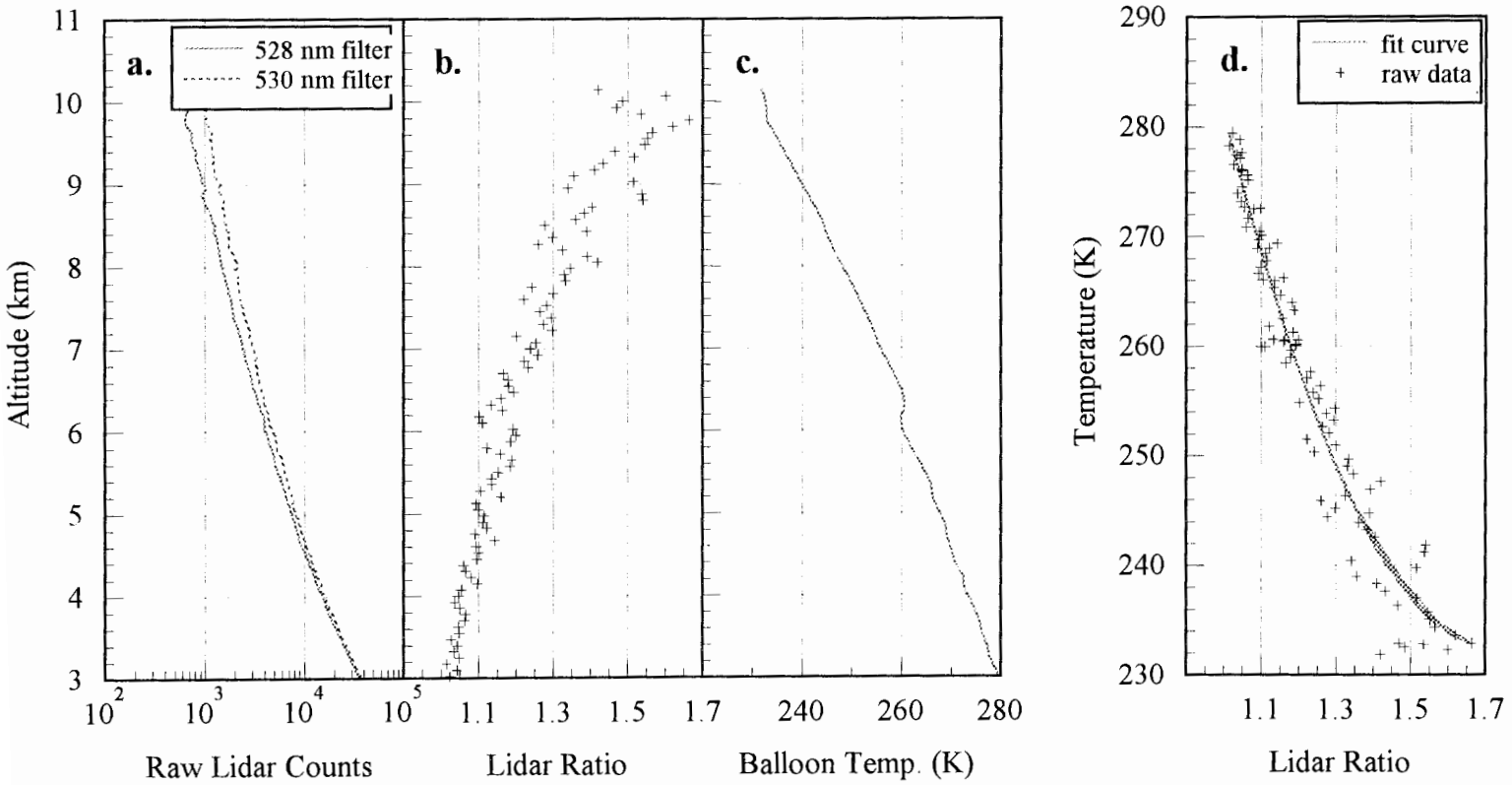

Figure 5.1. Procedure for obtaining a temperature versus ratio curve based on the regression of a second order polynomial of lidar rotational ratios to balloon temperatures. Lidar data was collected on 5/22/94 between 04:21 - 04:51 GMT, and balloon data was obtained from a launch at 04:35 GMT. (a.) Raw rotational lidar returns. (b.) Ratio of the 530 nm filter return to the 528 nm filter return. (c.) Balloon temperature profile. (d.) Raw lidar ratios to balloon temperatures and the resulting calibration curve.

Even though it can produce an adequate temperature versus ratio curve, their technique does not provide any information about the system itself. Another possible way to perform the regression would be to utilize the theoretical temperature versus curve and fit it to the lidar and balloon data profiles. The model would be based on system and rotational theory to obtain a corrected temperature versus ratio curve. In this way information about the system might be learned from the resulting coefficients.

Applying the above regression techniques assumes that the lidar system does not have any system drift, that the balloon travels in a vertical direction above the lidar system, and that the atmosphere does not change during the measurement period. The effects of system drift on the theoretical calibration curve has been explored by Nedeljkovic et al. [1993]. They calculated how changes in the thermal stability of the optics, laser line width, and laser position could change the temperature versus ratio curve. It was found that a stability of approximately 0.2 K is needed when using dielectric filters. Using metal oxide filters, which have a thermal coefficient which is an order of magnitude less than the dielectric filters, and which have been incorporated into the LAPS lidar, allows one to relax the thermal control by an order of magnitude. Nedeljkovic also determined that the laser line width had to be stable and narrow (single mode) so that the rotational spectrum in the filter bandpasses would not shift as the laser line position shifted.

One other system factor not discussed by Nedeljkovic was drift due to the thermal expansion of the system itself. Thermal expansion can cause optical paths to change in both length and direction. Optical path differences may cause the amount of light reaching the detectors to change significantly with respect to each other. This will then effect the ratio of the two lidar signals, giving data which cannot be meaningfully related back to the temperature versus ratio curve. To determine the amount of error thermal expansion has on the calibration curve one would need to calculate a number of calibration curves from a number of balloon and lidar profiles over a large atmospheric temperature change. This particular experiment was not performed on the LAMP and LAPS lidars for this thesis because of a lack of long term data under a constant system configuration. It is therefore

left for future work by others. However, Section 5.4 does show the drift for two all night data collection periods. In order for the true drift to be calculated, a number of these types of runs need to be measured.

5.1 Balloon Data and its Validity

Because it is necessary to calibrate the lidar temperature data to balloons, possible errors in balloon measurements must to be considered. With an understanding of these errors, a covariance matrix of the balloon data can be determined. This covariance matrix can then be used to develop the corresponding covariance matrix for the fitted lidar temperature profile (see Section 6.2).

The number of errors in the balloon temperature profiles can be potentially numerous. These errors include, instrument lag time, radiation sources, balloon flight path, and the manufacturer's specifications of the sensor. Lag time errors occur because the sensor can not respond fast enough to the temperature variations between successive balloon measurements. The temperature readings affected by lag time will either be too hot or too cold depending on whether or not the atmospheric thermal gradient is decreasing or increasing. Badgely (1957) showed that the lag time errors may be as high as 0.3 °C. Because the error caused by it is unknown and small in most cases, the effects of the lag rate on the balloon covariance matrix will be assumed to equal zero.

It has been pointed out that a potentially large source of error in balloon temperature measurements is due to radiative sources (Schmidlin, 1994). These radiative sources tend to increase the temperature of the sensor. However, the errors associated with the radiative sources have been shown to be most prevalent above the troposphere. Since the lidar data which is to be fitted with the balloon data in this thesis has been measured below the tropopause, the errors associated with radiative sources will be neglected.

The flight path of the balloon can also add to the errors of the balloon data. The balloon data has a tendency to follow the path of least resistance which is along wind

currents. The wind currents can take the balloon many kilometers away from the vertical before it reaches ten kilometers in altitude. The flight path trajectories of the balloon which are to be used in Sections 5.2, 5.3, and 5.4 are given in Figure 5.2 for 22 May 1994, and Figure 5.3 for 13 March 1995. Since it no longer takes measurements at the zenith, the balloon may no longer be an accurate measurement of the vertical temperature profile. The possible temperature errors associated with the balloon flight path are difficult to determine, and thus, are assumed zero for the calculation of the balloon covariance matrix.

Furthermore, for the purpose of the following calculations, the balloon data points are considered to be independent of each other, thus reducing the covariance matrix to a diagonal matrix consisting of only the variances of the data points, themselves. The variances at each point are then all equal, given by the square of the standard deviation of the balloons accuracy given on the manufacturer's specification sheet. This was given in Table 1.2 as $\sigma_b^2 = 0.04$ for the temperature range of +60 °C to -90 °C . The final balloon covariance matrix is then,

$$\Gamma_{balloon} = \boldsymbol{I}\vec{\sigma}_b^{\,2} \qquad 5.2$$

where **I** is the identity matrix.

Since the balloon data and the lidar data do not match in their altitude assignments, the balloon data had to be converted to the lidar altitudes. This can be done without adding any error into the balloon profile because there are a number of balloon data points within each lidar altitude range. The conversion was performed using a simple linear interpolation.

5.2 Linear Regression

When the relationship of the fit is based on sums of polynomials or exponentials, simple matrix algebra can be used to perform the regression analysis. For the case of polynomials, the relationship between the lidar (R) and balloon (T) data sets is,

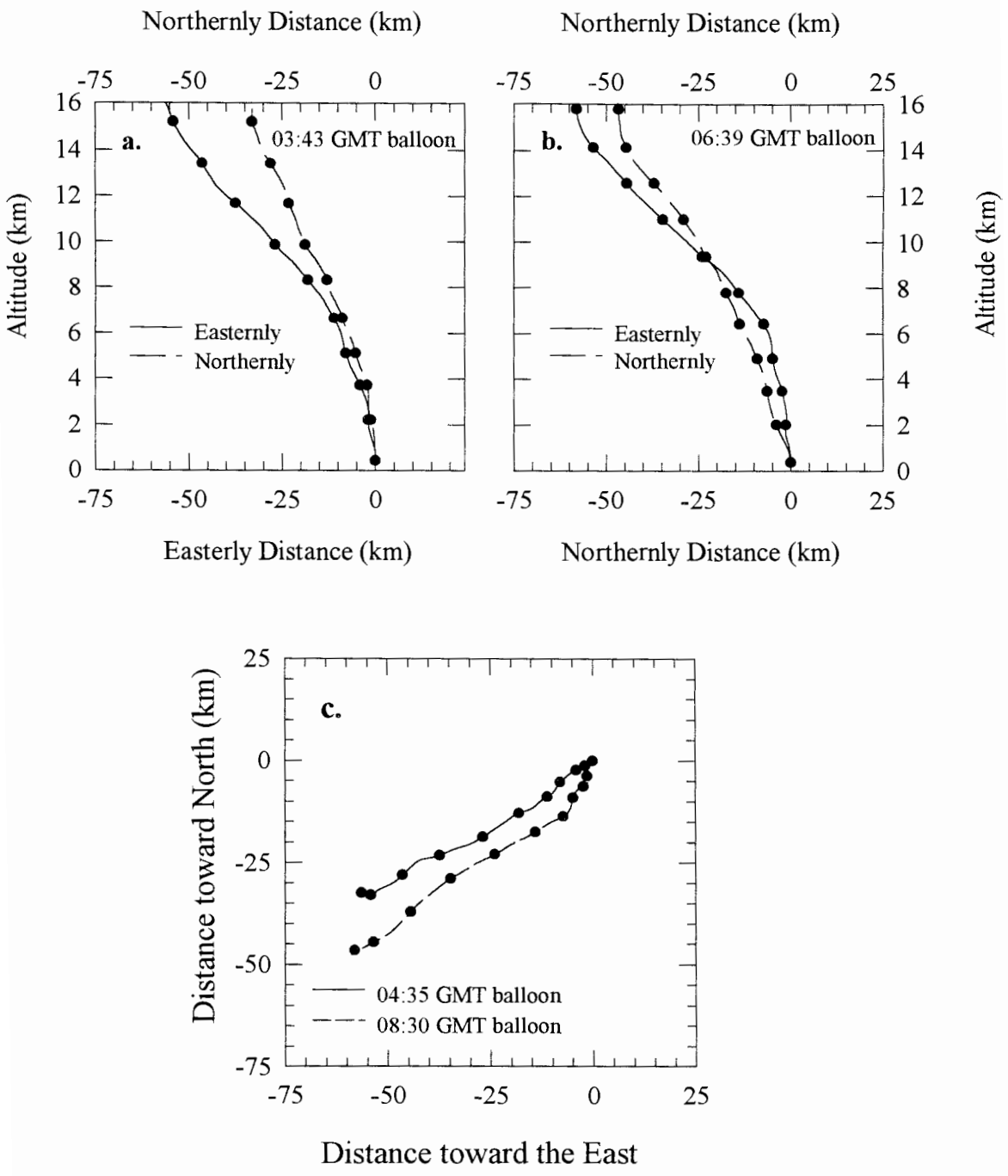

Figure 5.2. Flight path of radiosonde balloons launched on 05/22/94 at (a.) 03:43 GMT and (b.) 06:39 GMT. (c.) Topographical view of the flight paths from the two balloons to show the distance from the vertical while lidar measurements were being taken. Solid dots indicate 10 minute time lapse intervals in all plots.

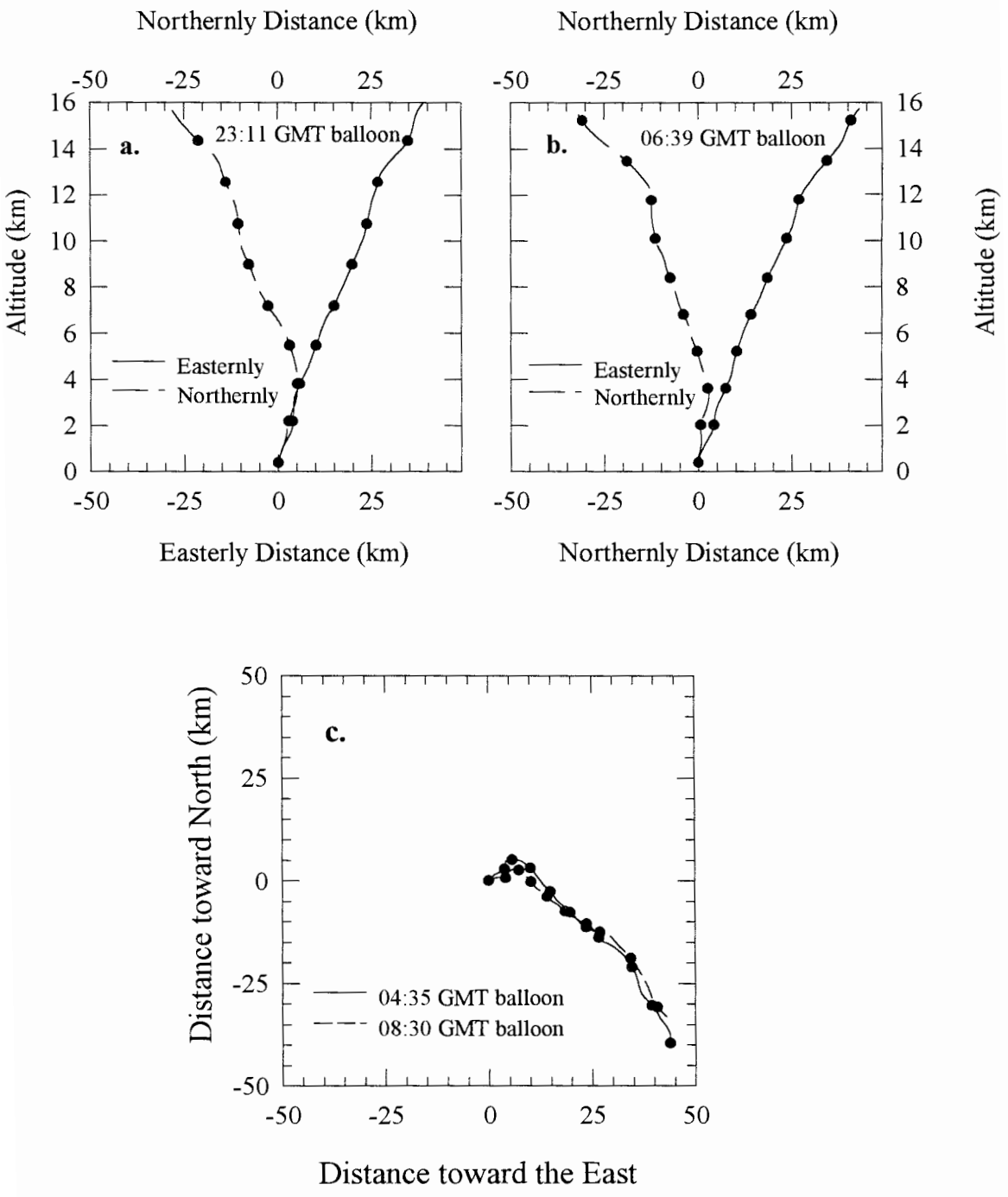

Figure 5.3. Flight path of radiosonde balloons launched on 03/13/95 at (a.) 04:35 GMT and (b.) 08:30 GMT. (c.) Topographical view of the flight paths from the two balloons to show the distance from the vertical while lidar measurements were being taken. Solid dots indicate 10 minute time lapse intervals in all plots.

$$T_i = C_0 + C_1 R_i + C_2 R_i^2 + \ldots + + C_N R_i^N \qquad 5.3$$

or for all data points,

$$\begin{bmatrix} T_1 \\ T_2 \\ \vdots \\ T_M \end{bmatrix} = \begin{bmatrix} 1 & R_1 & R_1^2 & \ldots & R_1^N \\ 1 & R_2 & R_2^2 & \ldots & R_2^N \\ \vdots & \vdots & \vdots & & \vdots \\ 1 & R_M & R_M^2 & \ldots & R_M^N \end{bmatrix} \begin{bmatrix} C_1 \\ C_2 \\ \vdots \\ C_M \end{bmatrix} \qquad 5.4$$

The object of the regression analysis is to determine the coefficients which minimize the mean squared error between the calculated and measured profiles and is given by,

$$\epsilon^2 = (\hat{\bar{T}} - \bar{T}) \cdot (\hat{\bar{T}} - \bar{T}) \qquad 5.5$$

where the dot indicate the dot product, and,

$$\hat{\bar{T}} = \boldsymbol{R}\bar{C} \qquad 5.6$$

Equation 5.5 becomes the measure of the goodness of the fit. Minimization requires that the derivative of Equation 5.5 be equal to zero,

$$\frac{\partial \epsilon^2}{\partial \bar{C}_k} = 0 = \epsilon_k \cdot (\boldsymbol{R}^* \boldsymbol{R} + (\boldsymbol{R}^* \boldsymbol{R})^*)\bar{C} - 2\epsilon_k \cdot \boldsymbol{R}^* \bar{T} \qquad 5.7$$

resulting in,

$$\bar{C} = (\boldsymbol{R}^* \boldsymbol{R})^{-1} \boldsymbol{R}^* \bar{T} \qquad 5.8$$

for the values of the coefficients in Equation 5.3

The determination of the coefficients in Equation 5.8 assumes that the quality of all the data points are equal. Though this may be true for the balloon data, it is not true for lidar data, because the lidar signal strength, and thus its standard deviation, is a function of altitude, telescope form factor, and atmospheric characteristics. Treating noisy data the same as more statistically sound data may induce errors in the calculated temperature versus ratio curve. This is because as the number of counts in the lidar data becomes small, the chances of collecting erroneous data points, and having them be significant to the total number of counts, increases. In non-weighted regression, the calculated temperature versus ratio curve will include these errors and thus be slightly different from the true curve. Avoiding these errors could be accomplished by applying a weighting factor to the calculation of the mean squared error given by Equation 5.5. This weighting factor is simply one over the variance of the lidar ratio (σ_R^2) at each successive data point in the profile and is given by,

$$\epsilon^2 = \frac{1}{\overline{\sigma_R^2}} \odot \left[(\boldsymbol{R}\overline{C} - \hat{\overline{T}}) \cdot (\boldsymbol{R}\overline{C} - \hat{\overline{T}}) \right] \qquad 5.9$$

where the $\odot$ notation is given by,

$$\overline{A} \odot \overline{B} = A_i B_i \qquad 5.10$$

Minimizing ϵ^2 in the weighted equation results in,

$$\overline{C} = (\boldsymbol{R}^* \boldsymbol{S} + (\boldsymbol{R}^* \boldsymbol{S})^*)^{-1} 2 \boldsymbol{S}^* \hat{\overline{T}} \qquad 5.11$$

where **S** is equal to,

$$\boldsymbol{S} = \frac{1}{\overline{\sigma_R^2}} \odot \boldsymbol{R} = \begin{bmatrix} \frac{1}{\sigma_{R_1}^2} & \frac{R_1}{\sigma_{R_1}^2} & \frac{R_1^2}{\sigma_{R_1}^2} & \cdots & \frac{R_1^N}{\sigma_{R_1}^2} \\ \frac{1}{\sigma_{R_2}^2} & \frac{R_2}{\sigma_{R_2}^2} & \frac{R_2^2}{\sigma_{R_2}^2} & \cdots & \frac{R_2^N}{\sigma_{R_2}^2} \\ \vdots & \vdots & \vdots & & \vdots \\ \frac{1}{\sigma_{R_M}^2} & \frac{R_M}{\sigma_{R_M}^2} & \frac{R_M^2}{\sigma_{R_M}^2} & \cdots & \frac{R_M^N}{\sigma_{R_M}^2} \end{bmatrix} \qquad 5.12$$

The determination of whether a weighted or a non-weighted regression technique should be used in either the general model fits or in the fits based on lidar system characteristics and rotational theory, requires the gathering of numerous data sets to make a statistical conclusion. This type of long term data base was not available for this thesis because the LAMP lidar has been under a number of system modifications over the past few years in order to make the system more stable. Modifications typically change the characteristics of the system and thus make comparisons of data difficult. However, two all night data sets were processed so that limited conclusions could be made about the different regression models. A secondary result of the data processing was an estimation of system drift over the course of 3 to 4 hours. This was accomplished by comparing the data profiles calculated from the regression of two data sets with successive balloon launches.

Each nightly data set consisted of a number of successive 30 minute lidar profiles and two balloon launches. The lidar profiles which were measured closest to the balloon launch times were used in the regression calculations. This was done to try and minimize any differences in the two measurements that might arise due to variability of the lower troposphere. The two lidar profiles chosen for each night were processed both as individual profiles and as a single stacked profile. This was done to see if a generated regression curve, calculated from all available data, could be used instead of a number of single profile curves taken during the course of a night.

Section 5.2.1 calculates the RMS difference of balloon profiles with calculated lidar temperatures for various general regression models which relate lidar ratios to balloon temperatures. Sections 5.2.2 calculates the same RMS values as Section 5.2.1 except that the ratio versus temperature curve for the LAMP lidar is calculated from rotational theory and system parameters.

5.2.1 Data Fit without using Theoretical Calculations or System Design Considerations

The general method in the literature to calculate a temperature versus ratio curve is to utilize either a linear polynomial or an exponential fit, of either first or second degree, of the balloon data to lidar ratio. For the LAMP lidar, this is only valid if the ratio of the two rotational signals is the 530 nm filter divided by the 528 nm filter. If the ratio is reversed, then the temperature versus ratio curve is no longer a polynomial, and other models must be chosen for the regression. Nedeljkovic et al. [1993] assumed that the signals received by the lidar were due to a single quantum line in each filter. Their relationship between the balloon temperature and the ratio of the lidar signals was calculated to be,

$$T = \frac{a}{\ln(b) + \ln(R)} \tag{5.13}$$

They further argued that because the theoretical curve behaves more like a second order polynomial than a linear curve, the relationship should be instead,

$$T = \frac{a}{\ln(b) + \ln(R)} + c\left(\frac{a}{\ln(b) + \ln(R)}\right)^2 + d \tag{5.14}$$

They found that Equation 5.14 provided a better fit by an order of magnitude. Their regression consisted of using an all night averaged lidar profile and a single balloon data profile. With a slight manipulation, Equation 5.14 can be reduced to a polynomial relationship as,

$$(T)^{-1} = C_o + C_1 \ln(R) + \ldots + C_N (\ln(R))^N \qquad 5.15$$

A comparison was made of polynomial fits up to fourth order, given by Equation 5.3, and exponential fits up to second order, given by Equation 5.15 for data taken on 22 May 1994 and 13 March 1995 to determine if any preliminary conclusions could be made as to what might be the best model for the regression. In each case both a weighted and a non-weighted regression was performed. The RMS difference between the calculated lidar temperature and the balloon profiles over all altitudes for the regression calculations are given in Table 5.1 for 5/22/94 and 3/13/95. The abbreviations for the models of the regression given in the first column of Table 5.1 are as follows,

$$\begin{aligned} TL1 &= C_0 + C_1 R \\ TL2 &= C_0 + C_1 R + C_2 R^2 \\ TL3 &= C_0 + C_1 R + C_2 R^2 + C_3 R^3 \\ TL4 &= C_0 + C_1 R + C_2 R^2 + C_3 R^3 + C_4 R^4 \\ TLE &= (C_0 + C_1 \ln(R))^{-1} \\ TLE2 &= (C_0 + C_1 \ln(R) + C_2 \ln(R)^2)^{-1} \end{aligned} \qquad 5.16$$

The tables give both the weighted and non-weighted fits for both the single lidar profiles and the combined lidar profile. Figures 5.4 and 5.5 show the resulting calibration curves from the calculation of the combined data sets for 5/22/94 for the weighted and non-weighted cases, respectively, and Figures 5.6 and 5.7 show the resulting curves for 3/13/95 for the weighted and non-weighted cases, respectively. In all cases shown, the non-weighted regression provided a smaller RMS difference between the calculated temperature profile and the balloon temperature profile than the weighted regression. There are three possible reasons for this result. First, the results may be just two rare cases which, in the midst of further measurements, may become insignificant. Secondly, if the data in the lower altitudes, which has good statistics, deviates at all from the balloon profile, which it sometimes does, then the weighting factor will cause the lidar profile to conform to the balloon temperatures when it should not. This will result in a bias at the higher altitudes because these data points will not be statistically strong enough to bring

Table 5.1. Comparison of weighted and non-weighted regressions of lidar rotational ratio data and balloon temperature data for various orders of polynomials and exponentials. Values indicate the RMS difference between the calculated lidar temperature profiles and the balloon temperature profiles. Data was collected on 5/22/94 and 3/13/95.

22 May 1994						
Regression Model	04:21 & 06:50 GMT Combined		04:21 GMT		06:50 GMT	
	Weighted	Non-Weighted	Weighted	Non-Weighted	Weighted	Non-Weighted
TL1	4.9 K	4.3 K	5.0 K	4.2 K	4.8 K	4.2 K
TL2	3.7 K	3.6 K	3.4 K	3.3 K	3.6 K	3.5 K
TL3	3.7 K	3.6 K	3.4 K	3.3 K	3.6 K	3.5 K
TL4	3.7 K	3.6 K	3.4 K	3.3 K	3.6 K	3.5 K
TLE	3.8 K	3.7 K	3.6 K	3.5 K	3.7 K	3.6 K
TLE2	3.8 K	3.6 K	3.6 K	3.3 K	3.7 K	3.6 K
13 March 1995						
	05:11 & 08:12 Combined		05:11 GMT		08:12 GMT	
TL1	4.9 K	4.4 K	5.7 K	5.0 K	4.0 K	3.6 K
TL2	4.5 K	4.0 K	5.1 K	4.7 K	3.4 K	3.2 K
TL3	4.5 K	4.0 K	5.1 K	4.7 K	3.4 K	3.2 K
TL4	4.4 K	4.0 K	5.1 K	4.6 K	3.4 K	3.2 K
TLE	4.7 K	4.3 K	5.5 K	4.9 K	3.7 K	3.4 K
TLE2	4.7 K	4.0 K	5.5 K	4.7 K	3.7 K	3.2 K

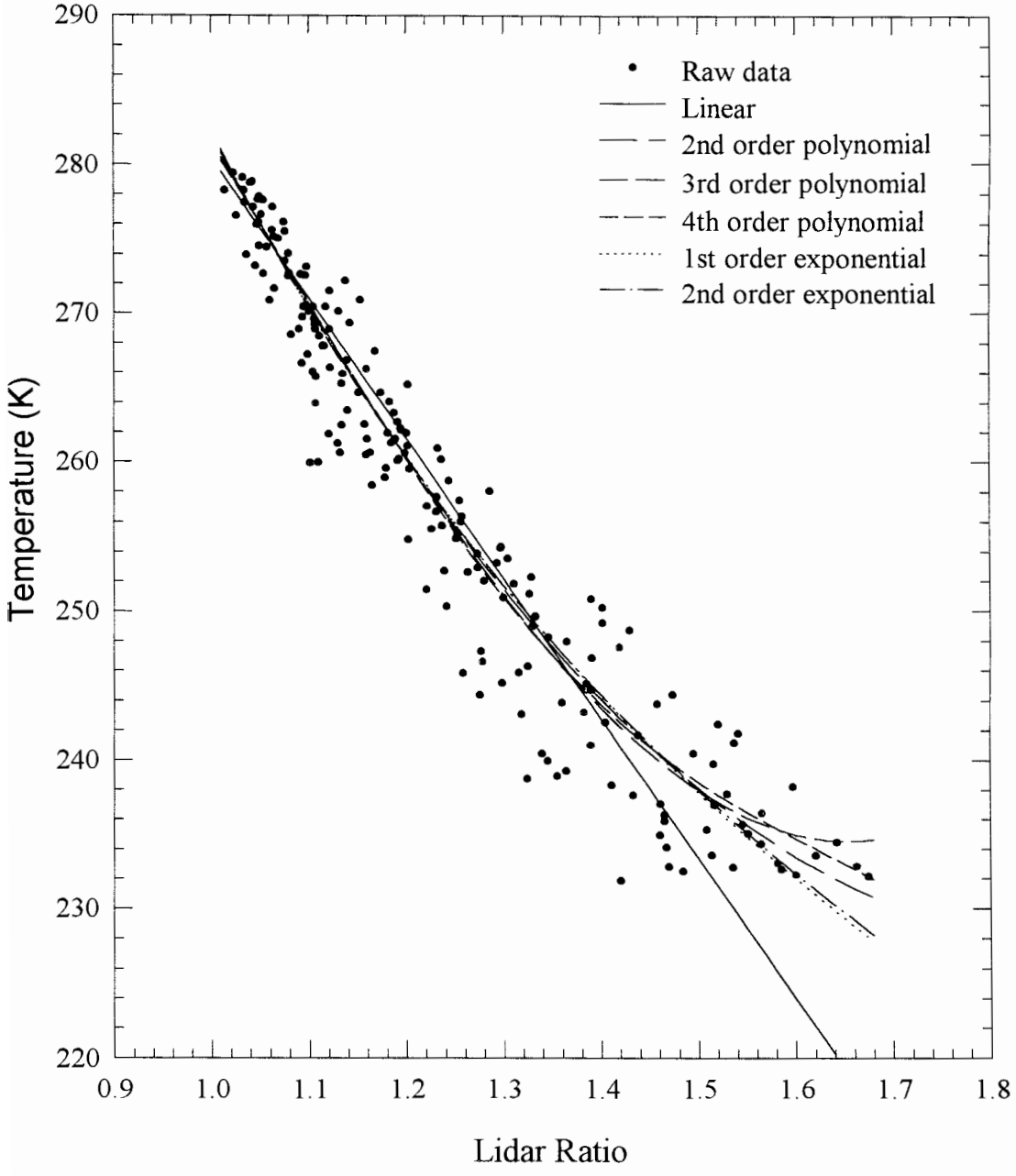

Figure 5.4. Comparison of the generated temperature versus ratio curves from raw lidar and balloon temperature data measured on 5/22/94. Regression calculations were weighted.

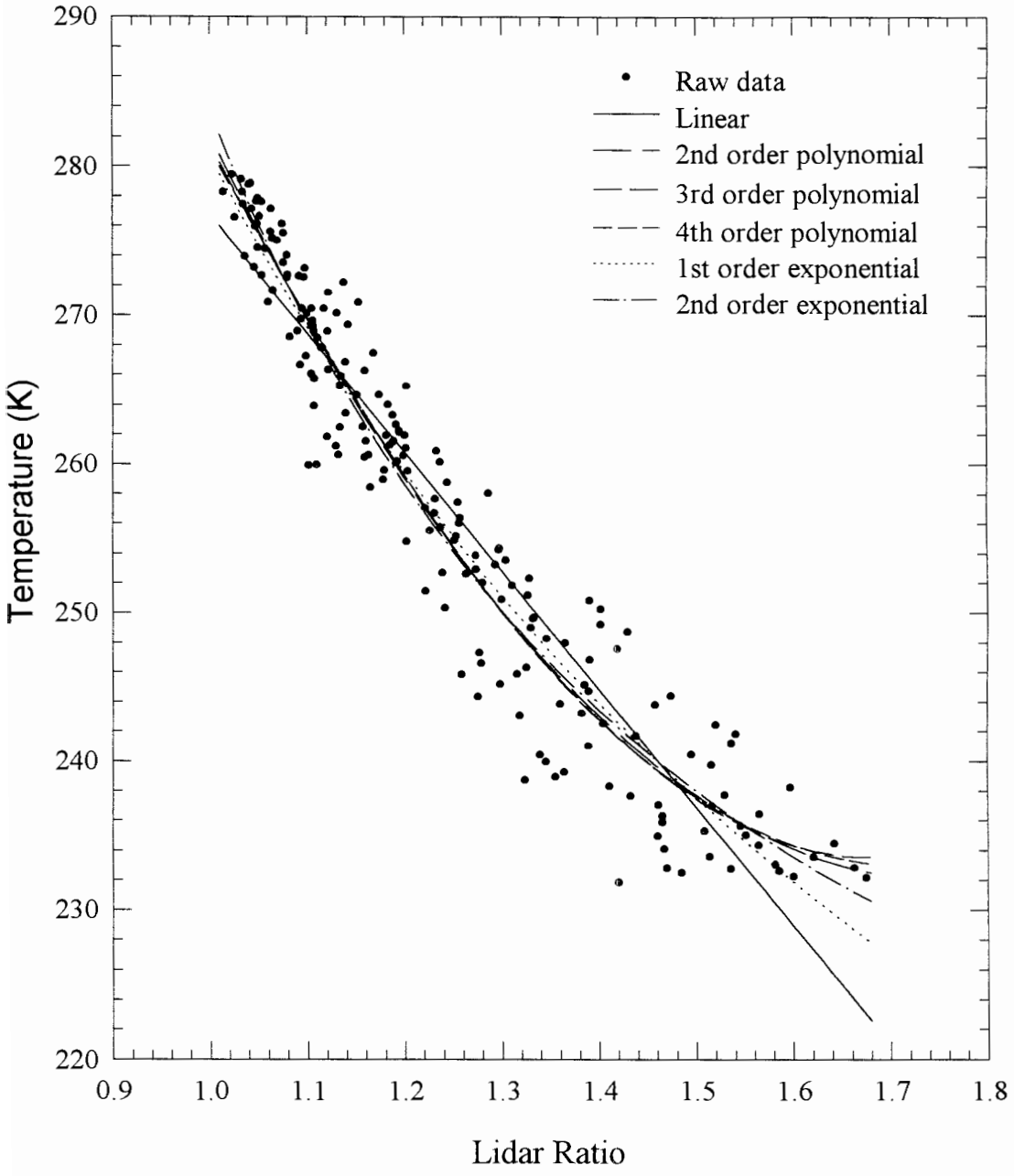

Figure 5.5. Comparison of the generated temperature versus ratio curves from raw lidar and balloon temperature data measured on 5/22/94. Regression calculations were not weighted.

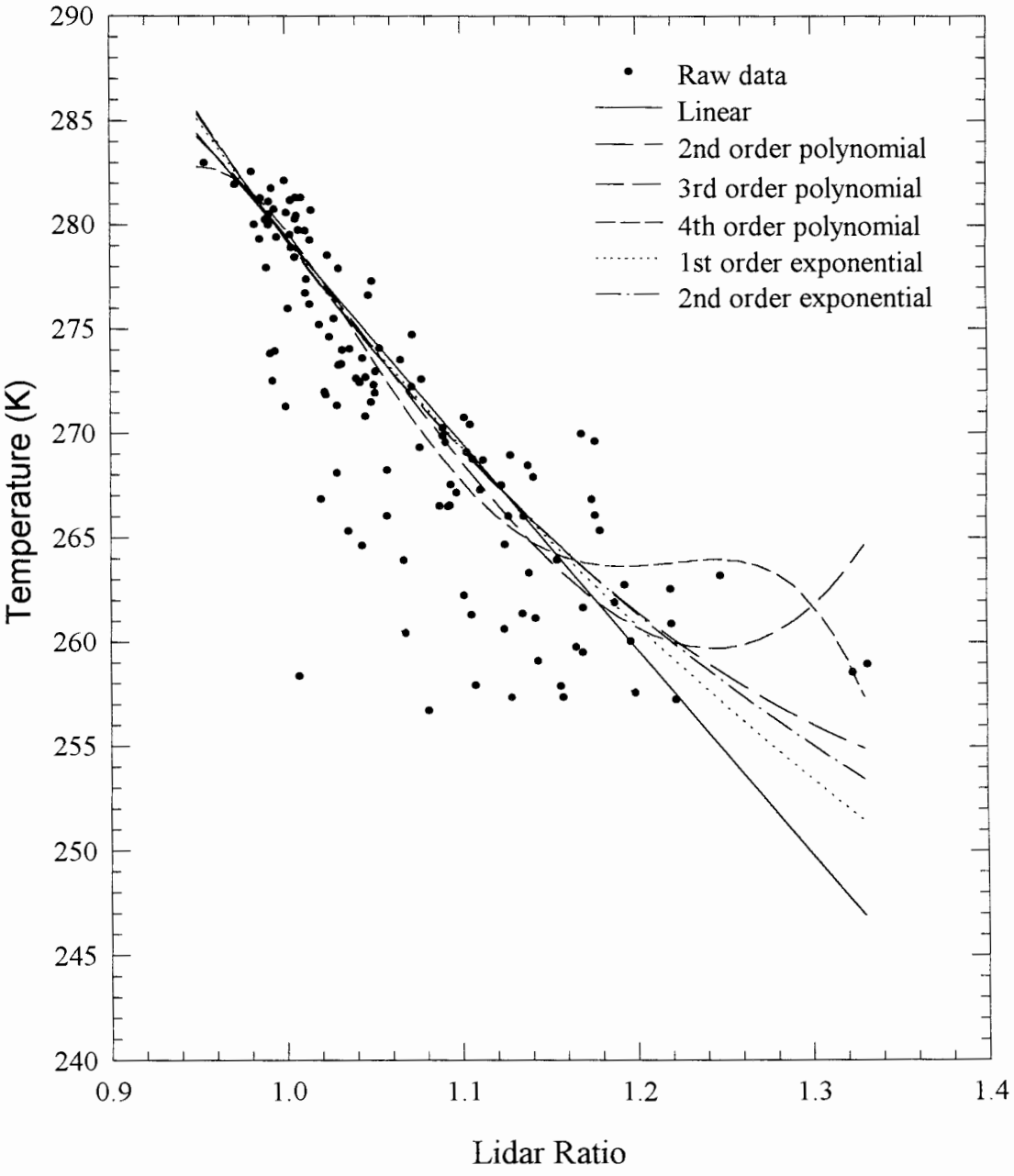

Figure 5.6. Comparison of the generated temperature versus ratio curves from raw lidar and balloon temperature data measured on 3/13/94. Regression calculations were weighted.

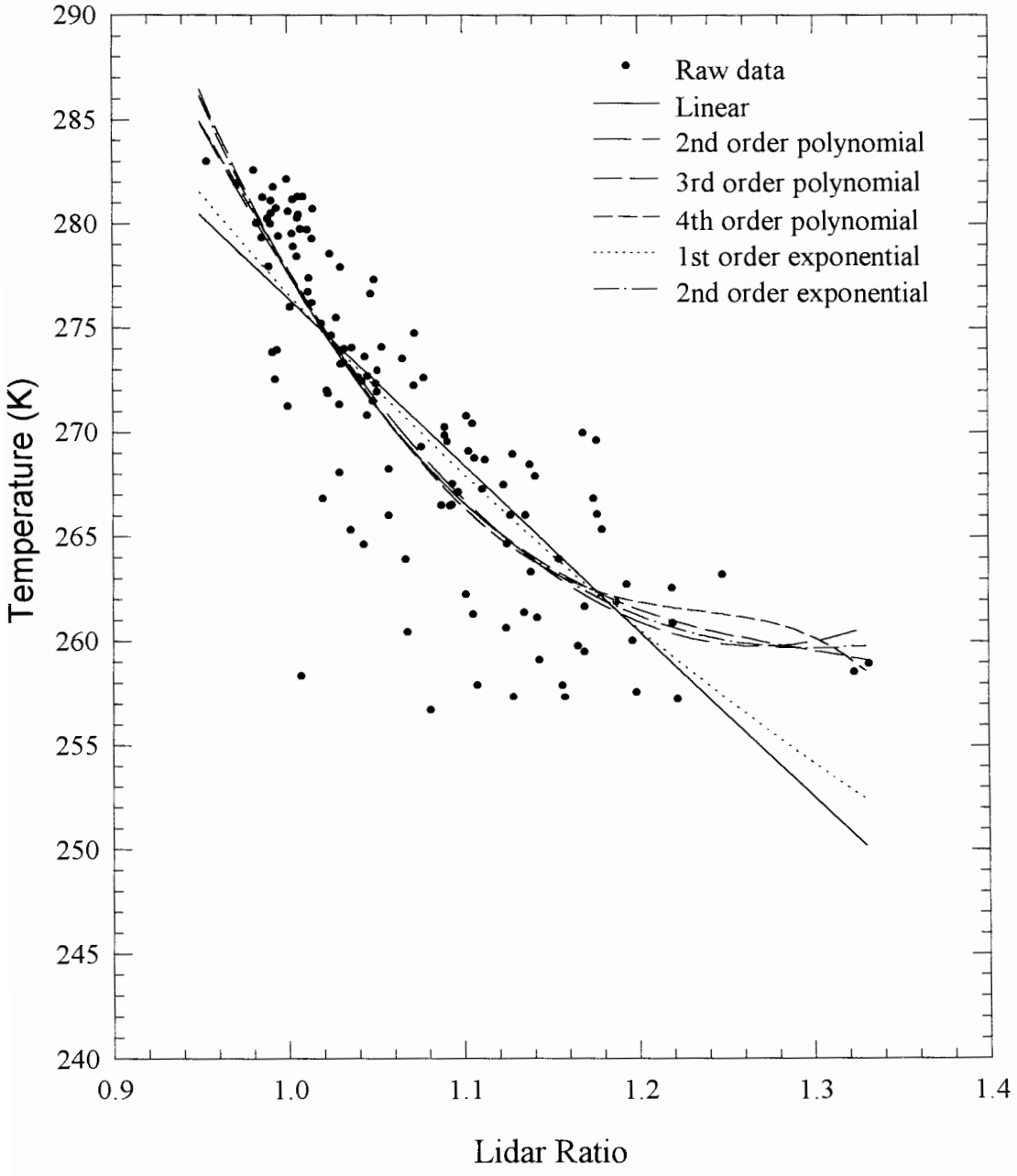

Figure 5.7. Comparison of the generated temperature versus ratio curves from raw lidar and balloon temperature data measured on 3/13/94. Regression calculations were not weighted.

the fitted curve back to its proper shape. Thirdly, because the dynamic range of the lidar counts is very large over the range of altitudes, the data found at these high altitudes will be trivialized compared to the data in the low altitudes even though they may still be statistically sound. For the same reason as was mentioned above, the regression will then tend to ignore these points and skew the calibration curve from its proper shape. However, it should be noted that if the lidar and the balloon do measure the same temperatures, then using a weighted regression would be better because it would not degrade the statistics of the lower altitudes.

From Table 5.1, all the polynomial fits above second order produced approximately the same RMS difference. For this reason, and by the fact that the third and fourth order polynomials might add oscillations into the regression curve which can not be described by theory, the second order polynomial appears to be the best choice of the general models. These oscillations can be clearly seen in the case of Figure 5.6. Data generated from the regions where the bow occurs are clearly not real.

Instead of the above general fits, another possible linear model for the regression analysis would be to use the theoretical calibration curve and the system design parameters to calculate the temperature versus ratio curve. By doing this, information about the system might be obtained if the fit is good enough. This type of model is explored in the following section.

5.2.2 Fit using Theoretical Calculations while Assuming Only Error due to Filter Gain

In order to take into account the theoretical temperature versus ratio curve in the regression analysis, the balloon temperature data must be converted into an expected lidar ratio based on this theoretical temperature versus ratio curve. This conversion can be accomplished with a linear extrapolation because the spacings between the temperature versus ratio data points are close enough to be considered linear with respect to each other.

The only model equation that could be used in a linear fit assumes that the only error in the temperature versus ratio curve was due to an inaccurate measurement of the two filter gains. Looking at Equation 2.5, if there is error in the filter gain, it can be factored out as a multiplicative constant. If both filters have this error then the ratio of the two produces a single coefficient allowing the model to be expressed as,

$$\overline{R}_{balloon} = C_0 \overline{R}_{lidar} \qquad 5.17$$

Using either Equation 5.8 or 5.11, the resulting temperature versus ratio curves for the two data sets can be calculated along with their respective RMS differences with the balloons, as was done in Section 5.2.1. The RMS differences for each data set are given in Table 5.2.

Table 5.2. RMS difference between the calculated lidar temperature profile and the balloon profile when using a regression model which consists of using the theoretical temperature versus ratio curve times a constant.

Date	Lidar Profiles (GMT)	Regression Type	
		Weighted	Non-weighted
05/22/94	04:21 and 06:50 combined	3.7 K	3.6 K
	04:21	3.4 K	3.3 K
	06:50	3.6 K	3.5 K
03/13/95	05:11 and 08:12 combined	4.5 K	4.0 K
	05:11	5.1 K	4.7 K
	08:12	3.4 K	3.2 K

A comparison of the results to the second order polynomial linear fit shows that they are equal for the two data sets presented. Thus, in these two cases, using either model is just as effective for the LAMP lidar. However, it is also important to note that unless a lidar system is perfectly stable, using the theoretical curve times a constant may not be effective

in describing the proper curve in the midst of this system drift. The reason for this is that thermal drifts in the detector box, changing optical path lengths due to mechanical expansion, or noise in the data units may cause the theoretical temperature versus ratio curve to distort to a point that it can no longer be used in the model given in Equation 5.17.

Because, the residual error in the above fit is still relatively high, there may be a possibility for improving the model. Since there are no other models which can be used in a linear regression, a non-linear technique must be explored. One model which has been applied to account for the error in the theoretical temperature versus ratio curve is the one that assumes that the subtraction of the background from the lidar signal and the filter gains are incorrect. This model is explored in Section 5.3.

5.3 Nonlinear Regression

The Newton-Raphson method is a non-linear technique which utilizes an iterative process to calculate the change in the coefficients which would produce the least amount of residual error. By adding the change in the coefficients to the previous set of coefficients, and determining if a noticeable reduction in the residual error occurs, one can approach a solution.

In the case where the error in the temperature versus ratio curve may be due solely to errors in the assumed filter gains and subtracted backgrounds, the fit model can be expressed using four coefficients,

$$\overline{R}_{balloon} = \frac{C_0\overline{R}_{lidar} + C_1}{C_2\overline{R}_{lidar} + C_3} \qquad 5.18$$

Calculating the coefficients in Equation 5.18 produced unreasonable values. Thus, the model indicated by Equation 5.18 was not a good model for the LAMP system.

5.4 Preliminary Calculations of LAMP System Drift

With the fact that the best regression model for the 5/22/94 and 3/13/95 data sets was a second order polynomial, an attempt to quantify the system drift of the LAMP lidar was made for both the weighted and non-weighted regressions. A calibration curve was calculated for each of the lidar profiles on a given night from its respective balloon profile. These temperature versus ratio curves were then used to calculate temperature profiles from both lidar ratio profiles, giving a total of 4 temperature data sets. RMS values of these resulting temperature profiles at each altitude were calculated for both nights. The RMS of the entire profiles were then calculated and are shown in Table 5.3. This approach provided a value of the drift in the calculated temperature versus ratio curve over 3 hours for the 5/22/94 data and 4 hours for the 3/13/95 data.

From the results of the two data sets, it appears as though the non-weighted regression provided temperature versus ratio curves which had less drift in them than the weighted regression. Also the drift for the 3/13/95 data was less than the 5/22/94 data by 23%. If it can be at all assumed that this is accurate in the midst of the limited data sets available, this was not at all unexpected because a number of steps were taken to improve the stability of the LAMP lidar during the lag time between the measurements. These steps included increasing the thermal stability of the detector box, stiffening the structure of the transmitter and receiver systems, and improving alignment techniques of the receiver, to name a few. In order to determine more accurately the drift in the system, more nights of data are required. This is suggested for future work for both the LAMP and LAPS systems.

Table 5.3. RMS difference between different calculated ratio versus temperature curves formulated from two lidar and two balloon profiles for each night. RMS values provide an indication as to how much drift might be in the LAMP system for the time lapse indicate in the table.

Date	Lapse time	Regression Type	
		Weighted	Non-weighted
05/22/94	3 hours	2.20 K	2.15 K
03/13/95	4 hours	2.19 K	1.65 K

Chapter 6

OPTIMAL ESTIMATION OF LIDAR TEMPERATURE DATA

In the past, the common procedure for filtering lidar temperature profiles has been to apply a general weighting function of some window size. Philbrick et al [1987] has demonstrated that the best weighting function is the raised cosine function (Hanning filter) given by,

$$WT(n) = \frac{1}{2g(w)}\left[1-\cos\left(2\pi\frac{n}{w+1}\right)\right] \qquad 6.1$$

where w is the window size, n is the window increment, and g(w) is the partition function of the window envelope given as the sum of all WT(n). Filtering is achieved at each point by specifying a window size, multiplying the resulting weighting coefficients to the pertinent data, and summing the results to achieve a new data point value. Figure 6.1a gives a typical raw lidar temperature profile taken on 8 November 1994 at 00:49 GMT and Figure 6.1b gives its standard deviation. Because it is determined by the amount of received backscattered photons, and because the atmospheric density drops off exponentially with altitude, lidar statistical error increases with increasing altitude. The data in the lower altitudes is statistically more sound than that at higher altitudes and thus requires a smaller filter window. However, if the filter window is too small then not enough noise will be filtered out, and if the window is too large, then small spacial temperature variations will be filtered out. The goal is to decide what is and what is not noise. This, unfortunately, is difficult to determine and requires a lot of personal decision making on the individual processing the data.

An alternative method for filtering is proposed which is based on climatology data, and which makes use of the optimal estimation technique. Optimal estimation theory and how it can be applied to lidar temperature profiles is described in Section 6.1 Sections

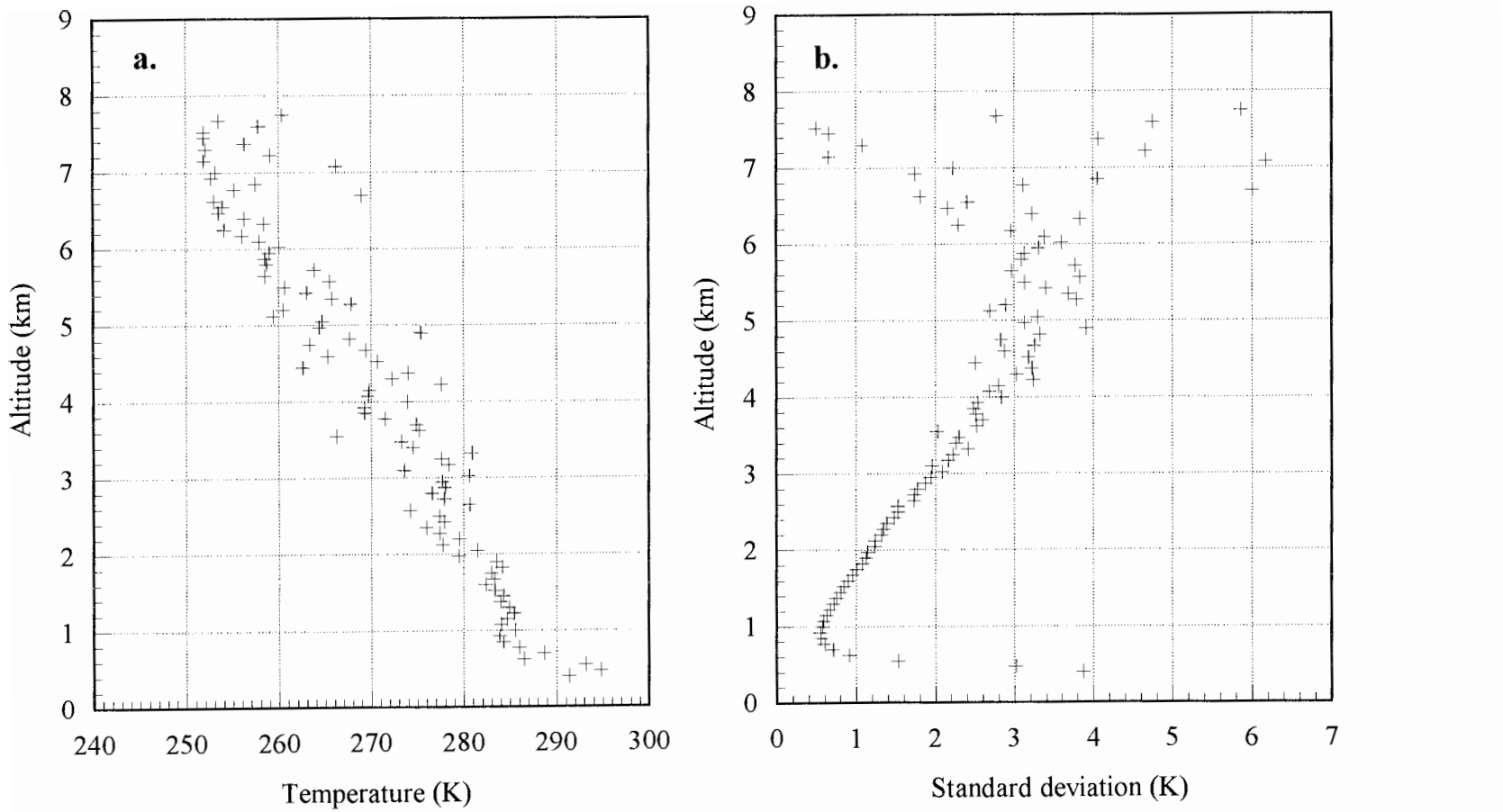

Figure 6.1: A typical raw rotational Raman lidar temperature profile (a.) and its corresponding standard deviation (b.) derived from assuming that the ratio versus temperature relation is a second order polynomial. Data was taken on 8 November 1994 from 00:49 - 01:21 GMT.

6.2 and 6.3 describe the calculations of a balloon climatology covariance matrix and a lidar temperature covariance matrix, respectively. And finally, Section 6.4 compares the results of filtering a temperature lidar profile using both the Hanning filter and the optimization filter.

6.1 Optimal Estimation Technique

Optimal estimation theory is based on the fact that there may be more than one independent data set which can describe a desired parameter. In this thesis, the two independent variables are temperature obtained from a lidar system and temperatures obtained from a balloon climatology data set which was calculated from a set of 20 meteorological balloons taken over the course of the month of November in 1993 and 1994 at State College.

Optimization makes use of the statistics of each data set to determine which is the most reliable, and thus, which should be weighted more heavily in the calculation of the real value of the parameter in question. The weighting of the data is given by,

$$x_{op} = \frac{a_1 x_1 + a_2 x_2}{a_1 + a_2} \tag{6.2}$$

where x_1 and x_2 are the two pieces of data, and a_1 and a_2 are the weighting coefficients. The best choice for the values of a_1 and a_2 can be calculated by minimizing the statistical error in x_{op}. This can be achieved by taking the partial derivatives of the standard deviation (σ) with respect to a_1 and a_2, setting the resulting equations to zero, and solving for a_1 and a_2. The standard deviation of Equation 6.2 is,

$$\sigma_{x_{op}} = \left[\left(\frac{a_1}{a_1 + a_2} \sigma_{x_1} \right)^2 + \left(\frac{a_2}{a_1 + a_2} \sigma_{x_2} \right)^2 \right]^{\frac{1}{2}} \tag{6.3}$$

The results of the minimization give values of a_1 and a_2 as,

$$a_1 = \frac{1}{\sigma_{x_1}^2}$$
$$a_2 = \frac{1}{\sigma_{x_2}^2} \qquad 6.4$$

which are simply the inverse of the variances of the two data points. If, on the other hand, two independent data vectors ($\vec{x}_1$ and $\vec{x}_2$) are being optimized, each with their own covariance matrix (Γ_{x1} and Γ_{x2}), then the optimization relation is given by,

$$\vec{x}_{opt} = \left(\Gamma_{x_1}^{-1} + \Gamma_{x_2}^{-1}\right)^{-1}\left(\Gamma_{x_1}^{-1}\vec{x}_1 + \Gamma_{x_1}^{-1}\vec{x}_2\right) \qquad 6.5$$

with its corresponding covariance matrix of,

$$\Gamma_{x_{opt}} = \left(\Gamma_{x_1}^{-1} + \Gamma_{x_2}^{-1}\right)^{-1} \qquad 6.6$$

The key to solving Equations 6.5 and 6.6 is to determine accurately what the covariance matrices are for the two data sets. The covariance matrix of a data profile describes how each point in the profile is related to all other points, and is given by,

$$\Gamma_{i,j} = r_{i,j}\sigma_i\sigma_j = \langle (x_i - \langle x_i \rangle)(x_j - \langle x_j \rangle) \rangle \qquad 6.7$$

or in matrix form by,

$$\Gamma_{i,j} = \begin{bmatrix} \sigma_1^2 & r_{1,2}\sigma_1\sigma_2 & \cdots & r_{1,N}\sigma_1\sigma_N \\ r_{2,1}\sigma_2\sigma_1 & \sigma_2^2 & \cdots & r_{2,N}\sigma_2\sigma_N \\ \vdots & \vdots & & \vdots \\ r_{N,1}\sigma_N\sigma_1 & r_{N,2}\sigma_N\sigma_2 & \cdots & \sigma_N^2 \end{bmatrix} \qquad 6.8$$

where σ_i and σ_j are the standard deviations of the ith and jth data point, respectively, and $r_{i,j}$ is the correlation coefficient between the ith and jth data points. Along the diagonal the

correlation coefficient is equal to 1 because every data point is perfectly correlated with itself. The diagonal, therefore, gives the variance of each data point. Given the above theory, the covariance matrices for the climatology data and the lidar temperature data can be calculated.

6.2 Lidar Temperature Covariance Matrix

The calculation of the lidar temperature covariance matrix in this section assumes that each data point in the lidar profile has been independently measured with respect to all other data points. In order for this to be true there can be no after pulsing in the photomultiplier tubes used in the detector system. Further, the data collection units must operate in the linear region where pulse-pile-up is insignificant. Pulse-pile-up of the data units can cause one data set to overlap into another, thus instilling a correlation term into the covariance matrix.

With the above assumption, the total covariance matrix of the lidar data profile can be expressed as a function of the covariance matrix associated with the regression coefficients, and the covariance matrix associated with the temperature lidar profile. The temperature covariance matrix, without the influence of the regression coefficients, is calculated by first determining the covariance matrix of the lidar ratio profile. Because it was assumed that all measured data points are independent, the lidar ratio covariance matrix ($\Gamma_{\mathbf{RL}}$) consists of only diagonal terms with all off diagonal terms equal to zero and is given by,

$$\Gamma_{RL} = \boldsymbol{I}\hat{\sigma}_{RL}^{2} \qquad 6.9$$

where **I** is the identity matrix. The covariance matrix for the calculated lidar temperature data is then given by,

$$\Gamma_{TL_{i,i}} = \Gamma_{RL_{i,i}} \left(\frac{\partial TL}{\partial RL} \right)_i^2 \qquad 6.10$$

where the derivative is simply the slope of the curve which relates lidar ratios to temperature.

Because Equation 6.10 is diagonal, the total covariance matrix associated with the calculated temperature profile (Γ_T) can be broken up into a simple summation of the covariance matrix from the calculated lidar temperature data (Γ_{TL}), and the covariance matrix of the calculated regression coefficients (Γ_C).

$$\Gamma_T = \Gamma_{TL} + \Gamma_C \qquad 6.11$$

The regression coefficient covariance matrix can be solved by noting that the covariance matrix of Y in the relation,

$$\vec{Y} = A\vec{X} \qquad 6.12$$

is given by,

$$\Gamma_Y = A\Gamma_X A^* \qquad 6.13$$

Since Equation 6.12 is similar to the equation for the coefficients (Equation 5.8), with $\mathbf{A} = (\mathbf{R}^*\mathbf{R})^{-1}\mathbf{R}^*$, the regression coefficient covariance matrix is given by,

$$\Gamma_C = [(R^*R)^{-1}R^*]\Gamma_{balloon}[(R^*R)^{-1}R^*]^* \qquad 6.14$$

where $\Gamma_{balloon}$ is given by Equation 5.1.

The covariance matrix was calculated for the temperature profile shown in Figure 6.1. For this data set, the ratio versus temperature curve was determined using a second order polynomial relating lidar ratios to balloon temperatures. Equation 6.10 can then be solved to equal,

$$\Gamma_{TL_{i,i}} = \Gamma_{RL_{i,i}}(a_2 + 2a_3 RL_i)^2 \qquad 6.15$$

The final calculated lidar temperature correlation matrix stemming from Equation 6.7 and 6.11, produced primarily a diagonal matrix with small off diagonal terms. This indicates that the data points in the lidar temperature profile are primarily uncorrelated, and is shown in Figure 6.2 for a number of different altitudes.

6.3 Climatology Model and its Covariance Matrix

The climatology model used in the optimization filter was derived from a grouping of a number of radiosonde balloons launched by the Penn State Meteorology Department and by the ARL Lidar Laboratory. The total number of balloons gathered was twenty. The processing of the balloon data consisted of first removing all erroneous data points caused by a failure of the system to lock on to the balloon signal, and then interpolating the data altitudes to match those of the lidar profile. The climatology model is the mean of all twenty balloons and is shown in Figure 6.3a. The calculation of the corresponding covariance matrix, $\Gamma_{\mathbf{climate}}$, stems from Equation 6.7 and is given by,

$$\Gamma_{TC_{x,y}} = \langle (T_i - \langle T_i \rangle)_x \, (T_j - \langle T_j \rangle)_y \rangle \qquad 6.16$$

where x and y are the altitudes in question, and i and j are all the data points at a particular altitude from all of the balloon data profiles. Equation 6.16 is equivalent to,

$$\Gamma_{TC_{x,y}} = \frac{1}{N^2} \sum_{i=1}^{N} \sum_{j=1}^{N} (T_i - \langle T_i \rangle)_x \, (T_j - \langle T_j \rangle)_y \qquad 6.17$$

Figure 6.3b shows the calculated standard deviation of the climatology model at each altitude. The correlation matrix calculated from Equations 6.7 and 6.17 is shown in Figure 6.4 in its entirety, and in Figure 6.5 for five different altitude points: 0.5, 1, 5, 7.5, 10 km. By definition, total correlation is equal to one, total decorrelation is equal to zero, and total anti-correlation is equal to -1. An important point in both Figure 6.4 and 6.5 is

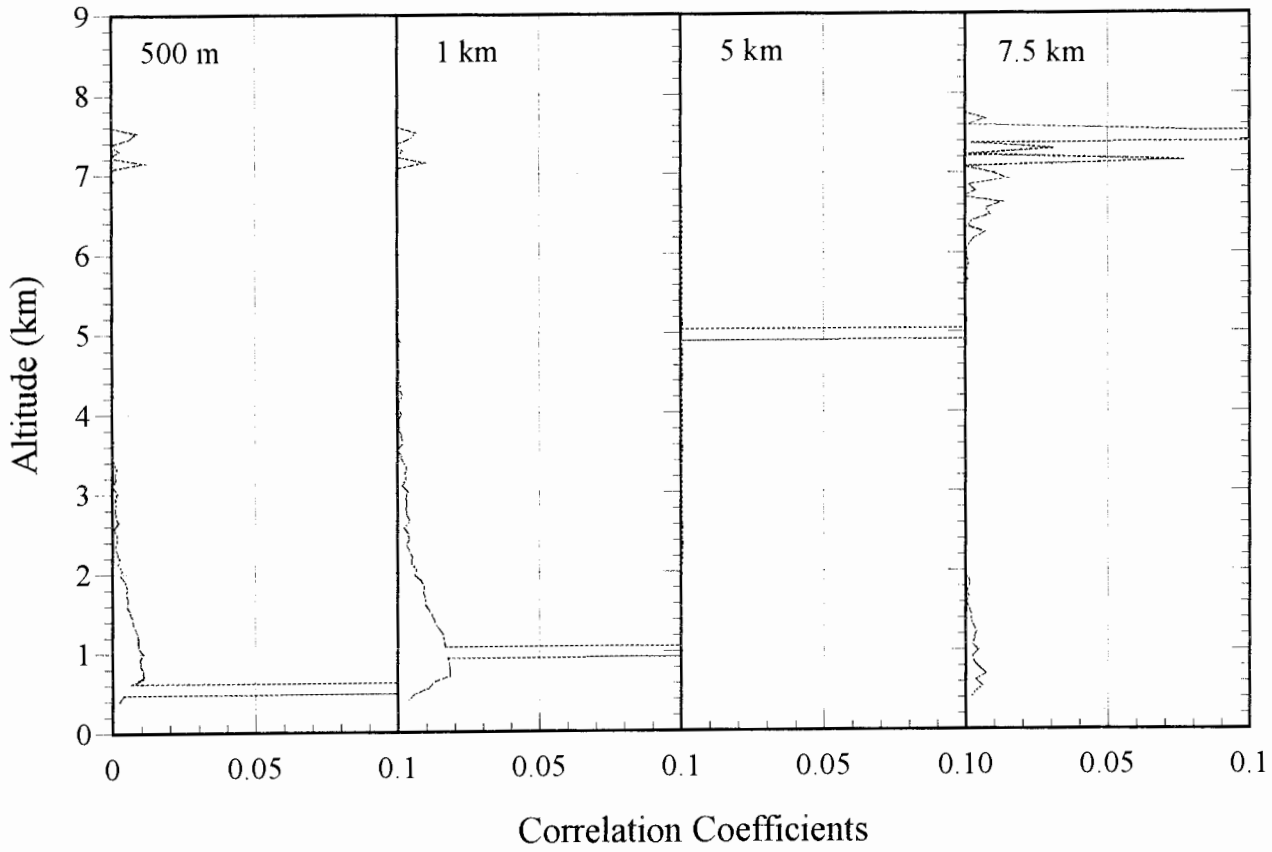

Figure 6.2. Correlation coefficients from a lidar rotational temperature profile measured at Penn State University on 8 November 1994 at 00:49 - 01:19 GMT. Correlation values are in relation to the altitude at the top left corner of each plot. Perfect correlation equals one.

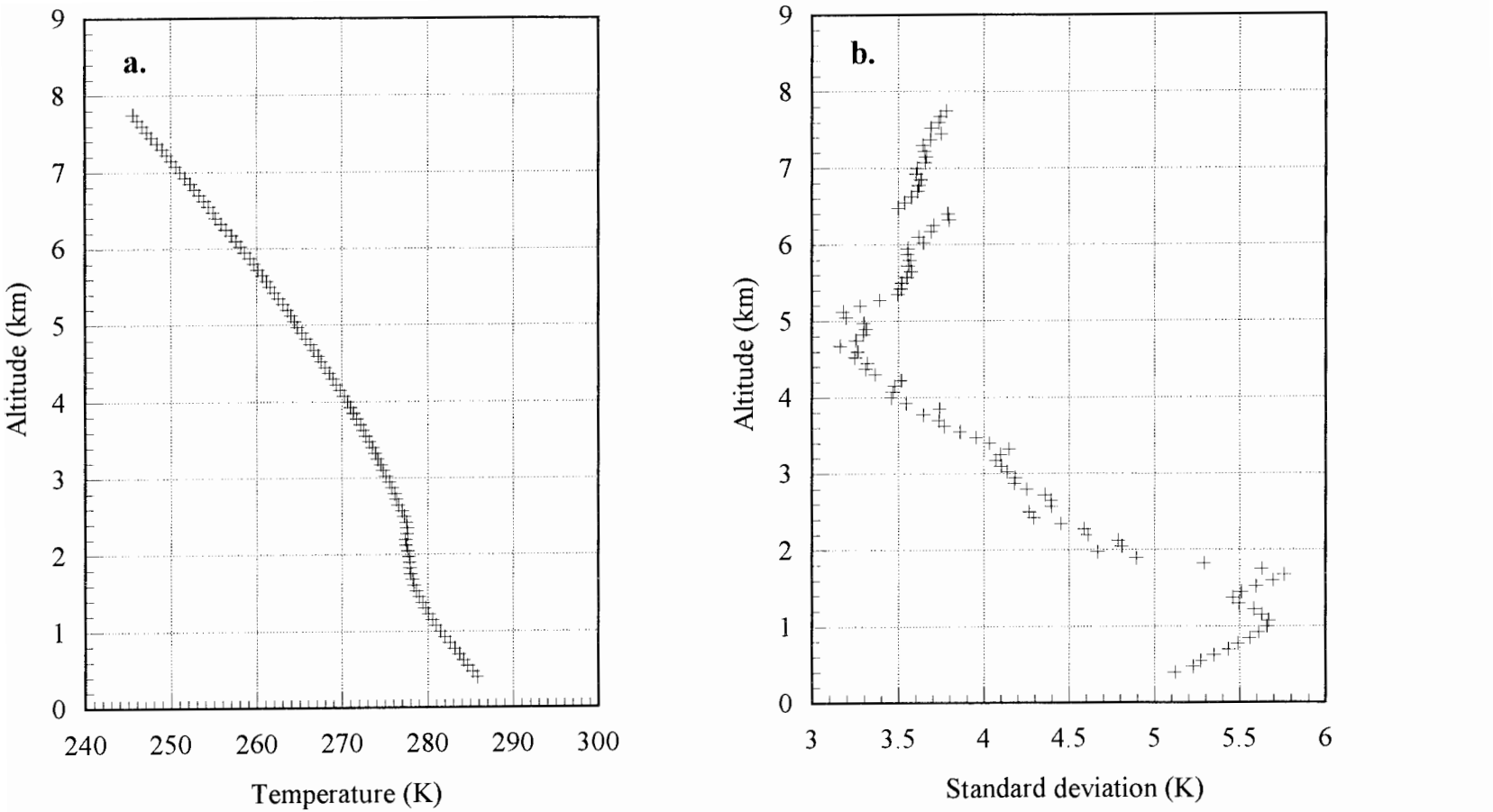

Figure 6.3: Mean November climatology temperature profile calculated from 20 radiosonde balloon launces (a.) and its corresponding standard deviation (b.)

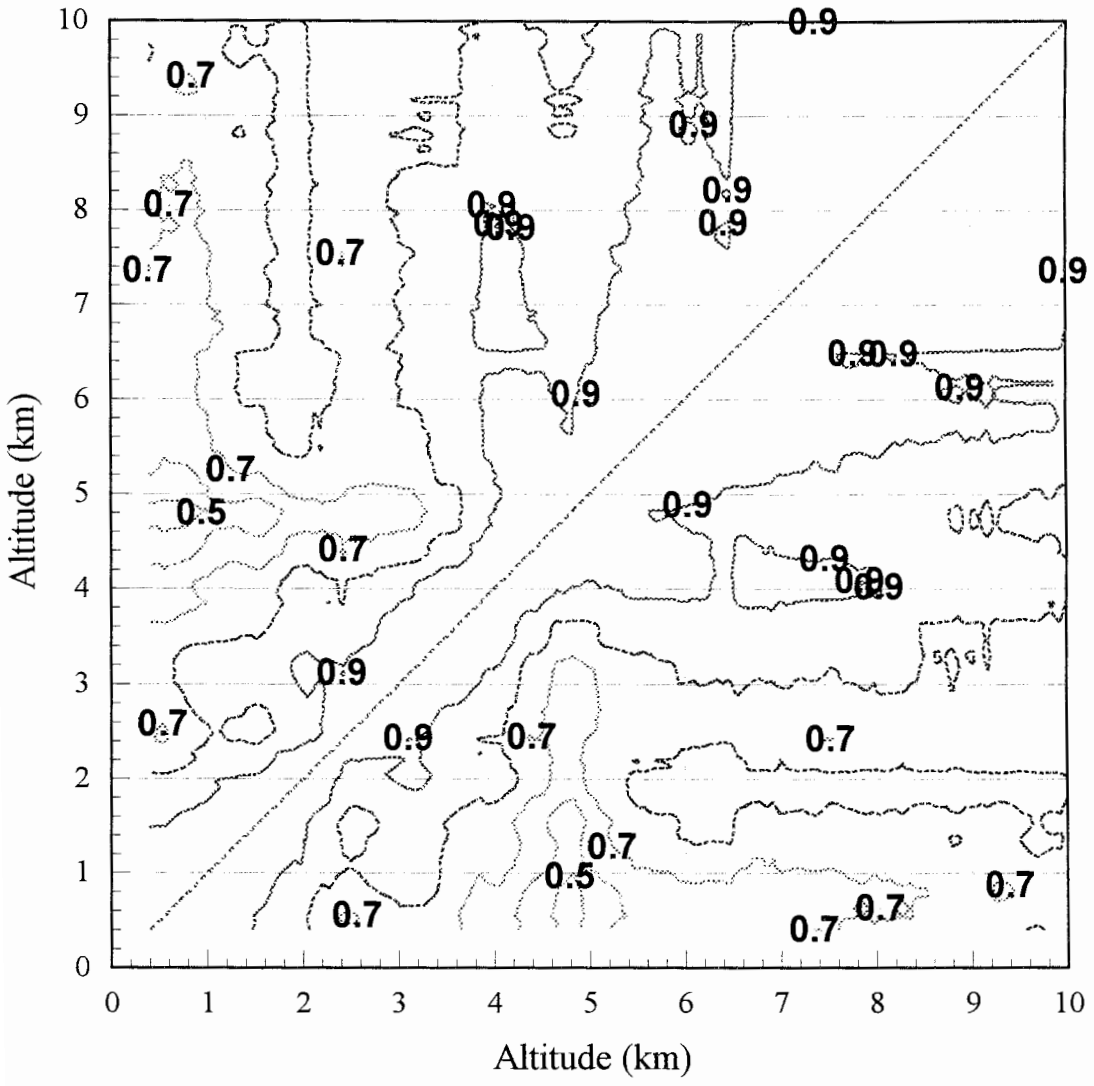

Figure 6.4. Correlation coefficients of the climatology covarience matrix for the month of November. Data calculations are based on 20 balloon profiles which were launched during both day and night.

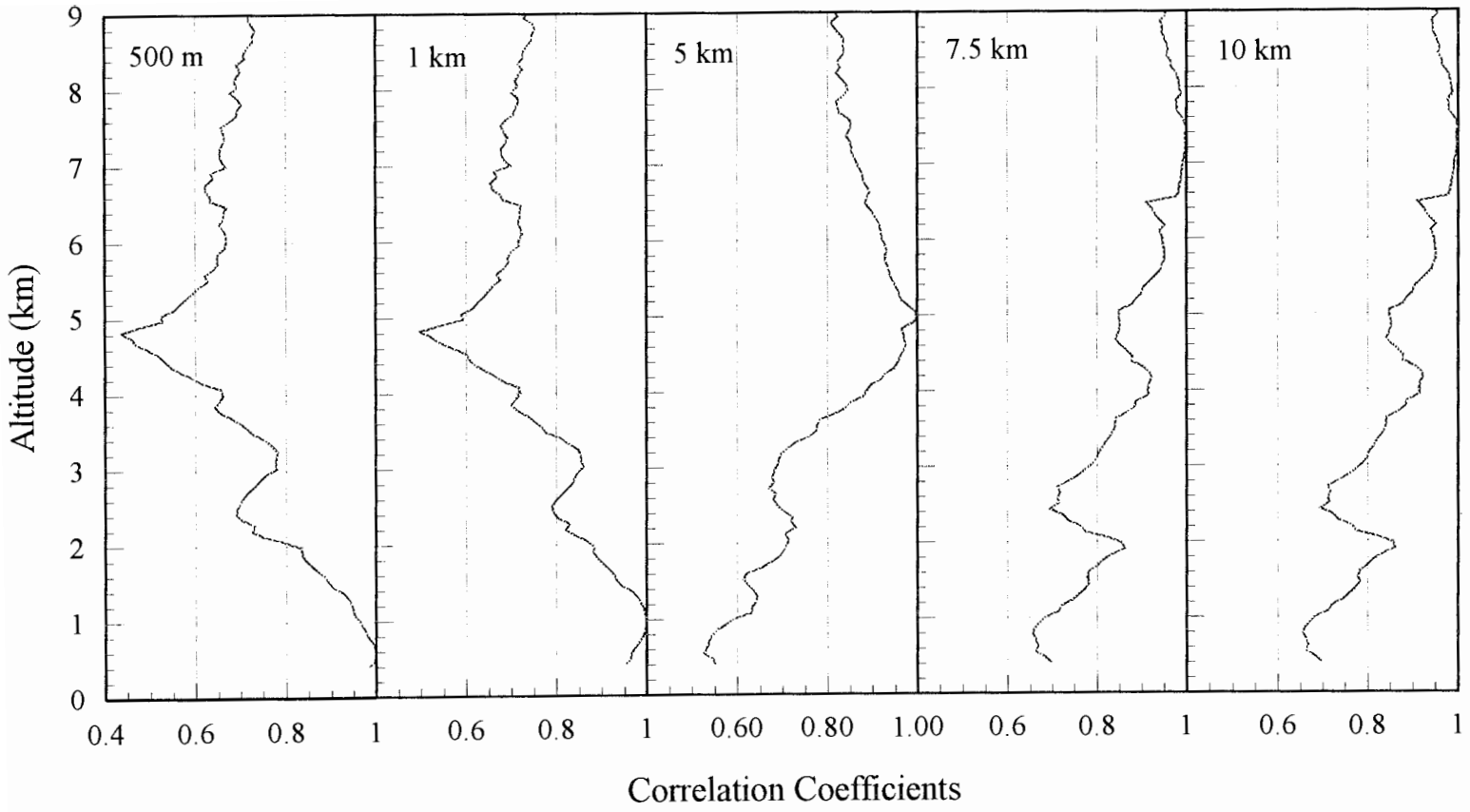

Figure 6.5. Correlation coefficients from a November climatology model based at Penn State University. Model consists of data from 20 radiosonde balloons. Correlation values are in relation to the altitude at the top left corner of each plot.

that, from the limited data set available, all points up to 10 km are in some way correlated to all other data points. Also, this correlation is typically greater than 0.6. This is the basis for the optimization technique to be able to filter out untrue variations in the lidar temperature profile. Very strong temperature variations, which are typically found because of high statistical lidar error, will be removed because of the strong weighting of the climatology model.

In order to improve the accuracy of the climatology model, more balloons need to be factored into the mean and covariance matrix This was not able to be done because there were only 20 balloons available at the time of the formulation of the model.

6.4 Comparison of Filtering Results from the Optimal Estimation Filter and the Hanning Filter

A comparison was made between the optimal estimation filter and a five point Hanning filter to determine the potential for use of the optimization technique for future data processing. The filtering was performed on the lidar profile taken on 8 November 1994 at 00:49 - 01:19 GMT which was shown in Figure 6.1. The balloon which was used in the regression analysis to determine the ratio versus temperature curve was launched 90 minutes prior to the taking of the lidar data. Its flight path is shown in Figure 6.6. The differences in the balloon and lidar temperature profiles shown in Figure 6.7 may be due to the differences in location and time when the balloon made its measurements. The results of the calculations are shown in Figure 6.7 for the temperature profile and Figure 6.8 for the corresponding standard deviations. In the regions where the lidar statistics outweigh those of the climatology model, the two processed profiles overlap each other, thus showing that information is not lost in these regions by the optimization calculation. In the other regions (below 600 m and above 3.5 km) the climatology model tends to smooth the noisy lidar data more than the Hanning filter. The reason for this is that because the statistics of the lidar data become worse with increasing altitude, a five point Hanning filter can no longer reduce the extra noise seen in the upper altitudes, and thus its results show more variations.

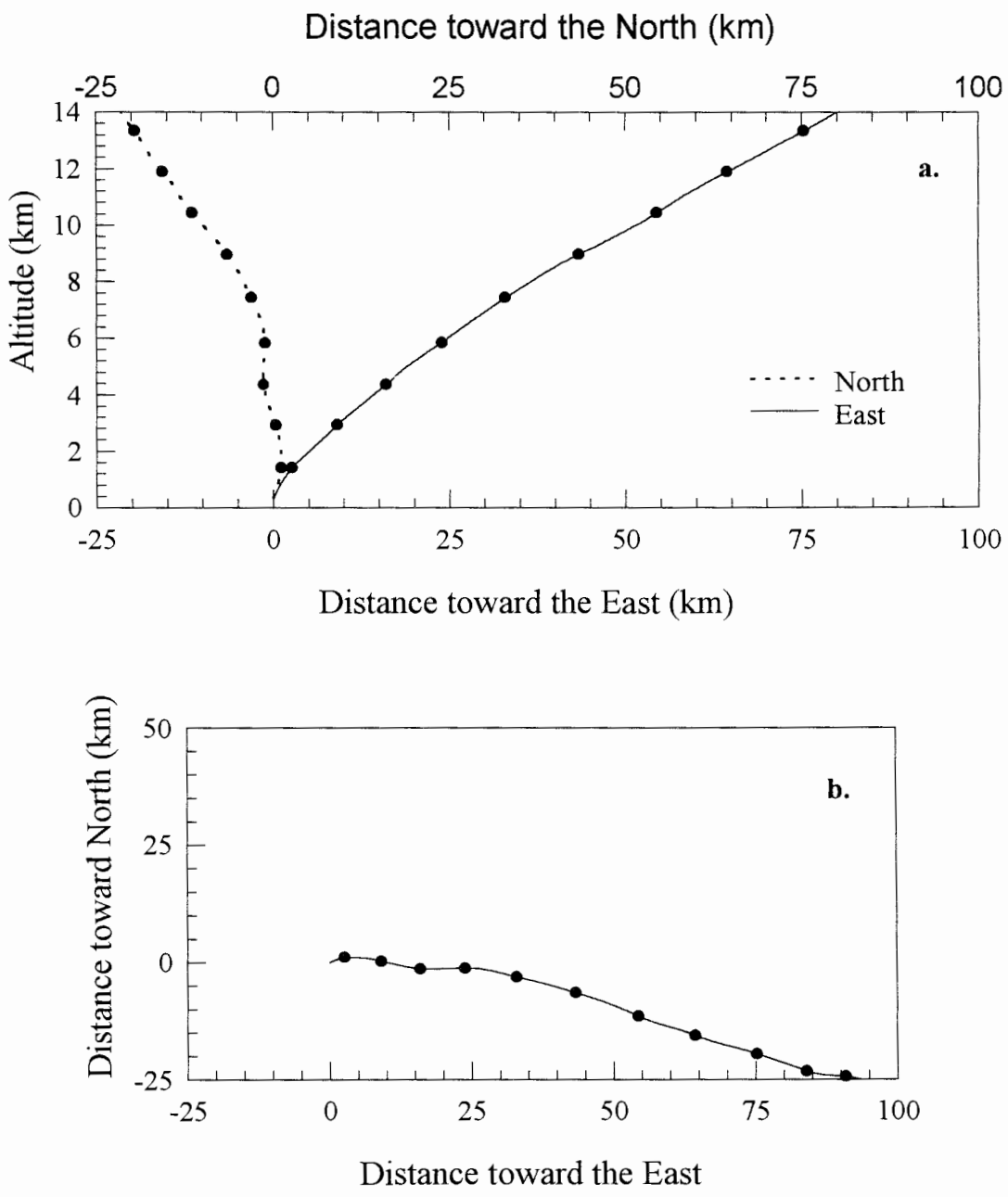

Figure 6.6. Flight path of a radiosonde balloon launched on 11/07/94 at 23:11 GMT. Lidar data was taken on 11/08/94 from 00:49 - 01:19 GMT. Solid dots indicate 5 minute lapse time intervals. **a**. Distance the balloon traveled to the North and the East as a function of altitude. **b**. Topographical view of the flight path to show the distance from the release of the balloon while lidar measurements were being taken.

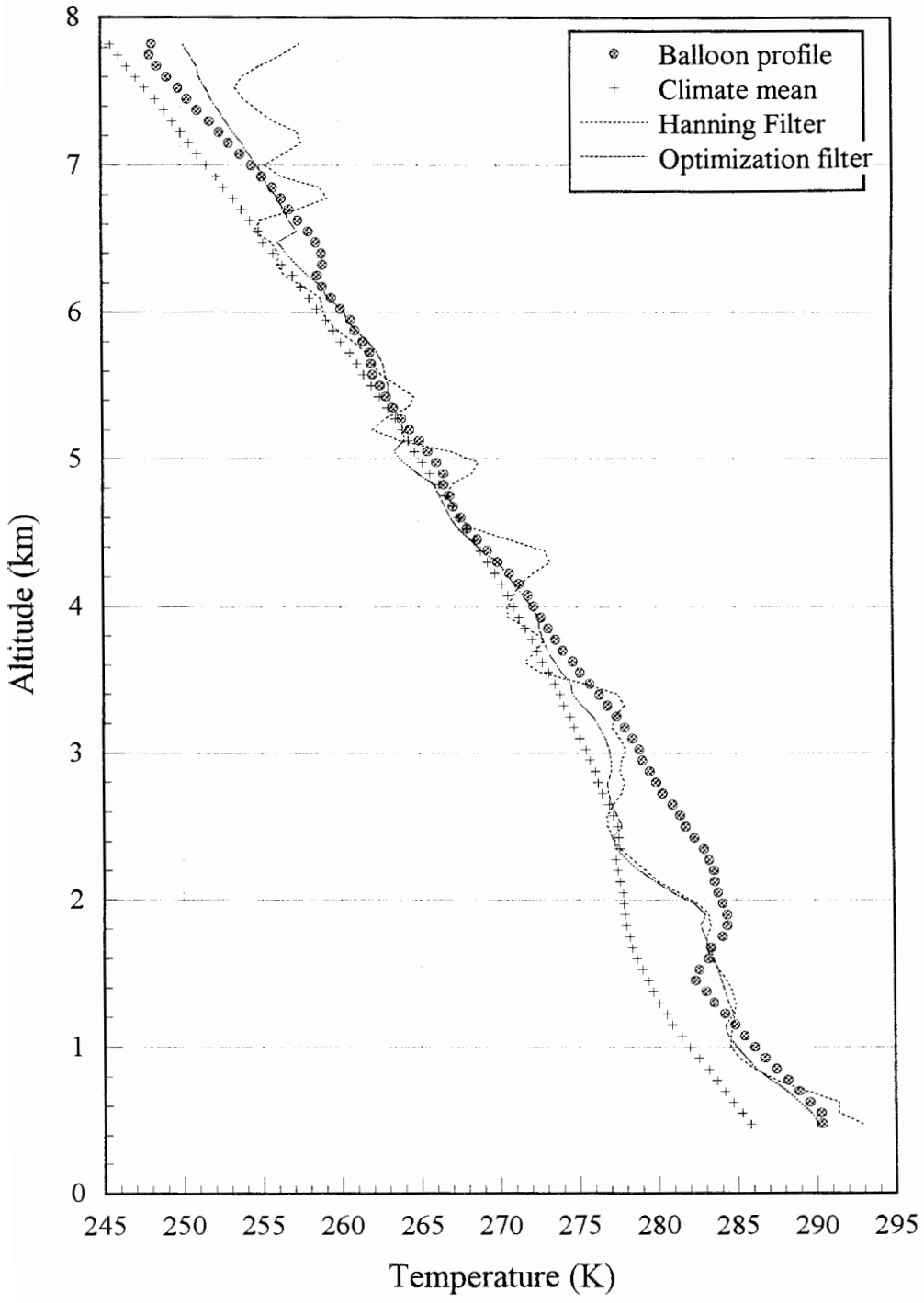

Figure 6.7. Comparison of processed lidar temperature data using a five point Hanning filter and an optimization filter which was based on a November climatology model calculated from 20 radiosonde balloons.

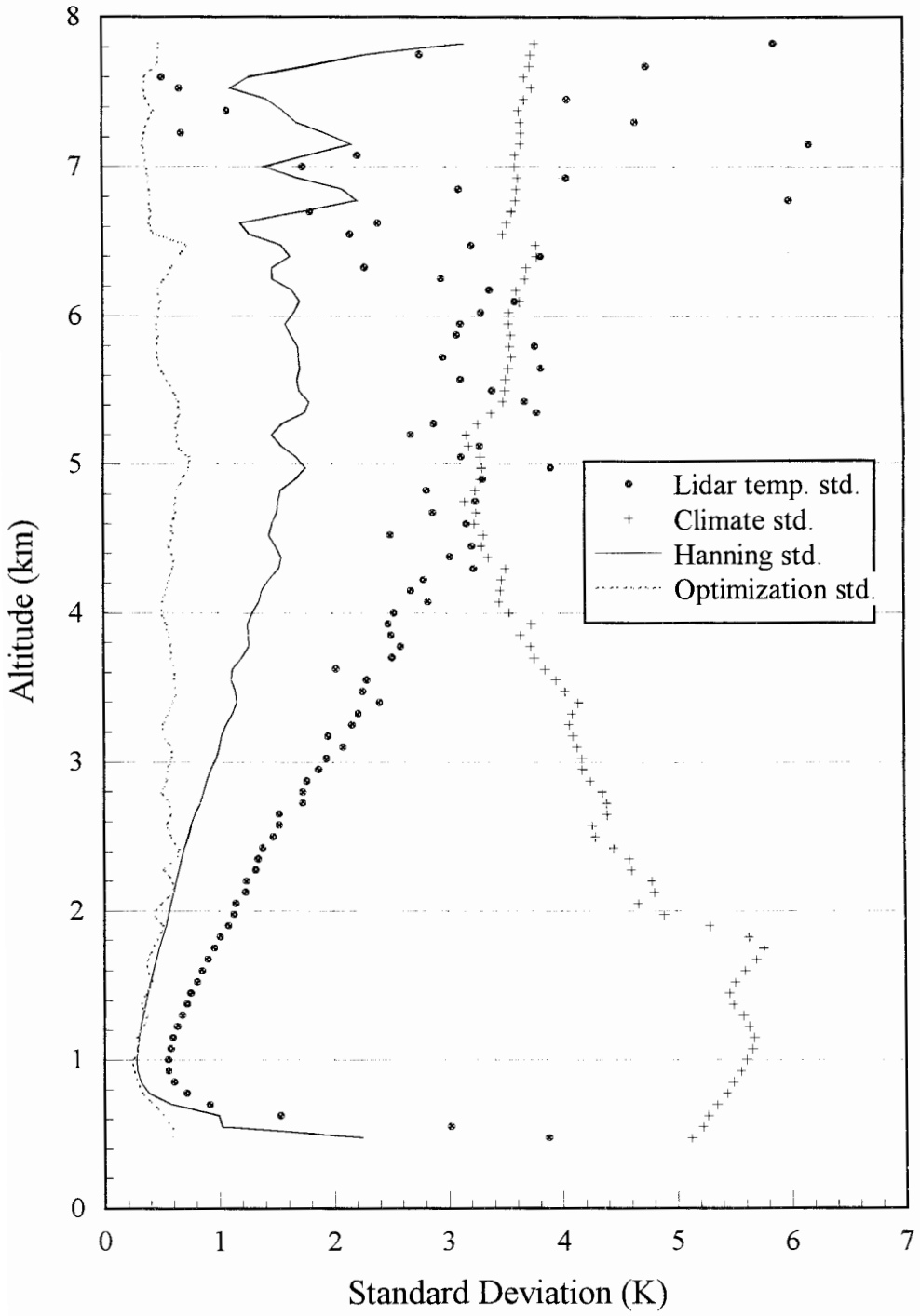

Figure 6.8 Comparison of the standard deviations from a raw lidar temperature profile taken on 8 November 1994, a climatology mean for the month of November, a Hanning filtered lidar temperature profile, and an optimization filtered lidar temperature profile.

The optimal estimation filter also acted to correct the tail end of the lidar temperature profile which is seen to trend towards warmer temperatures above 6.5 km in Figure 6.7. The regression to determine the ratio verses temperature curve is not capable of preventing the second order polynomial curve from bowing in the region of noisy lidar data. The fitting procedure can add extra error into the profile besides that based on the raw data. However, because of the weighting effect of the climatology model at those points, the lidar data is not permitted to move away from the mean too quickly, thus minimizing the potential error.

Figure 6.8 shows the standard deviations for the climatology model, raw lidar temperature data, and the two filtered temperature profiles. In the regions where the lidar data is statistically better than that of the model, both the Hanning filtered and optimization filtered data show the same decrease in standard deviation. However, in the regions where the climatology standard deviations become comparable or less in value to the lidar standard deviations, the optimized standard deviations become much more statistically sound than the Hanning filtered data. This is because the climatology model contains more information about the parameter in question than the Hanning filter does, and thus, has the ability to lower the uncertainty in its value. The use of the optimal estimation filter resulted in a lidar temperature profile whose standard deviation was less than 0.8 K below 7 km altitude with a minimum of 0.3 K at 1 km altitude. Lidar data above 7 km was ignored because of large errors which were added to the data due to the temperature versus ratio coefficients calculated during the regression analysis.

In order to determine how much error would be instilled in the processed data by using it as the second data set, three temperature profiles were substituted in for the climatology mean while maintaining the same climatology covariance matrix. These temperature profiles include the balloon profile at the time of the lidar measurement, and the balloon profiles generated by shifting the measured balloon profile by $\pm$ 20 K. The results are shown in Figure 6.9. For the case where the measured balloon profile was used, there was minimal deviation (RMS = 0.3 K) from the case where the climatology mean was used in the optimization. The difference in this case peaked at 0.5 K. From the

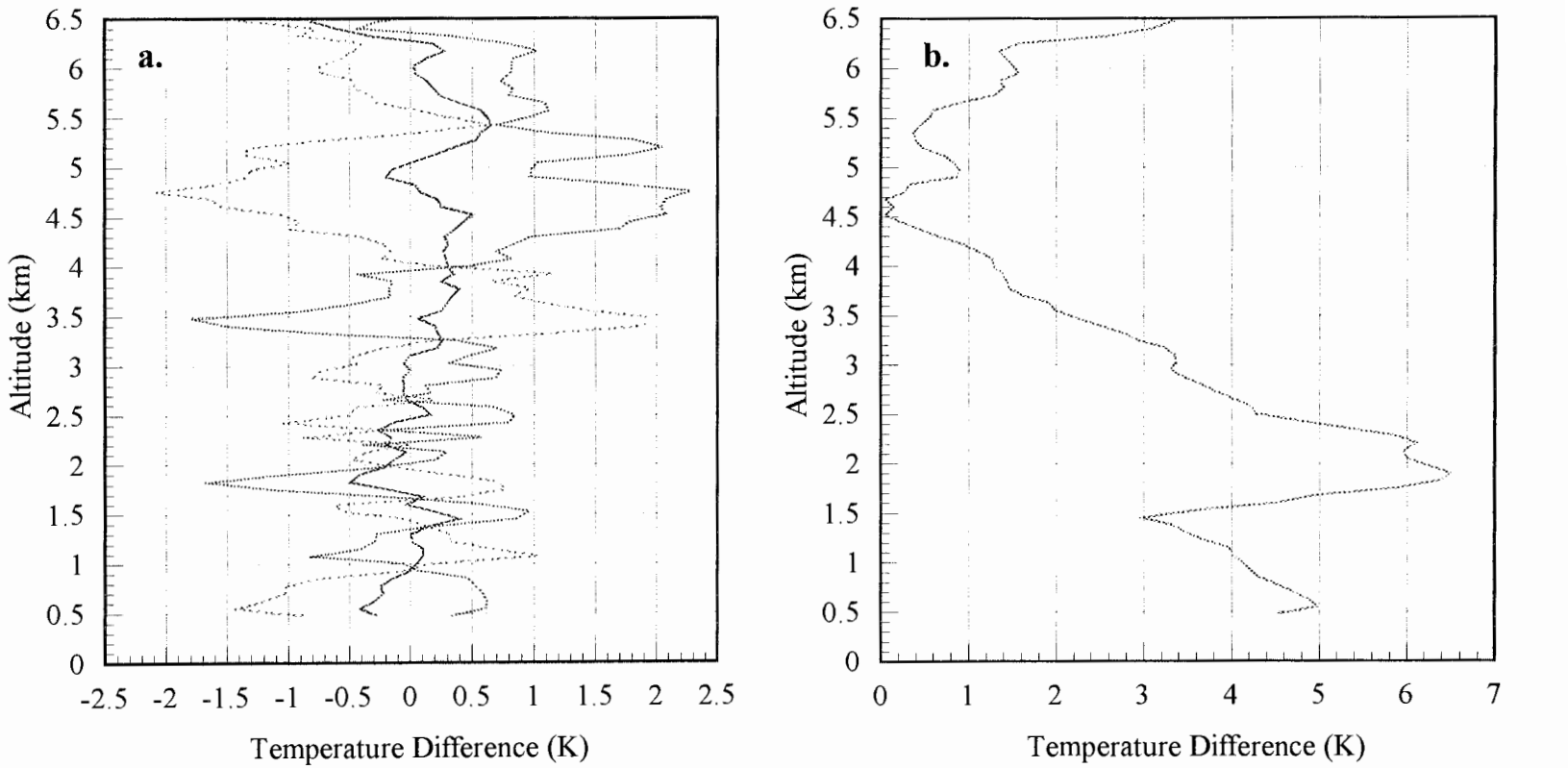

Figure 6.9. (a.) Calculation of the temperature differences from using the measured balloon profile (solid line), +20 from the measured balloon temperature profile (dash-dot line), and -20 K from the measured balloon temperature profile (dot line) as compared to using the mean climatology temperature profile (November) in the optimization filtering technique. (b.) Temperature difference between the mean climatology temperature profile and the measured temperature profile.

other two profiles whose temperatures were ±20 K from the measured profile, the deviation peaked at 2 K. The RMS values for the +20 K case was 0.9 K, and that for the -20 K was 0.9 K. This indicates that using a mean climatology temperature profile instead of a balloon temperature profile measured during the lidar run, instills little error into the lidar temperature profile.

Because of the lack of lidar data in the month of November, further comparisons were not able to be made between the Hanning filter and the optimization filter. However, the comparison in Figure 6.6 does show that the optimization technique has promise and should be further explored in the future.

Chapter 7

CONCLUSIONS

7.1 Summary

The purpose of this thesis was to develop experimental procedures and techniques for measurements of atmospheric temperature in the troposphere using the pure rotational Raman technique. To achieve this goal, it was necessary to determine if other contributions to optical scattering could alter temperature measurements, to establish design configurations for an ideal optical detector, to parameterize different analysis techniques for obtaining temperature versus ratio conversion curves, and to present a possible means of filtering the data to obtain the true temperatures.

Previous attempts by other groups to measure temperature profiles of the lower atmosphere using the pure rotational Raman technique have been made. These measurements either consisted of long all night averages, or were statistically weak and only demonstrated that the technique could be used, or were limited to altitudes above the lower troposphere. The question as to whether water vapor is a possible contaminant of the rotational Raman measurements had never been addressed. A thorough examination of water vapor's pure rotational Raman spectrum was presented in Chapter 3. The absolute values of the pure rotational Raman line intensities were calculated with the aid of a computer program originally developed by William Murphy [1977] which calculated the relative line intensities. The results showed that, when compared to the N_2 and O_2 spectrums, the peak in the spectrum of water vapor (529.46 nm or 83 cm^{-1}) was approximately 0.5% of the O_2 magnitude and 1.1% of the N_2 magnitude at 320 K. However, because of the broadness of it, the spectrum of water vapor becomes larger than that of N_2 and O_2 below approximately 525.6 nm N_2 and 526 nm for O_2 at 320 K, or 232 cm^{-1} and 217 cm^{-1}, respectively. Further analysis showed that there was no contamination

from the water vapor spectrum for the filters used in the LAMP and LAPS systems. In the case of a 0.2 nm FWHM filter and a 3% water vapor concentration at 320 K, the signal from the water vapor spectrum contributes less than 0.1% of the total signal for filter placements less than 163.9 cm^{-1} (greater than 527.5 nm) at 320 K. If the filters have a bandwidth of 3 nm FWHM this number would be 225.2 cm^{-1} (525.8 nm) at 320 K. If the LAMP theoretical temperature versus ratio curve is considered, then this 0.1 % error in the signal would equate to about a 0.2 K error in the temperature profile.

With the establishment that only N_2 and O_2 contribute to the signals which measure temperature, the ideal optical filter configurations for different thermal regions in the troposphere could be found. It was determined that it was sufficient to use the filter configurations optimized for the entire troposphere (200 K to 320 K) with minimal loss in statistics. These filters reside at 531.25 nm @ 0.5 nm FWHM and 528.15 nm @ 2.01 FWHM, or in wave numbers 30.1 cm^{-1} @ 17.7 cm^{-1} FWHM and 140.6 cm^{-1} @ 75.3 cm^{-1} FWHM. Further analysis showed that the lower wave number filter could be moved a little further from the primary laser frequency without too much loss in statistics.

A number of regression models were presented in Chapter 5 to try and determine what model might provide the best results for a temperature versus lidar ratio curve. For the data sets used in this thesis, it was shown that either a non-weighted second order polynomial, relating lidar ratios to balloon temperatures, or a non-weighted linear relation between the theoretical temperature versus ratio curve and the lidar and balloon data, provided the best results. One reason why the non-weighted fit worked a little better than the weighted fit, is that, if the balloon and the lidar did not measure the same temperatures in the lower altitudes, then a weighted regression would force the two measurements to be equal causing errors in the resulting curve. Another problem was that the weighted regression would eliminate the importance of some of the lidar data before it became statistically insignificant due to the large dynamic range of the lidar signal. For conditions where lidar system changes are non-existent, or where lidar system drift is not an issue, using the theoretical temperature versus ratio model would be the better choice for the regression analysis, since the model contains only one coefficient and it is based on

physical parameters of the system. However, in the case of the LAMP system, numerous changes have been made over the years to accommodate other experiments, test new equipment, and reduce system drift. Therefore, during these periods of changes, it was decided to use the model, based on a general second order polynomial, to avoid induced errors that could result from using the rigid model based on the lidar system.

With the calculation of a ratio versus temperature curve completed, the lidar temperature data has to be filtered. In the past, weighted averaged filters, such as the Hanning filter, were used, and required a lot of decision making by the analysist to try and eliminate what appeared to be noise. Improving this filtering procedure resulted in the application of an optimal estimation algorithm based on balloon climatology data. From the results shown in Chapter 6, the optimal estimation filter performed as well as, if not better than, a five point Hanning filter. In the regions where the standard deviation of the lidar data became large, the optimization filter was able to suppress more of the untrue variations in the data than the Hanning filter. It was also able to reduce the errors caused by inaccuracies found at the tail end of the calculated temperature versus ratio curve.

Using the optimal estimation filter on LAMP lidar data resulted in a temperature standard deviation less than 0.8 K below 7 km with a minimum of 0.3 K at 1 km. Further more, it was shown that using either the climatology mean or the measured balloon profile in the optimization calculation produced minimal differences in the resulting temperatures even in the regions where the two profiles differed by 6 K. These results show that the optimal estimation technique should be considered when filtering future lidar data.

7.2 Future Work

The results obtained from this thesis opened up a number of areas which could be further explored in the future. First, the effects of the water vapor's pure rotational Raman spectrum on temperature measurements taken in the Stoke's region, needs to be calculated for those wanting to take advantage of the greater intensities found in that region. Also, by looking at single quantum lines which are located in the far end of the spectrum, and

which are outside the N_2 and O_2 spectrums, and which are insensitive to the thermal changes typical to the atmosphere, the possibility of measuring water vapor concentrations might exist. In those far regions, the backscatter intensities of the pure rotational quantum lines are still significant when compared to the vibrational line of the water vapor molecule, thus making measurements plausible.

Future work should also explore the quantization of the backscatter cross section of liquid and solid water. Water molecules exist in high concentration in the liquid and solid states in the form of clouds, fog, rain, and ice to name a few. If these cross sections are high enough, then the scattered signals from them could pose a possible source of error in temperature measurements. Even if they do not cause errors, the results of the calculations might be applicable for developing techniques for underwater measurements.

Further studies to quantify statistically what the best model for the development of the ratio versus temperature curve needs to be made for both the LAMP and LAPS systems. This requires long term data collection periods which are taken without modifying system characteristics. The data could then also be used to determine system drift on time scales of hours, days, weeks, or months. Other possibilities for calibrating a rotational lidar system should also be explored in order to eliminate the need for balloon comparisons. One possibility would be to use a thermally stabilized chamber as a scattering volume. This calibration technique would only be practical if the spatial resolution of a lidar system could be reduced and if the lidar system was very stable over long periods of time.

Finally, the optimization filtering technique needs to be tested with more lidar data. This requires gathering balloon profiles for other months besides November, if practical experimentation is to be done through out the year. Other models should also be explored for substitution into the climatology data. One possibility is using a previously measured set of lidar data. A model based on this type of data would be important because it has been speculated that balloons are not capable of measuring true atmospheric variability because they travel along wind currents as they ascend. A lidar model would contain this information, and thus, would be a true model of the vertical atmosphere.

REFERENCES

Ahrens, C.D., *Meteorology Today: An Introduction to Weather, Climate, and the Environment*. New York: West Publishing (1994)

Alpers, M., J. Hoffner, U. von Zahn, "Sporadic Fe an E layers at polar, middle, and low latitudes," J.G.R. Vol. 99, 14971-14985 (1994)

Armstrong, R.L., "Rotational Raman Interferometric technique to measure gas temperature," Appl. Opt. Vol. 14, 383-387 (1975)

Arshinov, Y. F., S. M. Bobrovnikov, V. E. Zuev, and V. M. Mitev," Atmospheric temperature measurements using a pure rotational Raman lidar," Appl. Opt. Vol. 22, 2984- 2990 (1983)

Barry, R.G., R.J. Chorley, *Atmosphere, Weather & Climate*. New York: Routledge (1992).

Badgely, F.I., "Response of radiosonde thermistors, " Rev. Sci. Instr., Vol. 28, pp. 1079-1084 (1957)

Chanin, M.L., A. Hauchencorne, "LIDAR studies of temperature and density using Rayleigh scattering," MAP Handbook, Vol. 13, pp. 87-99 (1984)

Cohen, A., J. A. Cooney, and K. N. Geller, "Atmospheric temperature profiles from lidar measurements of rotational Raman and elastic scattering," Appl. Opt. Vol. 15, 2896-2901(1976)

Cooney, J. A., "Measurements of atmospheric temperature profiles by Raman backscatter," J. Appl. Meteorol. Vol. 11, 108-112 (1972)

COSPAR International Reference Atmosphere: 1986, Part II Middle Atmosphere Models, edited by D. Rees, J. J Barnett, K. Labitzke, Pergamon Press, Oxford (1990).

Elterman, L. B., "The measurements of stratospheric density distribution with the search light technique," J. Geophys. Res. Vol. 58, 519-530 (1953).

Fernandez-Sanchez, J.M., W.F. Murphy, "True and Effective polarizability tensors for asymmetric-top molecules: the rotational Raman spectra of H_2S and D_2S," J. Mol. Spectr., Vol 156, pp. 444-460 (1992).

Hainer, R.M., P.C. Cross, J. Chem. Phys. Vol. 11, pp. 27 (1943)

Haris, P.A.T., T.D. Stevens, S. Maruvada, C.R. Philbrick, "Latitudinal variation of middle atmospheric temperatures," Advances in Space Research, (1993)

Hauchecorne, A., M.L. Chanin, "Density and temperature profiles obtained by lidar between 35 and 70 km," Geophys. Res. Lett., Vol 7, pp. 565-568 (1980)

Hauchecorne, A., M.L. Chanin, P. Keckhut, D. Nedeljkovic, "Lidar monitoring of the temperature in the middle and lower atmosphere," Appl. Phys. Vol. B 55, 29-34 (1992)

Hertzberg, G., *Molecular Spectra and Molecular Structure: I. Spectra of Diatomic Molecules*, Florida: Robert E. Krieger Publishing (1989)

Hertzberg, G., *Molecular Spectra and Molecular Structure: II. Infrared and Raman Spectra of Polyatomic Molecules*, Florida: Robert E. Krieger Publishing (1991)

Johns, J.W.C., "High-resolution far-infrared (20-350-cm^{-1}) spectra of several isotopic species of H_2O," J. Opt. Soc. Am. Vol. 2, 1340-1354 (1985)

Leonard, D.A., "Observation of Raman scattering from the atmosphere using a pulsed nitrogen ultraviolet laser, "Nature Vol. 216, 142-143 (1967)

May, P.T., R.G. Strauch, K.P. Moran, W.L. Ecklund, "Temperature Sounding by RASS with wind profiler radars: A preliminary study," IEEE Trans. Geosci. Rem. Sens. Vol. 28, 19- 27 (1990)

Melfi, S. H., D. Whiteman, R. Ferrare, "Observation of atmospheric fronts using Raman lidar moisture measurements," J. Appl. Meteorol. Vol. 28, 789-806 (1989)

Measures, R. M., *Laser remote sensing*. New York: John Wiley & Sons (1984).

Machuga, D.W., "Daytime performance of the LAMP Rayleigh/Raman lidar system, "MS Thesis, The Pennsylvania State University (1993)

Murphy, W.F., "The Rayeigh depolarization ratio and rotational Raman spectrum of water vapor and the polarizability components for the water molecule," J. Chem. Phys. Vol. 67, 5877-5882 (1977)

Murphy, W.F., "The ro-vibrational Raman spectrum of water vapour υ_2 and $2\upsilon_2$," Mol. Phys., Vol 33, pp. 1701-1714 (1977).

Murphy, W.F., "Intensities of rotation and vibration-rotation Raman transitions in asymetric top molecules," J. Raman Spectr., Vol 11, pp. 339-345 (1981).

Nedelijkovic,D., A. Hauchecorne, and M.-L. Chanin, "Rotational Raman lidar to measure the atmospheric temperature from the ground to 30 km," IEEE Trans. Geosci. Rem. Sens. Vol. 31, 90-101 (1993)

Penney, C. M., R. L. St. Peters, and M. Lapp, "Absolute rotational Raman cross sections for N_2, O_2, and CO_2," J. Opt. Soc. Am. Vol. 64, 712-716 (1974)

Philbrick, C. R., F. J. Schmidlin, K. U. Grossmann, G. Lange, D. Offermann, K. D. Baker, D. Krankowsky, U. von Zahn, "Density and temperature structure over northern Europe," Journal of Atmospheric and Terrestrial Physics Vol. 47, No. 1-3, pp. 159-172 (1985).

Philbrick, C. R., D. P. Sipler, B. E. Dix, G. Davidson, W. P. Moskowitz, C. Trowbride, R. Sluder, F. J. Schmidlin, L.D. Mendenhall, K. H. Bhavnani, and K. J. Hahn, "Measurements of the high latitude middle atmosphere properties using LIDAR," AFGL-TR-87-0053, Environmental Research Papers, No. 976, Geophysics Laboratory, 129 pages (1987).

Philbrick, C. R., D. B. Lysak, T. D. Stevens, P. A. T. Haris, and Y. -C. Rau, "Atmospheric Measurements using the LAMP lidar during the LADIMAS campaign," Proceedings of the 16th International Laser Radar Conference, NASA Conference publications, No. 3158, pp. 651-654 (1992).

Philbrick, C.R., "Raman lidar measurements of atmospheric properties," Proceedings of Atmospheric Propogation and Remote Sensing III, SPIEE 2222, 922-931 (1994)

Placzek, G., "The Rayleigh and Raman Scattering," Translated by A. Werbin, UCRL Trans.Vol. 256(L) (1934)

Rau, Yi.-C, "Multi-wavelength Raman-Rayleigh lidar for atmospheric remote sensing," Ph.D. Thesis, The Pennsylvania State University (1994)

Ray, B.S., Z. Physik, Vol. 78, pp. 74 (1932)

Salzman, J.A., "Low temperature measurements by rotational raman scattering," in Laser Raman Gas Diagnostics, edited by M. Lapp and C.M. Penney, Plenum Press, NY (1974)

Schmidlin, F.J., "Radiosonde temperature and humidity measurement errors and their effect on global change," AMS 5th Symposium on global change studies, pp. 209-212 (1994)

Stevens, T. D., P. A. T. Haris, Y. -C. Rau, C. R. Philbrick, "Latitudinal lidar mapping of stratospheric particle layers," Adv. in Spac. Res., (1993)

Stevens, T. D., "An optical detection system for a Rayleigh/Raman lidar," MS Thesis, The Pennsylvania State University, 1992.

Stowe, L. L., R. M. Carey, and P. P. Pellegrino, "Monitoring the Mt. Pinatubo aerosol layer with NOAA/11 AVHRR data," Geophysical Research Letters Vol 19, No. 2, pp. 150-162 (1990).

Taylor, P.A., J.R. Salmon, R.E. Stewart, "Mesoscale observations of surface fronts and low pressure centres in Canadian east coast winter storms," Boundary-Layer Meteo. Vol 64, 15-54 (1993)

Theopold, F.A., J. Bosenberg, "Differential absorption lidar measurements of atmospheric temperature profiles: theory and experiment," J. Atmos. Oceanic Tech. Vol. 10, 165-178 (1993)

U.S. Standard Atmosphere, 1976, National Oceanic and Atmospheric Administration, Washington, D.C., 1976.

Vaughan, G., D. P. Wareing, S. J. Pepler, L. Thomas, and V. Mitev, "Atmospheric temperature measurements made by rotational Raman scattering," Appl. Opt. **32**, 2758-2764 (1993)

Watson, J.K.G., "Determination of centrifugal distortion coefficients of asymetric-top molecules," J. Chem. Phys., Vol 46, 1935-1949 (1967)

Appendix A

OPTICS FOR THE LAMP LOW ALTITUDE DETECTOR BOX

Optic numbers are in reference to Figure 1.2. All wavelengths are in nanometers when units are not specified.

Abbreviations:

R	Reflect
T	Transmit
f.	focal length

1	Fused silica optical fiber	1mm dia. core
2	Fused silica plano-convex lens; 38mm f.	25.4mm dia.
3	Beamsplitter: R: 277, 283, 294 T: 528, 530, 532, 607, 660 or R: 355, 387, 407 T: 528, 530, 532, 607, 660	2" dia. 1/16" thick 2" dia. 3/8" thick
4	Beamsplitter: R: 294, T: 277, 283 or R: 407, T: 355, 387	2" dia. 1/16" thick 2" dia. 3/8" thick
5	Metal oxide 294 or 407 narrow band filter, 0.35nm bandwidth	1" dia.
6	Fused silica plano convex lens; AR coated; 100mm f.	25.4mm dia.
7	Beamsplitter: R: 283, T: 277 or R: 387, T: 355	2" dia., 1/16" thick 2" dia., 3/8" thick
8	Metal oxide 283 or 387 narrow band filter, 0.35nm bandwidth	1" dia.
9	Fused silica plano convex lens; AR coated; 100mm f.	25.4mm dia.
10	Neutral density filter	1" dia.
11	Metal oxide 277 or 355 narrow band filter; 0.35nm bandwidth	1" dia.
12	Fused silica plano convex lens; AR coated; 100mm f.	25.4mm dia.
13	BK7 window; AR coated	2" dia., 3/8" thick
14	Beamsplitter: R: 528, 530, 532, T: 607, 660,	2" dia., 3/8" thick
15	Beamsplitter: R: 532, T: 528, 530; 15° optimal incident angle	1" dia., 1/8" thick
16	Highly reflective broadband mirror	2" dia., 3/8" thick
17	Neutral density filter	1" dia.
18a	BK7 window	1" dia.
18b	Dielectric 532 narrow band filter; 0.35nm bandwidth	1" dia.
19	BK7 plano convex lens; AR coated; 100mm f.	25.4mm dia.
20	BK7 plano convex lens; 500mm f.	2" dia.

21	Beamsplitter: R: 530, T: 528; 15° optimal incident angle	1" dia., 1/8" thick
22	Highly reflective broadband mirror	2" dia., 3/8" thick
23a	BK7 window	1" dia.
23b	2 dielectric 530 narrow band filters; 0.35nm bandwidth	1" dia.
24	BK7 plano convex lens; AR coated; 88mm f.	25.4mm dia.
25a	BK7 window	1" dia.
25b	2 dielectric 528nm narrow band filters; 0.35nm bandwidth	1" dia.
26	BK7 plano convex lens; AR coated; 88mm f.	25.4mm dia.
27	Beamsplitter: R: 660, T: 607	2" dia., 3/8" thick
28a	BK7 window	1" dia.
29	BK7 plano convex lens; AR coated; 88mm f.	25.4mm dia.
30	2 dielectric 607nm narrow band filters; 0.35nm bandwidth	1" dia.
31	Highly reflective broadband mirror	2" dia., 3/8" thick
32a	BK7 window	1" dia.
32b	2 dielectric 660nm narrow band filters; 0.35nm bandwidth	1" dia.
33	BK7 plano convex lens; AR coated; 88mm f.	25.4mm dia.
34	Thorn EMI photomultiplier tube, 9268B	
35	Thorn EMI photomultiplier tube, 9893Q/350B, photon counter	
36	Thorn EMI photomultiplier tube, 9893Q/350B, photon counter	
37	Thorn EMI photomultiplier tube, 9893Q/350B, photon counter	
38	Thorn EMI photomultiplier tube, 9863/350B, photon counter, thermally cooled with an Amherst cold housing	
39	Thorn EMI photomultiplier tube, 9863/350B, photon counter, thermally cooled with an Amherst cold housing	
40	Thorn EMI photomultiplier tube, 9863/350B, photon counter, thermally cooled with an Amherst cold housing	
41	Thorn EMI photomultiplier tube, 9863/350B, photon counter, thermally cooled with an Amherst cold housing	

Appendix B

COMPUTER PROGRAM FOR THE CALCULATION OF THE WATER VAPOR ENERGY TRANSITIONS AND EIGENFUNCTIONS

This program calculates the energies and wavefunctions of the water vapor molecule. It was originally developed by William F. Murphy [1977]. The input file which contains the parameters of the reduced molecular Hamiltonian is given below.

```
          12
     532.1e-007
   835839.672      435346.828      278140.312
     37.5917        -173.3183        974.444       15.22164       39.603
    0.016515         -0.05720        -0.5203         3.8620
   0.0081761         -0.02623         0.9305
 -0.00001107        0.0001315      -0.002070        0.00773      -0.02650
 -0.000004751       0.0000160       0.000577       -0.01035
0.00000000329    -0.000000294    -0.00000134
    0.0000263        -0.0000652       0.0001792
          0.0      -0.000000150             0.0    -0.00000960     0.0000590
-0.0000005670
```

```
CMMMMMMMMMMMMMMMMMMMMMMMMMMMMMMMMMMMMMMMMMMMMMMMMMMMMMMM
C
C                    PROGRAM ASYME
C              MAIN ROUTINE FOR CALCULATION OF
C       ASYMETRIC TOP ROTOR ENERGIES AND EIGENFUNCTIONS
C       USES DIRECT ACCESS I O, AND ISMLIB EIGENVALUE ROUTINE
C
CMMMMMMMMMMMMMMMMMMMMMMMMMMMMMMMMMMMMMMMMMMMMMMMMMMMMMMM
      IMPLICIT REAL*8 (A-H,O-Z)
      DIMENSION ED(100),EE(100),Z(100,100)
      CHARACTER*4 MOUT(2)/' NOT',' ARE'/
      CHARACTER*35 mrootdir

      COMMON /MOLCON/ XJJ1,EDK0,EDK2,EDK4,EDK6,EDK8,EDK10,EDK12,
     +            EEK0,EEK2,EEK4,EEK6,EEK8,KMAX
      DATA IDSRN/20/
      mrootdir = 'c:\thesis\phd\fortran\programs\h2o\'

      PRINT *, 'ENTER Jmax'
      READ (*,'(I4)') JMAX
      PRINT *, 'ENTER Jmin'
      READ (*,'(I4)') JMIN
      PRINT *, 'ENTER Kmax'
      READ (*,'(I4)') KMAX
      IF (JMAX.GT.100) STOP 1

C     STOP 1- ERROR STOP- PRESENT VERSION DIMENSIONED FOR JMAX.LE.100
C       NOTE: FOR JMAX>20,
C           USE VERSION OF 'SAVEWF' WHICH TRUNCATES WAVE FUNCTIONS
C                - MANDATORY FOR JMAX>60

      IF (JMAX.GT.60) ISW = 1
      IF (KMAX.LE.0.OR.KMAX.GT.JMAX) KMAX = JMAX

C     OPEN(3,FILE=mrootdir//'results\h2ocoef.dat')
      OPEN(3,FILE=mrootdir//'results\h2oengr.dat')
      WRITE (3,502) JMIN,JMAX,KMAX,MOUT(ISW+1)
      CALL INCONS
      WRITE (3,505)
      DO 60 J = JMIN,JMAX
    5 IZ = (J+2)/2
        XJJ1 = DFLOAT(J*(J+1))
        DO 50 ITMIN = 0,3
          CALL SETUPH (J,ITMIN,IZ,ED,EE,NTH,Z,N)
C             PRINT *, 'Tag3',J,ITMIN,N

          IF(N-1) 50,30,20
   20     CALL TQL2(IZ,NTH,ED,EE,Z,IERR)

C-------------------------------------------------
C       ADD CONSTANT OFFSET TO EIGENVALUES
C-------------------------------------------------
```

```
 30    DO 40 I=1,NTH
 40    ED(I) = ED(I)+EDK0
       CALL SAVEWF (IDSRN,J,ITMIN,ED,N,Z,IZ,ISW)
       CALL PREWF (J,ITMIN,ED,N,Z,IZ,0)
 50   CONTINUE
      WRITE (3,507)
 60 CONTINUE

 500 FORMAT (4I5)
 502 FORMAT ('1',10X,'ASYMMETRIC ROTOR ENERGIES AND EIGENFUNCTIONS'//
    +  11X,'IR REP.- WATSON A HAMILTONIAN    JMIN,JMAX,KMAX=',3I5/
    +  '0',10X,'OUTPUT WAVE FUNCTIONS',A4,' TRUNCATED.'//)
C  505 FORMAT ('0',4X,'J',4X,'TAU',4X,'KP',4X,'KO',2X,'SUBMAT',5X,
C    +       'ENERGY',8X,'WAVE FUNCTION'/
C    +  '0')
 505 FORMAT ('0',4X,'J',4X,'TAU',4X,'KP',4X,'KO',2X,'SUBMAT',5X,
    +       'ENERGY'/
    +  '0')
 507 FORMAT ('0')

      STOP
      END


CSSSSSSSSSSSSSSSSSSSSSSSSSSSSSSSSSSSSSSSSSSSSSSSSSSSSSSSSSSSSSSSSSSSSSSSSS
C
C     INPUT ROUTINE FOR ASYMMETRIC TOP MOLECULAR CONSTANTS
C     WATSON A REDUCTION
C
CSSSSSSSSSSSSSSSSSSSSSSSSSSSSSSSSSSSSSSSSSSSSSSSSSSSSSSSSSSSSSSSSSSSSSSSSS
      SUBROUTINE INCONS

      IMPLICIT REAL*8 (A-H,O-Z)
      COMMON /consc/ CONS(37)
      CHARACTER*35 mrootdir

      mrootdir = 'c:\thesis\phd\fortran\programs\h2o\'
C-----------------------------------
C     READ & PRINT TITLE
C-----------------------------------

      OPEN (1, FILE = mrootdir//'H2OCONS.DAT')

C     READ (1,500) (CONS(I),I=1,10)
C     WRITE (3,501) (CONS(I),I=1,10)
C     WRITE (3,501)

      READ (1,502) IORDER
      PRINT *, IORDER
      IF(IORDER.LE.0) RETURN

      DO 10 I = 1, 37, 1
```

```
      CONS(I) = 0.0D0
   10 CONTINUE

      READ (1,505) CONS(1)
      IF(IORDER.LT.2) RETURN

      READ (1,505) (CONS(I),I=2,4)
      IF(IORDER.LT.4) RETURN

      READ (1,505) (CONS(I),I=5,9)
      IF(IORDER.LT.6) RETURN

      READ (1,505) (CONS(I),I=10,13)
      READ (1,505) (CONS(I),I=14,16)
      IF(IORDER.LT.8) RETURN

      READ (1,505) (CONS(I),I=17,21)
      READ (1,505) (CONS(I),I=22,25)
      IF(IORDER.LT.10) RETURN

      READ (1,505) (CONS(I),I=26,28)
      READ (1,505) (CONS(I),I=29,31)
      READ (1,505) (CONS(I),I=32,36)
      IF(IORDER.LT.12) RETURN

      READ (1,505) CONS(37)

C     CONS(1) = 1/CONS(1)
c     DO 20 I = 2,37,1
C        CONS(I) = CONS(I)/2.9979258E10
C   20 CONTINUE

      WRITE (3,503) IORDER
      WRITE (3,506) CONS(1)
      WRITE (3,507) (CONS(I),I=2,4)
      WRITE (3,508) (CONS(I),I=5,9)
      WRITE (3,509) (CONS(I),I=10,16)
      WRITE (3,510) (CONS(I),I=17,25)
      WRITE (3,511) (CONS(I),I=26,36)
      WRITE (3,512) CONS(37)

C  500 FORMAT (10A8)
C  501 FORMAT ('0',10A8)
   501 FORMAT ('0')
   502 FORMAT (I15)
   503 FORMAT ('0  MOLECULAR CONSTANTS INCLUDING TERMS TO ORDER',I3)
   505 FORMAT (5F15.5)
   506 FORMAT ('0BAND ORIGIN =',E15.5E2)
   507 FORMAT ('0      A,B,C =',3F15.6)
   508 FORMAT ('0D(J),D(JK),D(K),DEL(J),DEL(K)=',T40,1P,5D14.5)
   509 FORMAT ('0       H(J),H(JK),H(KJ),H(K)=',T40,1P,4D14.5/
     +       '             h(J),h(JK),h(K)=',T40,3D14.5)
```

```
 510 FORMAT ('0L(J),L(JJK),L(JK),L(KKJ),L(K)=',T40,1P,5D14.5/
  +       '       l(J),l(JK),l(KJ),l(K)=',T40,4D14.5)
 511 FORMAT ('0P(J),P(JJK),P(JK),P(KJ),P(KKJ),P(K)=',T40,1P,6D14.5/
  +       '      p(J),p(JJK),p(JK),p(KKJ),p(K)=',T40,5D14.5)
 512 FORMAT ('0T(K)=',T40,1PD14.5)
     RETURN
     END

CSSSSSSSSSSSSSSSSSSSSSSSSSSSSSSSSSSSSSSSSSSSSSSSSSSSSSSSSSSSSSSSSSSSSSSSSSSS
C
C    ROUTINE TO SET UP HAMILTONIAN MATRIX
C        - FOR ASYM TOP CALC - interacting level case
C
CSSSSSSSSSSSSSSSSSSSSSSSSSSSSSSSSSSSSSSSSSSSSSSSSSSSSSSSSSSSSSSSSSSSSSSSSSSS
     SUBROUTINE SETUPH (J,ITMIN,IZ,ED,EE,NTH,Z,N)

     IMPLICIT REAL*8 (A-H,O-Z)
     DIMENSION ED(100),EE(100),z(100)
     COMMON /consc/ CONS(37)
     REAL*8 LLJ,LLJJK,LLJK,LLKKJ,LLK,LJ,LJK,LKJ,LK

     EQUIVALENCE (CONS(1),ORIGIN),
    +     (CONS(2),A),(CONS(3),B),(CONS(4),C),
    +     (CONS(5),DELTJ),(CONS(6),DELTJK),(CONS(7),DELTK),
    +       (CONS(8),DELJ),(CONS(9),DELK),
    +     (CONS(10),HHJ),(CONS(11),HHJK),(CONS(12),HHKJ),
    +       (CONS(13),HHK),
    +       (CONS(14),HJ),(CONS(15),HJK),(CONS(16),HK),
    +     (CONS(17),LLJ),(CONS(18),LLJJK),(CONS(19),LLJK),
    +       (CONS(20),LLKKJ),(CONS(21),LLK),
    +       (CONS(22),LJ),(CONS(23),LJK),(CONS(24),LKJ),(CONS(25),LK),
    +     (CONS(26),PPJ),(CONS(27),PPJJK),(CONS(28),PPJK),
    +       (CONS(29),PPKJ),(CONS(30),PPKKJ),(CONS(31),PPK),
    +       (CONS(32),PJ),(CONS(33),PJJK),(CONS(34),PJK),
    +       (CONS(35),PKKJ),(CONS(36),PK),
    +     (CONS(37),TTK)

     COMMON /MOLCON/ XJJ1,EDK0,EDK2,EDK4,EDK6,EDK8,EDK10,EDK12,
    +             EEK0,EEK2,EEK4,EEK6,EEK8,KMAX

     E00 = (B+C)/2D0

C----------------------------------------
C    set constant offset to 0
C----------------------------------------

     EDK0 = 0D0
     EDK2 = A-E00 +XJJ1*(-DELTJK+XJJ1*(HHJK  +XJJ1*(LLJJK
    +          +XJJ1* PPJJK)))
     EDK4 = -DELTK+XJJ1*(HHKJ   +XJJ1*(LLJK  +XJJ1* PPJK))
     EDK6 = HHK   +XJJ1*(LLKKJ  +XJJ1* PPKJ)
     EDK8 = LLK   +XJJ1* PPKKJ
```

```
      EDK10 = PPK
      EDK12 = TTK

      EEK0 = (B-C)/4D0 +XJJ1*(-DELJ  +XJJ1*(HJ    +XJJ1*(LJ
     +             +XJJ1* PJ)))
      EEK2 = (-DELK   +XJJ1*(HJK    +XJJ1*(LJK   +XJJ1* PJJK)))/2D0
      EEK4 = (HK      +XJJ1*(LKJ    +XJJ1* PJK))/2D0
      EEK6 = (LK      +XJJ1* PKKJ)/2D0
      EEK8 =  PK/2D0

      N = 0

C-----------------------------------------------------
C     for offset correction in one dimensional case
C-----------------------------------------------------
      Nth = 1
      EE(1) = 0D0

      GO TO (30,20,20,10),ITMIN+1

C       E-  CASE

   10 IF(J.LT.2) RETURN
      ED(1) = EDK0+4D0*(EDK2+4D0*(EDK4+
     +          4D0*(EDK6+4D0*(EDK8+4D0*(EDK10+4D0*EDK12)))))
      N = 1
      GO TO 45

C       O-,O+  CASES

   20 IF(J.LT.1) RETURN
      ED(1) = EDK0+EDK2+EDK4+EDK6+EDK8+EDK10+EDK12+
     +         DFLOAT(2*ITMIN-3)*XJJ1*(EEK0+2D0*(EEK2+EEK4+EEK6+EEK8))
      N = 1
      IK = 3
      GO TO 50

C       E+  CASE

   30 ED(1) = EDK0
      N = 1
      IF (J.LT.2) GO TO 60
      EE(2) = (EEK0+4D0*(EEK2+4D0*(EEK4+4D0*(EEK6+4D0*EEK8))))
     +         *DSQRT(2D0*XJJ1*(XJJ1-2D0))
      ED(2) = EDK0+4D0*(EDK2+4D0*(EDK4+
     +          4D0*(EDK6+4D0*(EDK8+4D0*(EDK10+4D0*EDK12)))))
      z(iz+2) = 1.0D0
      z(iz+1) = 0.0D0
      z(2) = 0.0D0

      N = 2
      NTH = 2
```

```
 45 IK = 4

C FINISH

 50 IF(J.GE.IK) CALL RESTH(J,N,IK,ED,EE,NTH,Z,IZ)

C----------------------------------------
C    calculate constant offset
C----------------------------------------
 60 EDK0 = ORIGIN
  +      + XJJ1*(E00+XJJ1*(-DELTJ+XJJ1*(HHJ+XJJ1*(LLJ+XJJ1*PPJ))))
    z(1) = 1.0D0

    RETURN
    END

CSSSSSSSSSSSSSSSSSSSSSSSSSSSSSSSSSSSSSSSSSSSSSSSSSSSSSSSSSSSSSSSSSSSSSSSSSS
C
C    ROUTINE TO SET UP PART OF HAMILTONIAN MATRIX FOR ASYM TOP CALC
C
CSSSSSSSSSSSSSSSSSSSSSSSSSSSSSSSSSSSSSSSSSSSSSSSSSSSSSSSSSSSSSSSSSSSSSSSSSS
    SUBROUTINE RESTH (J,N,IK,ED,EE,NTH,Z,IZ)

    IMPLICIT REAL*8 (A-H,O-Z)
    DIMENSION ED(100),EE(100),Z(IZ,IZ)
    COMMON /MOLCON/ XJJ1,EDK0,EDK2,EDK4,EDK6,EDK8,EDK10,EDK12,
   +           EEK0,EEK2,EEK4,EEK6,EEK8,KMAX

    DO 20 K=IK,J,2
     DO 10 L=1,N
     Z(N+1,L) = 0.0D0
 10  Z(L,N+1) = 0.0D0
     N = N+1
     Z(N,N) = 1.0D0
     IF (K.LE.KMAX) THEN
      NTH = N
      XK = DFLOAT(K)
      XKK = XK*XK
      XK22 = (XK-2.D0)**2
      ED(N) = EDK0+XKK*(EDK2+XKK*(EDK4+
   +         XKK*(EDK6+XKK*(EDK8+XKK*(EDK10+XKK*EDK12)))))
      EE(N) = (EEK0+EEK2*(XK22+XKK)
   +           +EEK4*(XK22**2+XKK**2)
   +           +EEK6*(XK22**3+XKK**3)
   +           +EEK8*(XK22**4+XKK**4))*
   +          DSQRT((XJJ1-XKK+XK)*(XJJ1-(XK-1.D0)*(XK-2.D0)))
     ELSE
      ED(N) = -1D0
     ENDIF
 20 CONTINUE
    RETURN
    END
```

```
CSSSSSSSSSSSSSSSSSSSSSSSSSSSSSSSSSSSSSSSSSSSSSSSSSSSSSSSSSSSSSSSSSSSSSSS
C
C    ROUTINE TO STORE ASYM TOP ENERGIES AND WAVE FUNCTIONS
C    AS REQUIRED BY INTENSITY CALC ROUTINES
C    VERSION USED CONTROLLED BY NLEV
C
CSSSSSSSSSSSSSSSSSSSSSSSSSSSSSSSSSSSSSSSSSSSSSSSSSSSSSSSSSSSSSSSSSSSSSSS
      SUBROUTINE SAVEWF (IDSRN,J,ITMIN,ED,N,Z,IZ,NLEV)

      REAL*8 ED(IZ),Z(IZ,IZ)
      REAL*8 SEZ(998)
      INTEGER*2 IZPNT(2,100)
      CHARACTER*43 mrootdir

      mrootdir = 'c:\thesis\phd\fortran\programs\h2o\results\'
      OPEN (20, FILE=mrootdir//'h2oasyme.dat')

      IF (NLEV-1) 10,100,200

C-----------------------------------------
C    SIMPLE VERSION
C-----------------------------------------
   10 WRITE (IDSRN, '(702E15.8E2)') (ED(I),I=1,N),
     +     ((Z(I,II),I=1,N),II=1,N)
      RETURN
C-----------------------------------------------------------------
C    OUTPUT ENERGIES AND WAVE FUNCTIONS INTO DA DATA SET
C    SINGLE PRECISION- PACK EIGENVECTORS, KEEPING ONLY THOSE > ZLIM
C    TO STAY WITHIN 4000 BYTE LIMIT FOR DA RECORD SIZE
C-----------------------------------------------------------------
C*****  FOR DEBUGGING - USE SIMPLE FORM
C-----------------------------------------------------------------

  100 IF(NLEV.EQ.1) GO TO 10
      ZLIM = 1D-6
  115 IPZ = N
      DO 150 JJ=1,N
        SEZ(JJ) = ED(JJ)
        DO 120 I=1,N
          IF(ABS(Z(I,JJ)).GE.ZLIM) GO TO 130
  120   CONTINUE

C     ---------------------------------------------------------
C       INDEX OF 1ST ELEMENT > ZLIM OF JJTH EIGENVECTOR (LESS 1)
C     ---------------------------------------------------------
  130   IZPNT(1,JJ) = I-1
        I1 = I
        DO 140 I=I1,N
          IF(ABS(Z(I,JJ)).LT.ZLIM) GO TO 145
          IPZ = IPZ+1
          IF(IPZ.LE.998-N) GO TO 140
```

```
C    ------------------------------------------------------------
C         THIS SECTION ENTERED IF RECORD LONGER THAN ALLOWED
C    ------------------------------------------------------------
       ZLIM = 1E1*ZLIM

C    ------------------------------------------------------------
C         STOP 99991- ERROR STOP; ZLIM = .001
C    ------------------------------------------------------------
       IF(ZLIM.GE.1E-3) STOP 99991
       WRITE (3,510) ZLIM
       GO TO 115
  140  SEZ(IPZ) = Z(I,JJ)

C    ------------------------------------------------------------
C      OUTPUT VECTOR INDEX OF LAST ELEMENT OF JJTH EIGENVECTOR
C    ------------------------------------------------------------
  145  IZPNT(2,JJ) = IPZ
  150 CONTINUE

      WRITE (IDSRN, '(100(E15.8E2))')
     +      ((IZPNT(I,II),I=1,2),II=1,N),(SEZ(I),I=1,IPZ)
      RETURN

C    ------------------------------------------------------------
C          VERSION FOR INTERACTING VIBRATIONAL LEVELS
C         STORED ENERGY VECTOR LENGTH DEPENDS ONLY ON J
C              (ONLY N VALID ENTRIES)
C    ------------------------------------------------------------
  200 ND = (J/2+1)*NLEV

C    ------------------------------------------------------------
C            ACTUAL DIMENSION OF WAVE FUNCTION
C    ------------------------------------------------------------
      NE = (J+2-(ITMIN+1)/2)/2
      WRITE (IDSRN, '(I15,702E15.8E2)') N,(ED(I),I=1,ND),
     +  ((Z(I,II),I=1,NE),II=1,N)

  510 FORMAT (' ***** WARNING- RECORD SIZE FOR',2I4,
     + ' GREATER THAN ONE PAGE,'/' TRUNCATION LIMIT RESET TO ',1PD10.1)

      RETURN
      END

CSSSSSSSSSSSSSSSSSSSSSSSSSSSSSSSSSSSSSSSSSSSSSSSSSSSSSSSSSSSSSSSSSSSSSSSSSSSS
C
C    ROUTINE TO PRINT ENERGIES AND WAVEFUNCTIONS AS CALCULATED
C       - FOR ASYMMETRIC TOP
C
CSSSSSSSSSSSSSSSSSSSSSSSSSSSSSSSSSSSSSSSSSSSSSSSSSSSSSSSSSSSSSSSSSSSSSSSSSSSS
      SUBROUTINE PREWF (J,ITMIN,ED,N,Z,IZ,ISW)

      IMPLICIT REAL*8 (A-H,O-Z)
```

```
      DIMENSION ED(100),Z(IZ,IZ)
      CHARACTER*4 LABEL(4)/' E+ ',' O- ',' O+ ',' E- '/
      ND = (J+2-(ITMIN+1)/2)/2
      KP = (ITMIN-4)/2
      KO = J-ITMIN/2+2
      DO 40 I=1,N
        KP = KP+2
        KO = KO-2
        IF(ISW.LE.1) GO TO 35
        KP = 0
        KO = 0
        IMAX = IABSMAX(ND,Z(1,I))
        IF(DABS(Z(IMAX,I)).LT.1D-1) GO TO 35
        KP = 2*IMAX-(4-ITMIN)/2
        KO = J+MOD(ITMIN,2)-KP
   35   ITAU = KP-KO
   40 WRITE (3,501) J,ITAU,KP,KO,LABEL(ITMIN+1),ED(I) !! ,(Z(K,I),K=1,ND)
  501 FORMAT (4I6,4X,A4,1X,E15.8E2,50E15.8E2)

      RETURN
      END


CSSSSSSSSSSSSSSSSSSSSSSSSSSSSSSSSSSSSSSSSSSSSSSSSSSSSSSSSSSSSSSSSSSSSSSSSSS
C
C     THIS SUBROUTINE FINDS THE EIGENVALUES AND EIGENVECTORS
C     OF A SYMMETRIC TRIDIAGONAL MATRIX BY THE QL METHOD.
C     THE EIGENVECTORS OF A FULL SYMMETRIC MATRIX CAN ALSO
C     BE FOUND IF  TRED2  HAS BEEN USED TO REDUCE THIS
C     FULL MATRIX TO TRIDIAGONAL FORM.
CC
CSSSSSSSSSSSSSSSSSSSSSSSSSSSSSSSSSSSSSSSSSSSSSSSSSSSSSSSSSSSSSSSSSSSSSSSSSS
C
C-----------------------------------------------------------------------C
C     THIS SUBROUTINE IS A TRANSLATION OF THE ALGOL PROCEDURE TQL2,
C     NUM. MATH. 11, 293-306(1968) BY BOWDLER, MARTIN, REINSCH, AND
C     WILKINSON.
C     HANDBOOK FOR AUTO. COMP., VOL.II-LINEAR ALGEBRA, 227-240(1971).
C
C
C     ON INPUT
C
C       NM MUST BE SET TO THE ROW DIMENSION OF TWO-DIMENSIONAL
C         ARRAY PARAMETERS AS DECLARED IN THE CALLING PROGRAM
C         DIMENSION STATEMENT.
C
C       N IS THE ORDER OF THE MATRIX.
C
C       D CONTAINS THE DIAGONAL ELEMENTS OF THE INPUT MATRIX.
C
C       E CONTAINS THE SUBDIAGONAL ELEMENTS OF THE INPUT MATRIX
C         IN ITS LAST N-1 POSITIONS.  E(1) IS ARBITRARY.
```

```
C
C      Z CONTAINS THE TRANSFORMATION MATRIX PRODUCED IN THE
C        REDUCTION BY  TRED2, IF PERFORMED.  IF THE EIGENVECTORS
C        OF THE TRIDIAGONAL MATRIX ARE DESIRED, Z MUST CONTAIN
C        THE IDENTITY MATRIX.
C
C     ON OUTPUT
C
C      D CONTAINS THE EIGENVALUES IN ASCENDING ORDER.  IF AN
C        ERROR EXIT IS MADE, THE EIGENVALUES ARE CORRECT BUT
C        UNORDERED FOR INDICES 1,2,...,IERR-1.
C
C      E HAS BEEN DESTROYED.
C
C      Z CONTAINS ORTHONORMAL EIGENVECTORS OF THE SYMMETRIC
C        TRIDIAGONAL (OR FULL) MATRIX.  IF AN ERROR EXIT IS MADE,
C        Z CONTAINS THE EIGENVECTORS ASSOCIATED WITH THE STORED
C        EIGENVALUES.
C
C      IERR IS SET TO
C        ZERO      FOR NORMAL RETURN,
C        J         IF THE J-TH EIGENVALUE HAS NOT BEEN
C                  DETERMINED AFTER 30 ITERATIONS.
C
C     CALLS PYTHAG FOR  DSQRT(A*A + B*B) .
C
C     QUESTIONS AND COMMENTS SHOULD BE DIRECTED TO BURTON S. GARBOW,
C     MATHEMATICS AND COMPUTER SCIENCE DIV, ARGONNE NATIONAL
C     LABORATORY
C
C     THIS VERSION DATED AUGUST 1983.
C
C------------------------------------------------------------------------
      SUBROUTINE TQL2(NM,N,D,E,Z,IERR)

      INTEGER I,J,K,L,M,N,II,L1,L2,NM,MML,IERR
      DOUBLE PRECISION D(N),E(N),Z(NM,N)
      DOUBLE PRECISION C,C2,C3,DL1,EL1,F,G,H,P,R,S,S2,TST1,TST2,PYTHAG

      IERR = 0
      IF (N .EQ. 1) GO TO 1001

      DO 100 I = 2, N
  100 E(I-1) = E(I)

      F = 0.0D0
      TST1 = 0.0D0
      E(N) = 0.0D0

      DO 240 L = 1, N
        J = 0
        H = DABS(D(L)) + DABS(E(L))
```

```
      IF (TST1 .LT. H) TST1 = H

C     ------------------------------------------------------------
C          .... LOOK FOR SMALL SUB-DIAGONAL ELEMENT ....
C     ------------------------------------------------------------
      DO 110 M = L, N
        TST2 = TST1 + DABS(E(M))
        IF (TST2 .EQ. TST1) GO TO 120

C       ------------------------------------------------------
C            ... E(N) IS ALWAYS ZERO, SO THERE IS NO EXIT
C                  THROUGH THE BOTTOM OF THE LOOP ...
C       ------------------------------------------------------
  110   CONTINUE

  120   IF (M .EQ. L) GO TO 220
  130   IF (J .EQ. 30) GO TO 1000
        J = J + 1

C     ----------------------------------
C          ..... FORM SHIFT .....
C     ----------------------------------
      L1 = L + 1
      L2 = L1 + 1
      G = D(L)
      P = (D(L1) - G) / (2.0D0 * E(L))
      R = PYTHAG(P,1.0D0)
      D(L) = E(L) / (P + DSIGN(R,P))
      D(L1) = E(L) * (P + DSIGN(R,P))
      DL1 = D(L1)
      H = G - D(L)
      IF (L2 .GT. N) GO TO 145

      DO 140 I = L2, N
  140   D(I) = D(I) - H

  145   F = F + H

C     ---------------------------------------
C          .... QL TRANSFORMATION ....
C     ---------------------------------------
      P = D(M)
      C = 1.0D0
      C2 = C
      EL1 = E(L1)
      S = 0.0D0
      MML = M - L

C     ------------------------------------------------------
C          .... FOR I=M-1 STEP -1 UNTIL L DO -- ....
C     ------------------------------------------------------
      DO 200 II = 1, MML
```

```
        C3 = C2
        C2 = C
        S2 = S
        I = M - II
        G = C * E(I)
        H = C * P
        R = PYTHAG(P,E(I))
        E(I+1) = S * R
        S = E(I) / R
        C = P / R
        P = C * D(I) - S * G
        D(I+1) = H + S * (C * G + S * D(I))

C       ---------------------------------
C            ... FORM VECTOR ...
C       ---------------------------------
        DO 180 K = 1, N
          H = Z(K,I+1)
          Z(K,I+1) = S * Z(K,I) + C * H
          Z(K,I) = C * Z(K,I) - S * H
 180     CONTINUE
 200   CONTINUE

      P = -S * S2 * C3 * EL1 * E(L) / DL1
      E(L) = S * P
      D(L) = C * P
      TST2 = TST1 + DABS(E(L))
      IF (TST2 .GT. TST1) GO TO 130
 220   D(L) = D(L) + F
 240 CONTINUE

C    ----------------------------------------------------------
C         .... ORDER EIGENVALUES AND EIGENVECTORS ....
C    ----------------------------------------------------------
    DO 300 II = 2, N
      I = II - 1
      K = I
      P = D(I)
      DO 260 J = II, N
        IF (D(J) .GE. P) GO TO 260
        K = J
        P = D(J)
 260   CONTINUE
      IF (K .EQ. I) GO TO 300
      D(K) = D(I)
      D(I) = P
      DO 280 J = 1, N
        P = Z(J,I)
        Z(J,I) = Z(J,K)
        Z(J,K) = P
 280   CONTINUE
 300 CONTINUE
```

```
      GO TO 1001

C    --------------------------------------------------------
C          .... SET ERROR -- NO CONVERGENCE TO AN
C             EIGENVALUE AFTER 30 ITERATIONS ....
C    --------------------------------------------------------
 1000 IERR = L

 1001 RETURN
      END


CFFFFFFFFFFFFFFFFFFFFFFFFFFFFFFFFFFFFFFFFFFFFFFFFFFFFFFFFFFFFFFFFFFFFFFF
C
C    FINDS DSQRT(A**2+B**2) WITHOUT OVERFLOW OR DESTRUCTIVE
C    UNDERFLOW
C
CFFFFFFFFFFFFFFFFFFFFFFFFFFFFFFFFFFFFFFFFFFFFFFFFFFFFFFFFFFFFFFFFFFFFFFF
      DOUBLE PRECISION FUNCTION PYTHAG(A,B)

      DOUBLE PRECISION A,B
      DOUBLE PRECISION P,R,S,T,U
      P = DMAX1(DABS(A),DABS(B))
      IF (P .EQ. 0.0D0) GO TO 20
      R = (DMIN1(DABS(A),DABS(B))/P)**2
   10 CONTINUE
         T = 4.0D0 + R
         IF (T .EQ. 4.0D0) GO TO 20
         S = R/T
         U = 1.0D0 + 2.0D0*S
         P = U*P
         R = (S/U)**2 * R
      GO TO 10
   20 PYTHAG = P

      RETURN
      END


CFFFFFFFFFFFFFFFFFFFFFFFFFFFFFFFFFFFFFFFFFFFFFFFFFFFFFFFFFFFFFFFFFFFFFFF
C
C        FINDS THE SMALLEST INDEX I HAVING THE
c         MAXIMUM ABSOLUT VALUE IN AN ARRAY
C
CFFFFFFFFFFFFFFFFFFFFFFFFFFFFFFFFFFFFFFFFFFFFFFFFFFFFFFFFFFFFFFFFFFFFFFF
      INTEGER FUNCTION IABSMAX(N,A)

      INTEGER N, I
      DOUBLE PRECISION A(N), AA(100)
      x = 0.0
      IABSMAX = 0
      DO 10 I = 1,N,1
```

```
   AA(I) = DABS(A(I))
   IF (AA(I) .GT. x) THEN
     IABSMAX = I
     x = AA(I)
   END IF
10 CONTINUE

  RETURN
  END
```

Appendix C

COMPUTER PROGRAM FOR THE CALCULATION OF THE WATER VAPOR LINE INTENSITIES OF THE ALLOWED ENERGY TRANSITIONS

This program calculates the relative intensities of the Stoke's and anti-Stoke's pure rotational Raman quantum lines. It was originally developed by William F. Murphy [1977]. Input to this program consists of the output file which contains the energies and wavefunctions of the water vapor molecule, and the file which contains information on the temperature of the gas and its polarizability components. The input file which was used in the research of this thesis is given below.

```
$$$$$$$$  input file for cond0 - H2O  $$$$$$$$
  15   0   0   0   1
  20   0
  20   0
  300.     1.       1.       3.       3.
 -500.     500.     .25
   0.0706
   0.0530
H2O   H2O - cond0 - pure rotation, T=300
```

```
CMMMMMMMMMMMMMMMMMMMMMMMMMMMMMMMMMMMMMMMMMMMMMMMMMMMMMMMMMMMMM
C
C                 driver program
C
C       ASYMMETRIC TOP- RAMAN BAND CONTOUR CALCULATION
C            DRIVER FOR Q=0,(2+2) TRANSITIONS
C
C
CMMMMMMMMMMMMMMMMMMMMMMMMMMMMMMMMMMMMMMMMMMMMMMMMMMMMMMMMMMMMMM

      PROGRAM COND0

      EXTERNAL SACAL0
      INTEGER KI, KF
C       CHARACTER*50 FMT(3)
C      1  /'("0",T23,"2",T30,"2",T38,"2"/            ',
C      2   "' MATRIX ELEMENTS: ALFA ,",A1,"ALFA  + ALFA"/ ',
C      3   'T23,"0",T30,"2",T38,"-2")                 '/
      COMMON/CASYM/JI,KI,NDI,ITI,JF,KF,NDF,ITF,DUMMY(11)

C     ---------------------------------------------------------------
C        FOR SELECTION RULES - INDICES 0,1,2,3 => STATES E+,O-,O+,E-
C        ITAU IS DUMMY HERE
C     ---------------------------------------------------------------

      CALL ASMIPR (JMAX,ITAU)
C     CALL ASMIPR (JMAX,ITAU,FMT)
      PRINT *, 'taga'
      DO 100 JI=0,JMAX
C       --------------------------------------------
C            DELTA J = 0,+-2 TRANSITIONS
C       --------------------------------------------
        DO 20 JF=JI-2,JI+2,2
          IF (JI+JF.GT.1) THEN
            CALL SCAL0
C             PRINT *, 'JI=',JI, 'JF=',JF
C             ----------------------------------------------------
C                 SELECTION RULE - E+- => E+- , O+- => O+-
C             ----------------------------------------------------
            DO 10 ITI=0,3
              ITF = ITI
10              CALL ASINC
C             PRINT *, 'tagb2'
          END IF
20      CONTINUE
C       PRINT *, 'tagc'

C       --------------------------------------------
C            DELTA J = +-1 TRANSITIONS
C       --------------------------------------------
        DO 40 JF=JI-1,JI+1,2
          IF (JI+JF.GT.1) THEN
```

```
          CALL SCAL0
C           PRINT *, 'JI=',JI, 'JF=',JF
C          ------------------------------------------------
C              SELECTION RULE - E+ <=> E- , O+ <=> O-
C          ------------------------------------------------
          DO 30 ITI=0,3
            ITF = 3-ITI
30            CALL ASINC
        END IF
40     CONTINUE
100   CONTINUE
      CALL ASMIEP
      STOP
      END

CSSSSSSSSSSSSSSSSSSSSSSSSSSSSSSSSSSSSSSSSSSSSSSSSSSSSSSSSSSSSSSSSSSSSSSSSSSSSSSS
C
C              rotational line strength routine
C
C           ROUTINE FOR ASYMMETRIC TOP RAMAN CONTOURS
C         THIS ENTRY COMPUTES LINE STRENGTH FACTOR TERMS
C             FOR PURE ROTATIONAL TRANSITIONS
C         IN TERMS OF CONTACT TRANSFORMED POLARIZABILITY
C
CSSSSSSSSSSSSSSSSSSSSSSSSSSSSSSSSSSSSSSSSSSSSSSSSSSSSSSSSSSSSSSSSSSSSSSSSSSSSSSS
      SUBROUTINE SCAL0

      COMMON /CASYM/ JI,KI,NDI,ITI,JF,KF,NDF,ITF,SIGN,
     1  A20, T200, T002,T202,T402,
     2  A22, T220,     T222,T422,
     3                 T442
      REAL*4 S(100),SP2(100),SM2(100),SP4(100),SM4(100)
C     ------------------------------------
C         DIMENSION FOR SACAL0 ENTRY
C     ------------------------------------
      REAL*4 AI(50),SA(50)

      JS = JI+JF+1
      FJ = SQRT(FLOAT((2*JI+1)*(2*JF+1))/
     1       (FLOAT((JS+2)*(JS+1))*FLOAT(JS)*FLOAT((JS-1)*(JS-2))))

      JI1 = JI*(JI+1)
      JF1 = JF*(JF+1)


C     V^l_q = alpha^l_q + sum f_12  T^l_q
C     ------------------------------------------------------------
C         V2q SCALED BY FACTOR OF 1/2 IN MATRIX ELEMENT FOR q>0
C     ------------------------------------------------------------
C     f_12(J',J;2,0,2)
      C20 = -0.5*FLOAT(JI1 + JF1)/SQRT(3.)
```

```
C    f_12(J',J;2,2,2)
     C22 = 0.25*FLOAT((JI1 - JF1)**2 - 4*(JI1 + JF1) + 30)/SQRT(21.)

     V20 = FJ*(A20 + C20*T200 + C22*T202)
     V22 = 0.5*FJ*(A22 + C20*T220 + C22*T222)

     V40 = +FJ*T402
     V42 = +0.5*FJ*T422
     V44 = +0.5*FJ*T442

     NP221 = JI*(JI+2)
     NP222 = JI*JI-1
     SP = SQRT(2.*FLOAT(NP221)*FLOAT(NP222))
     NP441 = NP221-8
     NP442 = NP222-8
     ND0 = 1
     NPD4 = 5

     IF(JI.EQ.JF) THEN

C       DELTA J = 0 CASE

        V00 = +T002*FLOAT(JS)/(FJ*SQRT(120.))

C       ------------------------------------------------------------
C            CONSTANT FACTORS FROM f_12        3-j SYMBOL
C       ------------------------------------------------------------
        V20 = V20*                2.
        V22 = V22*              SQRT(6.)

C               SQRT(3/35)/2       2
        V40 = V40*        SQRT(3./35.)
C               SQRT(3/35)/2   2*SQRT(10)
        V42 = V42*        SQRT(6./7.)
C               SQRT(3/35)/2     SQRT(70)
        V44 = V44*        .5*SQRT(6.)

        N201 = -JI1
        S20 = FLOAT(N201)
        N401 = N201+2
        N402 = 0
        N403 = -1
        S40 = FLOAT(N401)
        S(1) = V00+(V20+3.*V40*S40)*S20
        SM2(2) = -(V22+V42*S40)*S20
        SM4(2) = -V44*S20*SQRT(S40*FLOAT(N201+6))
        SM4(3) = V44*S20*S40
        SM4(4) = SM4(2)
        NP42 = N201+9
        SP2(1) = (V22+V42*FLOAT(NP42))*SP
        SP4(1) = V44*SP*SQRT(FLOAT(NP441)*FLOAT(NP442))
        DO 500 K=1,JF
```

```
      N201 = N201+3*ND0
      N401 = N401+7*ND0
      N402 = N402+7*ND0
      N403 = N403+4*ND0
      S(K+1) = V00+(V20+3.*V40*FLOAT(N401))*FLOAT(N201)
     1          -V40*FLOAT(N402)*FLOAT(N403)

      ND0 = ND0+2
      NP221 = NP221-ND0
      NP222 = NP222-ND0
      SP = SQRT(FLOAT(NP221)*FLOAT(NP222))
      NP42 = NP42+7*ND0
      SP2(K+1) = (V22+V42*FLOAT(NP42))*SP
      IF(K.GT.1) SM2(K+1) = SP2(K-1)

      NPD4 = NPD4+2
      NP441 = NP441-NPD4
      NP442 = NP442-NPD4
      SP4(K+1) = V44*SP*SQRT(FLOAT(NP441)*FLOAT(NP442))
      IF(K.GT.2) SM4(K+2) = SP4(K-2)

  500 CONTINUE

    ELSE

C     ------------------------------
C         DELTA J NOT 0 CASES
C     ------------------------------
      IF(JF.GT.JI) THEN
        N201 = JF*JF
      ELSE
        N201 = JI*JI
      END IF

      NM221 = NP221
      NM222 = NP222
      NM441 = NP441
      NM442 = NP442
      NMD4 = 7

C     ------------------------------
C         DELTA J = 1 CASE
C     ------------------------------
      IF(IABS(JI-JF).EQ.1) THEN


C       ------------------------------------
C           CONSTANT FACTORS FROM
C           f_12       3-j SYMBOL
C       ------------------------------------
        V20 = V20*            2.*SQRT(6.)
        V22 = V22*             2.
```

```
C               1/(2 SQRT(14))  4*SQRT(5)
      V40 = V40*        SQRT(10./7.)
C               1/(2 SQRT(14))  2*SQRT(2)
      V42 = V42/        SQRT(7.)
C               1/(2 SQRT(14))  2*SQRT(14)
C      V44 = V44*          1

      IF(JF.GT.JI) THEN
        NPD42 = JI+3
        NMD42 = -7-JI
        NP42 = -(JI-8)*NPD42
        NPD221 = -1
        NPD222 = -2*JI-1
        P = 1.
        N = 2
      ELSE
        NPD42 = 2-JI
        NMD42 = -6+JI
        NP42 = (JI+9)*NPD42
        NPD221 = 2*JI+1
        NPD222 = -1
        P = -1.
        N = -2
        SP = -SP
      END IF

      NPD42 = 7*NPD42
      NMD42 = 7*NMD42
      N401 = -3*N201+5
      NM42 = NP42
      NMD221 = -NPD221+N
      NMD222 = -NPD222-N
      S(1) = 0.
      SP2(1) = (V22+V42*FLOAT(NP42))*SP
      SP4(1) = V44*SP*SQRT(FLOAT(NP441)*FLOAT(NP442))

      DO 700 K=1,JF
        ND0 = ND0-2
        N201 = N201+ND0
        N401 = N401-7*ND0
        S(K+1) = FLOAT(K)*(V20+V40*FLOAT(N401))*
     +                          SQRT(FLOAT(N201))

        NPD221 = NPD221-N
        NP221 = NP221+NPD221
        NPD222 = NPD222+N
        NP222 = NP222+NPD222
        SP = P*SQRT(FLOAT(NP221)*FLOAT(NP222))
        NPD42 = NPD42+28
        NP42 = NP42+NPD42
        SP2(K+1) = SP*(V22+V42*FLOAT(NP42))
```

```
          NPD4 = NPD4+2
          NP441 = NP441-NPD4
          NP442 = NP442-NPD4
          SP4(K+1) = V44*SP*SQRT(FLOAT(NP441)*FLOAT(NP442))

          NMD221 = NMD221-N
          NM221 = NM221+NMD221
          NMD222 = NMD222+N
          NM222 = NM222+NMD222
          SM = -P*SQRT(FLOAT(NM221)*FLOAT(NM222))
          NMD42 = NMD42+28
          NM42 = NM42+NMD42
          SM2(K+1) = SM*(V22+V42*FLOAT(NM42))

          NMD4 = NMD4-2
          NM441 = NM441+NMD4
          NM442 = NM442+NMD4
          SM4(K+1) = V44*SM*SQRT(FLOAT(NM441)*FLOAT(NM442))
700       CONTINUE

C-------------------------------------------------------
C         DELTA J = 2 CASE
C-------------------------------------------------------
        ELSE

C         ---------------------------------
C            CONSTANT FACTORS FROM
C            f_12      3-j SYMBOL
C         ---------------------------------
          V20 = V20*              SQRT(6.)
C         V22 = V22*                1

C                 1/(4 SQRT(7))  2*SQRT(10)
          V40 = V40*      SQRT(5./14.)
C                 1/(4 SQRT(7))  2
          V42 = V42/     (2.*SQRT(7.))
C                 1/(4 SQRT(7))  2*SQRT(7)
          V44 = V44/          2.

          IF(JF.GT.JI) THEN
            N202 = (JI+1)**2
            N401 = -JI*(JI+3)
            NPD221 = -2*JI-3
            NPD222 = NPD221+2
            NPD42 = 14*JI+35
            NP42 = 2*(JI+3)*(JI+7)
          ELSE
            N202 = (JF+1)**2
            N401 = -JF*(JF+3)
            NPD221 = 2*JI+1
            NPD222 = NPD221-2
            NPD42 = 21-14*JI
```

```
        NP42 = 2*(JI-2)*(JI-6)
      END IF

      NM42 = NP42
      NMD42 = -NPD42-28
      NMD221 = -NPD221-2
      NMD222 = -NPD222-2
      S(1) = (V20+V40*FLOAT(N401))*FLOAT(2-N401)
      SP2(1) = (V22+V42*FLOAT(NP42))*SP
      SP4(1) = V44*SP*SQRT(FLOAT(NP441)*FLOAT(NP442))

      DO 1100 K=1,JF
        ND0 = ND0-2
        N201 = N201+ND0
        N202 = N202+ND0
        N401 = N401-7*ND0
        S(K+1) = (V20+V40*FLOAT(N401))*
     +                    SQRT(FLOAT(N201)*FLOAT(N202))

        NPD221 = NPD221+2
        NP221 = NP221+NPD221
        NPD222 = NPD222+2
        NP222 = NP222+NPD222
        SP = SQRT(FLOAT(NP221)*FLOAT(NP222))
        NPD42 = NPD42+28
        NP42 = NP42+NPD42
        SP2(K+1) = SP*(V22+V42*FLOAT(NP42))

        NPD4 = NPD4+2
        NP441 = NP441-NPD4
        NP442 = NP442-NPD4
        SP4(K+1) = V44*SP*SQRT(FLOAT(NP441)*FLOAT(NP442))

        NMD221 = NMD221+2
        NM221 = NM221+NMD221
        NMD222 = NMD222+2
        NM222 = NM222+NMD222
        SM = SQRT(FLOAT(NM221)*FLOAT(NM222))
        NMD42 = NMD42+28
        NM42 = NM42+NMD42
        SM2(K+1) = SM*(V22+V42*FLOAT(NM42))

        NMD4 = NMD4-2
        NM441 = NM441+NMD4
        NM442 = NM442+NMD4
        SM4(K+1) = V44*SM*SQRT(FLOAT(NM441)*FLOAT(NM442))
1100    CONTINUE
      END IF

      SM2(3) = SQRT(2.)*SM2(3)
      SM4(5) = SQRT(2.)*SM4(5)
    END IF
```

```
C    ------------------------------------------------
C       ******  END OF DELTA J NOT 0 CASES
C    ------------------------------------------------
     RETURN


CEEEEEEEEEEEEEEEEEEEEEEEEEEEEEEEEEEEEEEEEEEEEEEEEEEEEEEEEEEEEEEEEEEEEEEEEEEEE
C
C    THIS ENTRY COMPUTES VECTOR WHICH IS MULTIPLIED BY
C    FINAL LEVEL EIGENVECTOR TO GIVE LINE STRENGTH FACTOR
C
CEEEEEEEEEEEEEEEEEEEEEEEEEEEEEEEEEEEEEEEEEEEEEEEEEEEEEEEEEEEEEEEEEEEEEEEEEEEE

     ENTRY SACAL0 (AI,SA)

     IA = (KF-KI)/2
     IP4 = IA + 2
     IP2 = IA + 1
     IM2 = IA - 1
     IM4 = IA - 2
     KS = KF - 1
     DO 1600 I=1,NDF
       KS = KS + 2
       IA = IA + 1

       IF((IA.GE.1).AND.(IA.LE.NDI)) THEN
         SAI = S(KS) * AI(IA)
       ELSE
         SAI = 0.
       END IF

       IP2 = IP2 + 1
       IF(IP2.LE.NDI) SAI = SAI + SP2(KS) * AI(IP2)

       IP4 = IP4 + 1
       IF(IP4.LE.NDI) SAI = SAI + SP4(KS) * AI(IP4)

       IM2 = IM2 + 1
       IF(IM2.GE.1)   SAI = SAI + SM2(KS) * AI(IM2)

       IM4 = IM4 + 1
       IF(IM4.GE.1)   SAI = SAI + SM4(KS) * AI(IM4)

1600   SA(I) = SAI

     P = (-1.)**ITI

C    PRINT *, 2-KI/2
     IF(KI.EQ.1) THEN
       SA(1) = SA(1) + P * (SM2(2) * AI(1) + SM4(2) * AI(2))
       SA(2) = SA(2) + P * SM4(4) * AI(1)
     ELSE
```

```
      I = 2-KF/2
C       PRINT *,I
      IF (I .LE. NDI) THEN
        SA(I) = SA(I) + P * SM4(3) * AI(2-KI/2)
      ELSE
        SA(I) = SA(I)
      END IF
    END IF

    RETURN
C

CEEEEEEEEEEEEEEEEEEEEEEEEEEEEEEEEEEEEEEEEEEEEEEEEEEEEEEEEEEEEEEEEEEEEEEEE
C
C  THIS ENTRY RESCALES LINE STRENGTH FACTORS CORRESPONDING TO K=0
C    BY SQRT(2) AND THEN PRINTS ALL OF THEM
C  IF COEFFICIENTS SUITABLY CHOSEN IN CALLING ROUTINE,
C    THIS WILL GIVE THREE J SYMBOLS FOR PROGRAM CHECK OUT
C
CEEEEEEEEEEEEEEEEEEEEEEEEEEEEEEEEEEEEEEEEEEEEEEEEEEEEEEEEEEEEEEEEEEEEEEEE
    ENTRY SAPRT0

    SP2(1) = SP2(1)/SQRT(2.)
    SP4(1) = SP4(1)/SQRT(2.)
    SM2(1) = 0.
    SM2(3) = SM2(3)/SQRT(2.)
    SM4(1) = 0.
    SM4(5) = SM4(5)/SQRT(2.)
    PRINT *,'JI',JI,'JF',JF
    PRINT 5000, '0     ', (S(K),K=1,JF+1)
5000  FORMAT ('0',A6,6F12.6/(7X,6F12.6))
    PRINT 5000, '2  +  ', (SP2(K),K=1,JF+1)
    PRINT 5000, '2  -  ', (SM2(K),K=1,JF+1)
    PRINT 5000, '4  +  ', (SP4(K),K=1,JF+1)
    PRINT 5000, '4  -  ', (SM4(K),K=1,JF+1)
    RETURN
    END

CSSSSSSSSSSSSSSSSSSSSSSSSSSSSSSSSSSSSSSSSSSSSSSSSSSSSSSSSSSSSSSSSSSSSSSS
C
C     $$$$$$$$   general calculation control routine   $$$$$$$$
C
C  SUBROUTINE TO CONTROL CALCULATION OF ASYMMETRIC TOP RAMAN CONTOURS
C  CALLING ROUTINE AND CALCULATION ROUTINES SCAL AND SACAL ARE UNIQUE
C     TO VALUES OF Q
C  DIMENSIONED FOR MAXIMUM JMAX OF 98
C
CSSSSSSSSSSSSSSSSSSSSSSSSSSSSSSSSSSSSSSSSSSSSSSSSSSSSSSSSSSSSSSSSSSSSSSS

    SUBROUTINE ASINT (NDN1,NDN2,IEZI,IEZF)
    parameter (ndez = 3601, iydim = 18192, iin = 1, iout = 3,
   +        h = 6.6260755e-34, xk = 1.380658e-23, c = 2.9979258e10,
```

```
     +        pi = 3.1415926, ctheta = xk/(h*c) )

      REAL*4 SA(50),AI(50,50),AF(50,50), EI(1000), EF(1000),
     +     Temporary(50)
      INTEGER*4 ISWT(0:3)/1,3,2,4/
      INTEGER IYIMAX, tzn, IEZI, IEZF
      CHARACTER ih2ofile*47, rootdir4*35

C     ---------------------------------------------------------------
C          SPIN WEIGHT- A,BX,BY,BZ -> E+,O+,O-,E-, J EVEN;
C                              E-,O-,O+,E+, J ODD.
C              *** DECLARATIONS FOR PROLOG SECTION ***
C     ---------------------------------------------------------------
      COMMON/CASYM/JI,KI,NDI,ITI,JF,KF,NDF,ITF,SGN,ALF1(5),ALF2(5)
      CHARACTER*8 FILNAM,BLANKS/'       '/
      CHARACTER*4 TITLE(20)/20*'    '/
      REAL*4 SWT(4),RC(3)
C     CHARACTER *50 FMT(3)
C     CHARACTER LSIGN(-1:1) /'-',' ','+'/
      CHARACTER carT*3
      COMMON /CYINT/ YI(iydim)
      COMMON/CIO/ISWI,ISWF,KDK
      N = ISWT(ITI)
      IF ((-1)**JI.LT.0) N=5-N
      IF(SWT(N).EQ.0.0) RETURN

      NDII = NDI
      NDFF = NDF

      CALL EWF (IDSRNI,JI,ITI,NDII,EI)
C     WRITE (*,'(I2,2E10.4E2)') NDII,EI(NDII),EI(NDII+1)
      DO 32 I = 1,NDII,1
        DO 30 I1 = 1,NDII,1
          AI(I1,I) = EI(IEZI + (I-1)*NDII + I1-1)
C           WRITE (*,'(I2,I2,E10.4E2)') I1,I,AI(I1,I)
   30   CONTINUE
   32 CONTINUE
      CALL EWF (IDSRNF,JF,ITF,NDFF,EF)
      DO 37 I = 1,NDFF,1
        DO 35 I1 = 1,NDFF,1
          AF(I1,I) = EF(IEZF + (I-1)*NDFF + I1-1)
C           WRITE (*,'(I2,I2,E10.4E2)') I1,I,AF(I1,I)
   35   CONTINUE
   37 CONTINUE
C     PRINT *, 'Tag20'
      KPI = (ITI+1)/2
      KOI = JI-ITI/2
      DO 60 NI=1,NDII
        IF(EI(NI).GE.0.0 .and. EI(NI).LT.ELIM) THEN
          NF1 = MAX0(1,NI+NDN1)
          IF(NF1.LE.NDFF) THEN
            FACT = SWT(N)/(QR*EXP(EI(NI)/THETA))
```

```
          DO 39 I = 1,NDII,1
C              WRITE (*,'(E10.4E2)') AI(I,NI)
C     PRINT *, 'tag21'
            Temporary(I) = AI(I,NI)
  39       CONTINUE
          CALL SACAL0(Temporary,SA)

          KPF = 2*NF1-(4-ITF)/2
          KOF = JF+MOD(ITF,2)-KPF
          NF2 = MIN0(NDFF,NI+NDN2)
          DO 50 NF=NF1,NF2
            IF(EF(NF).GE.0.0) THEN
                      FREQ = EF(NF)-EI(NI)
                      YINT = 0.0
                      DO 40 I=1,NDF
 40                     YINT = YINT+AF(I,NF)*SA(I)
                      YINT = YINT*YINT

                      IF(YINT.GE.YLIM) THEN
                        YINT = FACT*YINT
                IF ((FREQ .GE. XLO) .OR. (FREQ .LE. XHI)) THEN
                  I = ABS(NINT((FREQ - XLO)/DX)) + 1
                  YI(I) = YI(I) + YINT
                END IF
                        ytot = ytot + yint
                        IF(IPRTSW.NE.0) THEN
*                 IF(ISWF.gt.1) then
C-----------------------------------------------------------------------
C     FOR CASE OF INTERACTIN6 VIB. LEVELS,
C       LABEL FINAL STATE USING LARGEST ELEMENT IN WAVE FUNCTION
C     KP=KO=-1 FOR STATE ASSGNED TO ANOTHER VIBRATION
C-----------------------------------------------------------------------
*                   KPF = -1
*                   KOF = -1
*                   IMAX = ISAMAX(NDF,AF(1,NF),1)
*                   IF(ABS(AF(IMAX,NF)).LT.0.1) GO TO 43
*                   KPF = 2*IMAX-(3-ITF)/2
*                   KOF = JF+MOD(ITF,2)-KPF
*                 END IF
                  IF ((FREQ .GE. XLO)
     +                      .AND. (FREQ .LE. XHI)
     +                      .AND. (FREQ .NE. 0.0)) THEN
                    WRITE (iout,503)
     +                   JI,KPI,KOI,JF,KPF,KOF,FREQ,YINT
                  END IF
                END IF
              END IF
            ELSE
              IF(IPRTSW.NE.0) WRITE (iout,501) JF,KPF,KOF
            END IF
 45         KPF = KPF+2
 50       KOF = KOF-2
```

```
        END IF
      ELSE
        IF(IPRTSW.NE.0) WRITE (iout,500) JI,KPI,KOI
      END IF
55      KPI = KPI+2
60    KOI = KOI-2

503   FORMAT (2(I8,2I4),5X,F15.3,1PE15.5)
501   FORMAT ('0FINAL LEVEL NOT IN INPUT DATA SET. J,KP,KO=',3I5/1X)
500   FORMAT ('0INITIAL LEVEL NOT IN INPUT DATA SET. J,KP,KO=',3I5/1X)

      RETURN

CEEEEEEEEEEEEEEEEEEEEEEEEEEEEEEEEEEEEEEEEEEEEEEEEEEEEEEEEEEEEEEEEEE
C
CEEEEEEEEEEEEEEEEEEEEEEEEEEEEEEEEEEEEEEEEEEEEEEEEEEEEEEEEEEEEEEEEEE
      ENTRY ASMIPR (JMAX,ISIGN)
C     ENTRY ASMIPR (JMAX,ISIGN,FMT)

      rootdir4 = 'C:\THESIS\PHD\FORTRAN\PROGRAMS\H2O\'
C     print *, 'tAG1'
      OPEN (iin, FILE = rootdir4//'h2ointn.dat')
      READ (iin, '(A47)') ih2ofile
      WRITE (*, '(A47)') ih2ofile
      READ (iin,'(5I5)') JMAX,KDK,ISIGN,IYLIM,IPRTSW
      WRITE (*, '(5I5)') JMAX,KDK,ISIGN,IYLIM,IPRTSW
      SGN = SIGN(1.,FLOAT(ISIGN))

      READ (iin,'(2I5)') IDSRNI,ISWI
      WRITE (*, '(2I5)') IDSRNI,ISWI
      READ (iin,'(2I5)') IDSRNF,ISWF
      WRITE (*, '(2I5)') IDSRNF,ISWF
      IF(IDSRNF.EQ.0) IDSRNF = IDSRNI
      IF(IDSRNF.EQ.IDSRNI) ISWF = ISWI
      IF(ISWI.GE.2.OR.ISWF.GE.2) KDK = 999

      READ (iin,601) T, (SWT(tzn), tzn = 1,4)
      WRITE (*, 601) T, (SWT(tzn), tzn = 1,4)
      PRINT *, 'Enter the temperature (K):'
      READ (*,'(F10.0)') T
      PRINT *, 'Enter the temperature (K):'
      READ (*,'(A3)') carT
      PRINT *, 'Temperature =', T
      THETA = ctheta*T

      READ (iin,'(3F10.0)') XLO,XHI,DX
      WRITE (*, '(3F15.3)') XLO,XHI,DX
      READ (iin, 601) (ALF1(tzn), tzn = 1,5)
      WRITE (*, 601) (ALF1(tzn), tzn = 1,5)
      READ (iin, 601) (ALF2(tzn), tzn = 1,5)
      WRITE (*, 601) (ALF2(tzn), tzn = 1,5)
```

```
      READ (iin,611) FILNAM,(TITLE(I),I=1,18)
      WRITE (*, 611) FILNAM,(TITLE(I),I=1,18)


      CLOSE(iin)


      IF (IYLIM.EQ.0) THEN
        YLIM = 0
        ELIM = 1E10
      ELSE
        YLIM = 1.5*(ALF1(1)**2 + 0.5*ALF2(1)**2)*10.**(-IYLIM)
        ELIM = 2.303*FLOAT(IYLIM)*THETA
      END IF
C     print *, 'tAG2'

      OPEN (iout, FILE = rootdir4//'results\h2o'//carT//'.dat')
      WRITE (iout,700)
C     WRITE (iout,603) TITLE
C     WRITE (iout, '(FMT(2))') LSIGN(ISIGN)

C     -------------------------------------------------------
C           OPEN ENERGY-WAVE FUNCTION FILES
C     -------------------------------------------------------
      CALL EWFOP (IDSRNI, JMAX)
      IF (IDSRNF.EQ.IDSRNI) THEN
        WRITE (iout,701)
      ELSE
        CALL EWFOP (IDSRNF, JMAX)
        WRITE (iout,702)
      END IF

      WRITE (iout,703) JMAX,ELIM,YLIM,KDK,T,SWT,ALF1,ALF2

C     -------------------------------------------------------------
C           CALCULATE ROTATIONAL PARTITION FUNCTION
C           INCLUDE CONTRIBUTIONS FROM J LEVELS
C           UNTIL CONVERGED TO MACHINE PRECISION
C           (OR ALL LEVELS IN ENERGY FILE USED)
C     -------------------------------------------------------------

      QR = 0.
      QROLD = 0.
      PRINT *, JMAX
      DO 200 JI=0,JMAX
        QR = QR/FLOAT(2*JI+1)
        DO 195 ITI=0,3
          KI = (ITI+1)/2
          NDI = (JI+2-KI)/2
          IF (NDI.GE.1) THEN
            N = ISWT(ITI)
            IF ((-1)**JI.LT.0) N=5-N
```

```
          IF(SWT(N).GT.0.0) THEN
          QR = QR/SWT(N)
          CALL EWF (IDSRNI,JI,ITI,NDI,EI)
C          ---------------------------------------------------------
C           SUM UNTIL CONTRIBUTION SMALLER THAN MACHINE PRECISIQN
C           THIS ASSUMES EI INCREASING WITH NI,
C           TERM THEN DECREASES
C           ***WATCH OUT FOR CASES WHERE NOT ALL ENERGIES KNOWN!
C          ---------------------------------------------------------

          DO 190 NI=1,NDI
            IF(EI(NI).GE.0.0) THEN
              TERM = EXP(-EI(NI)/THETA)
              IF(QR+TERM.EQ.QR) GOTO 191
              QR = QR + TERM
            END IF
190         CONTINUE
191         QR = SWT(N)*QR
        END IF
      END IF
195   CONTINUE
    QR = FLOAT(2*JI+1)*QR
              PRINT *, QROLD, QR
    IF(QR.EQ.QROLD) GO TO 201
200   QROLD = QR
201   WRITE (iout,704) QR

C    ---------------------------------------------------------
C        COMPARE CLASSICAL PARTITIQN FUNCTION
C        OBTAIN ROTATIONAL CONSTANTS FROM J=1 LEVELS,
C        ASSUME RIGID ROTOR, SYMMETRY NUMBER = 2
C    ---------------------------------------------------------
    DO 210 I=1,3
210   RC(I) = 0.0
    JI = 1
    NDI = 1
    DO 250 ITI=0,2
      CALL EWF (IDSRNI,JI,ITI,NDI,EI)
      DO 240 I=1,3
        IF(I.EQ.ITI+1) THEN
          RC(I) = RC(I) - EI(1)/2.
        ELSE
          RC(I) = RC(I) + EI(1)/2.
        END IF
240     CONTINUE
250   CONTINUE
    QCLASS = 0.25*(SWT(1)+SWT(2)+SWT(3)+SWT(4))/
   +       SQRT(RC(1)*RC(2)*RC(3)/(pi*THETA**3))
    WRITE (iout,705) QCLASS

C    ---------------------------------------------------
C          initialize total intensity
```

```
C     --------------------------------------------------
      ytot = 0.

C       IF(FILNAM.NE.BLANKS) WRITE (iout,706) FILNAM,TITLE

C     -------------------------------------------------------------
C            SET UP SPECTRUM PARAMETERS
C     -------------------------------------------------------------
      DO 260 I = 1, IYDIM, 1
        YI(I) = 0.
 260  CONTINUE
      IF(IPRTSW.NE.0) WRITE (iout,604)

600   FORMAT (16I5)
601   FORMAT (5F10.5)
611   FORMAT (A8,18A4)
700   FORMAT ('1CALCULATE THE ROTATIONAL SPECTRUM OF AN ASYMMETRIC',
    1       ' TOP MOLECULE')
603   FORMAT ('0',20A4)
701   FORMAT ('0PURE ROTATION TRANSITIONS')
702   FORMAT ('0VIBRATION-ROTATION TRANSITIONS')
703   FORMAT ('0ROTATIONAL LEVEL OF INITIAL STATES: FROM J = 0 TO',I4/
    1       '0   FOR INITIAL ENERGY LEVELS UP TO',G12.3/
    2       '0   AND SQUARE OF MATRIX ELEMENTS GREATER THAN',1PE12.4/
    3       '0TRANSITIQNS INVOLVING CHANGES IN KP AND/OR KO UP TO',I3/
    4       '0SAMPLE TEMPERATURE - ',0PF10.1/
    5       '0NUCLEAR SPIN WEIGHTS - ',4F5.0/
    6       '0MATRIX ELEMENT COEFFICIENTS - ',1P,5E12.5/31X,5E12.5)
704   FORMAT ('OROT. PARTITIQN FUNCTIQN -',1PE12.4)
705   FORMAT ('0     (CLASSICAL APPRQX) -',1PE12.4)
706   FORMAT ('OSPECTRUM SAVED IN FILE ',A,' SPEC'/' TITLE: ',20A)
604   FORMAT ('1',5X,'JI  KPI KOI     JF  KPF KOF',10X,
    +       'FREQUENCY INTENSITY'/)

      RETURN

CEEEEEEEEEEEEEEEEEEEEEEEEEEEEEEEEEEEEEEEEEEEEEEEEEEEEEEEEEEEEEEEEEEEEEE
C
CEEEEEEEEEEEEEEEEEEEEEEEEEEEEEEEEEEEEEEEEEEEEEEEEEEEEEEEEEEEEEEEEEEEEEE
      ENTRY ASMIEP

C     --------------------------------
C          CLOSE D A DATA SETS
C     --------------------------------
      CALL EWFCL

C     --------------------------------
C          SAVE SPECTRUM
C     --------------------------------
      IF (FILNAM.NE.BLANKS) THEN
      print *, 'tAG3'
```

```
      OPEN (8, FILE = rootdir4//'results\h20spec.'//carT)
C       YIMAX = 0.0
C       DO 270 I = 2000,IYDIM,1
C         IF (YI(I) .GT. YIMAX) THEN
C           YIMAX = YI(I)
C           IYIMAX = I
C         END IF
C 270    CONTINUE
      IYIMAX = ((XHI - XLO)/DX) + 1
      PRINT *, 'XHI =', XHI
      PRINT *, 'XLO =', XLO
      PRINT *, 'IYIMAX =', IYIMAX
      DO 280 I = 1,IYIMAX,1
        FREQ = XLO + DX*(I-1)
C         IF ( YI(I) .GT. 0.0 ) THEN
          WRITE (8, 606) FREQ, YI(I)
C         END IF
 280    CONTINUE
    END IF

C   ---------------------------------
C       total area
C   ---------------------------------
    WRITE (iout,605) ytot
    CLOSE (iout)
    CLOSE (8)

 605  FORMAT ('0 Total intensity ',1pe12.5)
 606  FORMAT (1P, 2E15.8E2)

    RETURN
    END

CSSSSSSSSSSSSSSSSSSSSSSSSSSSSSSSSSSSSSSSSSSSSSSSSSSSSSSSSSSSSSSSSSSSSSSSSSS
C
C    CALCULATE INITIAL K VALUES FOR EIGENVECTORS, EIGENVECTOR
C    DIMENSIIINS, AND CALL MAIN CALCULATION ROUTINE
C    INPUT PARAMETERS: IT - INDICES OF INITIAL LEVELS - VIA COMMON
C              E+,O-,O+,E- =' 0,1,2,3
C
CSSSSSSSSSSSSSSSSSSSSSSSSSSSSSSSSSSSSSSSSSSSSSSSSSSSSSSSSSSSSSSSSSSSSSSSSSS
    SUBROUTINE ASINC

    COMMON/CASYM/JI,KI,NDI,ITI,JF,KF,NDF,ITF,DUMMY(11)
C   ---------------------------------------------------------------
C     THESE COMMONS DIMENSIONED FOR MAXIMUM JMAX OF 98
C     ITRUNCATED WAVE FUNCTION VERSION (ISW=1) REQUIRED FOR JMAX>58)
C              **** NOT FOR VM VERSION ****
C   ---------------------------------------------------------------
    parameter (ndez = 3601, iydim = 8192)

    COMMON/CIO/ISWI,ISWF,KDK
```

```
C    ---------------------------------------------------------------
C         SELECTION RULES: DELTA KP OR DELTA KO .LE. KDK
C         KP,KO CORRESPOND TO CASE IR
C    ---------------------------------------------------------------
     INTEGER*4 KP0(0:3)/2,1,1,0/,KO0(0:3)/2,2,1,1/
     KI = (ITI+1)/2
     NDI = (JI+2-KI)/2
     IF(NDI.LT.1) RETURN
     KF = (ITF+1)/2
     NDF = (JF+2-KF)/2
     IF(NDF.LT.1) RETURN
     NDP = (KP0(ITF)-KP0(ITI)-KDK)/2
     NDO = (JF+KO0(ITF)-JI-KO0(ITI)-KDK)/2
     NDN1 = MIN0(NDP,NDO)
     NDP = (KP0(ITF)-KP0(ITI)+KDK)/2
     NDO = (JF+KO0(ITF)-JI-KO0(ITI)+KDK)/2
     NDN2 = MAX0(NDP,NDO)
*    IF(ISWI.EQ.O)
     IEZI = NDI+1
*    IF(ISWI.EQ.1) IEZI = 1001
*    IF(ISWI.GT.1) IEZI = (JI/2+1)*ISWI+1
*    IF(ISWF.EQ.0)
     IEZF = NDF+1
*    IF(ISWF.EQ.1) IEZF = 1OO1
*    IF(ISWF.GT.1) IEZF = (JF/2+1)*ISWF+1
     CALL ASINT (NDN1,NDN2,IEZI,IEZF)
     RETURN
     END

CSSSSSSSSSSSSSSSSSSSSSSSSSSSSSSSSSSSSSSSSSSSSSSSSSSSSSSSSSSSSSSSSSSSSSSSSSSSSSSS
C
C    SUBROUTINE TO READ ENERGIES AND WAVE FUNCTIONS FROM D A DATA SET
C    FOR ASYMMETRIC ROTOR PROGRAM
C    CALLED FROM ASINT - INPUT USING RWPACK ROUTINES
C      A, ISW NOT USED- FOR COMPATIBILITY WITH CALLING ROUTINE
C
CSSSSSSSSSSSSSSSSSSSSSSSSSSSSSSSSSSSSSSSSSSSSSSSSSSSSSSSSSSSSSSSSSSSSSSSSSSSSSSS
     SUBROUTINE EWF(IDSRN,J,IT,N,E)
     DIMENSION E(1000), EE(800,200)
C     REAL*4 A(N,N)
C     CHARACTER*5 WCHFIL
     CHARACTER*3 FILNAM
     CHARACTER*43 rootdir5
     INTEGER IDSRN, nnret(200), I1
     CHARACTER*12000 Astr
     CHARACTER*55 Filtnam
     parameter (c = 2.9979258e10)

C    ----------------------------------------
C         CALCULATE RETRIEVAL ADDRESS
C    ----------------------------------------
     IF (J-1) 10,20,30
```

```
C      ---------------------------
C           CASE J = 0
C      ---------------------------
10     IRA = 1
       GO TO 40

C      ---------------------------
C           CASE J = 1
C      ---------------------------
20     IRA = IT +2
       GO TO 40

C      ---------------------------
C           CASE J > 1
C      ---------------------------
30     IRA = 4*J + IT - 3

C    ---------------------------
C         READ RECORD
C    ---------------------------
C     PRINT *, 'Tag10',IRA
  40 IF (nnret(IRA).NE.N*(N+1)) THEN
      PRINT *,' ****ERROR - EWF RECORD LENGTH INCORRECT - FILE',
     1      IDSRN,'    J',J,' IT',IT,' DIM',N,' EXPECTED',N*(N+1),
     2      ' RETURNED',NRET
      STOP
     END IF
     DO 45 I = 1,N*(N+1),1
C       PRINT *, I
       IF (I .LE. N) THEN
         E(I) = (EE(I,IRA) * 1.0E6)/c
       ELSE
         E(I) = EE(I,IRA)
       END IF
  45 CONTINUE
C    DO 50 I = 1,N,1
C       DO 60 I1 = 1,N,1
C         A(I1,I) = EE(I*N+1+I1,IRA)
C  60    CONTINUE
C  50 CONTINUE

     RETURN

C-------------------------------------------------------------------
C  END OF FILE ENCOUNTERED - SET ENERGY VALUES TO FLAG UNAVAILABLE
C-------------------------------------------------------------------
100  DO 110 I=1,N
110     E(I) = -1.
     RETURN

C-------------------------------------------------------------------
C  READ ERROR ENCOUNTERED
```

```
C-----------------------------------------------------------------
200   PRINT *,' ****ERROR - READ ERROR FOR FILE',IDSRN
     1   ,'    TYPE',NRET
      STOP

      ENTRY EWFOP (IDSRN, JMAX)

      rootdir5 = 'C:\THESIS\PHD\FORTRAN\PROGRAMS\H2O\RESULTS\'
      Filtnam = rootdir5//'h2oasyme.dat'
      print *, 'tAG4'
      FILNAM = 'h2o'
      OPEN (IDSRN, FILE = Filtnam)
      PRINT *,'FILEID - ',FILNAM,' ASYME A4 - OPENED'
      PRINT *, JMAX*4+8
      DO 80 I = 1,JMAX*4+8,1
        READ (IDSRN, '(A12000)') Astr
        NRET = LEN_TRIM(Astr)
        nnret(I) = NRET/15
   80 CONTINUE
      REWIND (IDSRN)
      DO 220 I = 1,JMAX*4+8,1
        READ (IDSRN, '(800E15.0E2)') (EE(I1,I), I1=1,nnret(I),1)
  220 CONTINUE
      CLOSE (IDSRN)
      RETURN

      ENTRY EWFCL
      CLOSE (IDSRN)
      RETURN
      END
```

Appendix D

PURE ROTATIONAL RAMAN ENERGY LEVELS OF THE WATER VAPOR MOLECULE

J	TAU	KP	KO	SUBMAT	ENERGY (MHz)
0	0	0	0	E+	0
1	-1	0	1	E+	713336.9
1	0	1	1	O-	1113342.8
1	1	1	0	O+	1270272.7
2	-2	0	2	E+	2101269.6
2	2	2	0	E+	4082090.9
2	-1	1	2	O-	2383241.4
2	0	1	1	O+	2853302.4
2	1	2	1	E-	4044248.8
3	-3	0	3	E+	4100011.1
3	1	2	1	E+	6360287.1
3	-2	1	3	O-	4265401
3	2	3	1	O-	8550660.1
3	-1	1	2	O+	5197375.7
3	3	3	0	O+	8556633
3	0	2	2	E-	6184760.3
4	-4	0	4	E+	6656973.9
4	0	2	2	E+	9466831.6
4	4	4	0	E+	14633896
4	-3	1	4	O-	6740484.5
4	1	3	2	O-	11467568
4	-2	1	3	O+	8259193
4	2	3	1	O+	11507309
4	-1	2	3	E-	9004634
4	3	4	1	E-	14633103
5	-5	0	5	E+	9753684.5
5	-1	2	3	E+	13386053
5	3	4	1	E+	18297571
5	-4	1	5	O-	9791984.5
5	0	3	3	O-	15108585
5	4	5	1	O-	22246796
5	-3	1	4	O+	11975435
5	1	3	2	O+	15253803
5	5	5	0	O+	22246894
5	-2	2	4	E-	12477624
5	2	4	2	E-	18290774
6	-6	0	6	E+	13391627
6	-2	2	4	E+	18070696
6	2	4	2	E+	22717683
6	6	6	0	E+	31330074
6	-5	1	6	O-	13408288
6	-1	3	4	O-	19455895

6	3	5	2	O-	26639526
6	-4	1	5	O+	16275906
6	0	3	3	O+	19832740
6	4	5	1	O+	26640542
6	-3	2	5	E-	16575867
6	1	4	3	E-	22686043
6	5	6	1	E-	31330063
7	-7	0	7	E+	17575141
7	-3	2	5	E+	23456060
7	1	4	3	E+	27917793
7	5	6	1	E+	36460613
7	-6	1	7	O-	17582205
7	-2	3	5	O-	24483883
7	2	5	3	O-	31767416
7	6	7	1	O-	41815519
7	-5	1	6	O+	21111807
7	-1	3	4	O+	25253219
7	3	5	2	O+	31773075
7	7	7	0	O+	41815520
7	-4	2	6	E-	21273521
7	0	4	4	E-	27813070
7	4	6	2	E-	36460471
8	-8	0	8	E+	22306471
8	-4	2	6	E+	29466957
8	0	4	4	E+	33929788
8	4	6	2	E+	42319985
8	8	8	0	E+	53633717
8	-7	1	8	O-	22309439
8	-3	3	6	O-	30162605
8	1	5	4	O-	37628966
8	5	7	2	O-	47687805
8	-6	1	7	O+	26468388
8	-2	3	5	O+	31482941
8	2	5	3	O+	37651294
8	6	7	1	O+	47687824
8	-5	2	7	E-	26549630
8	-1	4	5	E-	33657964
8	3	6	3	E-	42319072
8	7	8	1	E-	53633717
9	-9	0	9	E+	27585959
9	-5	2	7	E+	36032708
9	-1	4	5	E+	40778841
9	3	6	3	E+	48907668
9	7	8	1	E+	60252347
9	-8	1	9	O-	27587208
9	-4	3	7	O-	36461707
9	0	5	5	O-	44218833
9	4	7	3	O-	54280017
9	8	9	1	O-	66710773

9	-7	1	8	O+	32349995
9	-3	3	6	O+	38460956
9	1	5	4	O+	44288282
9	5	7	2	O+	54280157
9	9	9	0	O+	66710773
9	-6	2	8	E-	32389146
9	-2	4	6	E-	40198727
9	2	6	4	E-	48903545
9	6	8	2	E-	60252344
10	-10	0	10	E+	33412843
10	-6	2	8	E+	43109225
10	-2	4	6	E+	48460056
10	2	6	4	E+	56224975
10	6	8	2	E+	67581279
10	10	10	0	E+	80949676
10	-9	1	10	O-	33413374
10	-5	3	8	O-	43353848
10	-1	5	6	O-	51525923
10	3	7	4	O-	61587708
10	7	9	2	O-	74080388
10	-8	1	9	O+	38763714
10	-4	3	7	O+	46112572
10	0	5	5	O+	51705392
10	4	7	3	O+	61588411
10	8	9	1	O+	74080388
10	-7	2	9	E-	38782181
10	-3	4	7	E-	47407269
10	1	6	5	E-	56210324
10	5	8	3	E-	67581259
10	9	10	1	E-	80949676
11	-11	0	11	E+	39785764
11	-7	2	9	E+	50684857
11	-3	4	7	E+	56930846
11	1	6	5	E+	64276922
11	5	8	3	E+	75614045
11	9	10	1	E+	89075570
11	-10	1	11	O-	39785992
11	-6	3	9	O-	50816896
11	-2	5	7	O-	59532371
11	2	7	5	O-	69605980
11	6	9	3	O-	82147425
11	10	11	1	O-	96166636
11	-9	1	10	O+	45713797
11	-5	3	8	O+	54359088
11	-1	5	6	O+	59928384
11	3	7	4	O+	69608753
11	7	9	2	O+	82147428
11	11	11	0	O+	96166636
11	-8	2	10	E-	45722437
11	-4	4	8	E-	55252646

11	0	6	6	E-	64233512
11	4	8	4	E-	75613930
11	8	10	2	E-	89075570
12	-12	0	12	E+	46703007
12	-8	2	10	E+	58765556
12	-4	4	8	E+	66123822
12	0	6	6	E+	73074418
12	4	8	4	E+	84344010
12	8	10	2	E+	97876760
12	12	12	0	E+	111921060
12	-11	1	12	O-	46703107
12	-7	3	10	O-	58834495
12	-3	5	8	O-	68214011
12	1	7	6	O-	78329173
12	5	9	4	O-	90903583
12	9	11	2	O-	105056530
12	-10	1	11	O+	53201668
12	-6	3	9	O+	63132364
12	-2	5	7	O+	68972761
12	2	7	5	O+	78338292
12	6	9	3	O+	90903602
12	10	11	1	O+	105056530
12	-9	2	11	E-	53205713
12	-5	4	9	E-	63704451
12	-1	6	7	E-	72963522
12	3	8	5	E-	84343518
12	7	10	3	E-	97876760
12	11	12	1	E-	111921060
13	-13	0	13	E+	54162623
13	-9	2	11	E+	67359927
13	-5	4	9	E+	75961253
13	-1	6	7	E+	82634954
13	3	8	5	E+	93764576
13	7	10	3	E+	107343870
13	11	12	1	E+	121592090
13	-12	1	13	O-	54162668
13	-8	3	11	O-	67395295
13	-4	5	9	O-	77542287
13	0	7	7	O-	87750280
13	4	9	5	O-	100340050
13	8	11	3	O-	114565300
13	12	13	1	O-	127128150
13	-11	1	12	O+	61226948
13	-7	3	10	O+	72391649
13	-3	5	8	O+	78825302
13	1	7	6	O+	87776174
13	5	9	4	O+	100340130
13	9	11	2	O+	114565300
13	13	13	0	O+	127128150
13	-10	2	12	E-	61228855

13	-6	4	10	E-	72735565
13	-2	6	8	E-	82385887
13	2	8	6	E-	93762814
13	6	10	4	E-	107343870
13	10	12	2	E-	121592090
14	-14	0	14	E+	62162482
14	-10	2	12	E+	76473537
14	-6	4	10	E+	86365389
14	-2	6	8	E+	92977983
14	2	8	6	E+	103869500
14	6	10	4	E+	117464760
14	10	12	2	E+	131588140
14	14	14	0	E+	139374320
14	-13	1	14	O-	62162502
14	-9	3	12	O-	76491555
14	-5	5	10	O-	87486933
14	-1	7	8	O-	97860086
14	3	9	6	O-	110447490
14	7	11	4	O-	124687030
14	11	13	2	O-	137640990
14	-12	1	13	O+	69788236
14	-8	3	11	O+	82126109
14	-4	5	9	O+	89439600
14	0	7	7	O+	97925103
14	4	9	5	O+	110447810
14	8	11	3	O+	124687030
14	12	13	1	O+	137640990
14	-11	2	13	E-	69789145
14	-7	4	11	E-	82323763
14	-3	6	9	E-	92480816
14	1	8	7	E-	103864070
14	5	10	5	E-	117464740
14	9	12	3	E-	131588140
14	13	14	1	E-	139374320
15	-15	0	15	E+	70700312
15	-11	2	13	E+	86108591
15	-7	4	11	E+	97271090
15	-3	6	9	E+	104112340
15	1	8	7	E+	114653470
15	5	10	5	E+	128224840
15	9	12	3	E+	142009850
15	13	14	1	E+	151102170
15	-14	1	15	O-	70700322
15	-10	3	13	O-	86117772
15	-6	5	11	O-	98018658
15	-2	7	9	O-	108646200
15	2	9	7	O-	121215620
15	6	11	5	O-	135332460
15	10	13	3	O-	140994030
15	14	15	1	O-	149924180

15	-13	1	14	O+	78883551
15	-9	3	12	O+	92341599
15	-5	5	10	O+	100747610
15	-1	7	8	O+	108792820
15	3	9	6	O+	121216690
15	7	11	4	O+	135332460
15	11	13	2	O+	140994030
15	15	15	0	O+	149924180
15	-12	2	14	E-	78883991
15	-8	4	12	E-	92452039
15	-4	6	10	E-	103223820
15	0	8	8	E-	114638640
15	4	10	6	E-	128224780
15	8	12	4	E-	142009850
15	12	14	2	E-	151102170

Appendix E

ALLOWED ENERGY TRANSITIONS AND THEIR ABSOLUTE INTENSITIES FOR THE PURE ROTATIONAL RAMAN SPECTRA OF THE WATER VAPOR MOLECULE

Initial Energy Level			Final Energy Level				Absolute Intensity (m^2)	
J	KP	KO	J	KP	KO	Wave # (cm^{-1})	320 K	200 K
9	6	4	8	4	4	-499.471	6.5989E-041	1.6295E-042
14	4	11	13	2	11	-499.14	9.3025E-042	1.1353E-044
15	4	11	14	4	11	-498.589	9.3322E-043	2.9673E-046
14	3	11	13	3	11	-491.367	3.1467E-042	3.9092E-045
7	3	5	5	1	5	-490.069	1.6365E-039	3.6376E-040
11	2	9	9	2	7	-488.743	9.1823E-040	1.9316E-041
10	3	7	8	3	5	-487.992	7.3376E-040	2.3292E-041
7	4	3	5	2	3	-484.726	7.653E-039	1.2489E-039
10	4	6	8	4	4	-484.677	4.1876E-040	1.0762E-041
13	2	12	12	0	12	-484.53	4.2649E-041	3.4739E-043
13	1	12	12	1	12	-484.463	1.2796E-040	1.0425E-042
12	1	11	10	1	9	-481.598	1.8881E-040	3.1669E-042
12	2	11	10	2	9	-481.117	5.6451E-040	9.465E-042
13	5	9	12	3	9	-480.663	4.3072E-042	8.083E-045
8	6	3	7	4	3	-480.375	4.0616E-040	1.8138E-041
13	0	13	11	0	11	-479.56	4.6615E-040	7.171E-042
13	1	13	11	1	11	-479.554	1.5538E-040	2.3902E-042
11	3	9	9	3	7	-478.837	2.7924E-040	5.8047E-042
13	3	11	12	1	11	-473.448	2.5421E-041	1.1888E-043
13	2	11	12	2	11	-472.134	7.643E-041	3.5856E-043
10	5	5	8	5	3	-468.794	1.7487E-040	3.3558E-042
13	4	10	12	2	10	-465.989	1.1903E-041	3.4425E-044
10	8	3	8	8	1	-465.24	6.5655E-042	3.0194E-044
10	8	2	8	8	0	-465.24	2.1885E-042	1.0065E-044
10	6	4	8	6	2	-463.82	5.8507E-041	7.4759E-043
10	7	3	8	7	1	-463.674	1.4558E-041	1.148E-043
10	7	4	8	7	2	-463.651	4.3673E-041	3.4442E-043
10	5	6	8	5	4	-463.552	5.2372E-040	1.0214E-041
10	6	5	8	6	3	-463.362	1.755E-040	2.2454E-042
15	13	3	13	13	1	-462.516	1.7611E-046	1.0951E-051
15	13	2	13	13	0	-462.516	5.2832E-046	3.2852E-051
12	5	8	11	3	8	-462.15	4.0183E-041	1.7457E-043
10	4	7	8	4	5	-458.627	1.2202E-039	3.4472E-041
7	6	2	6	4	2	-458.41	2.2557E-040	1.7066E-041
7	2	5	5	0	5	-457.062	6.5802E-039	1.6044E-039
5	5	1	3	3	1	-456.854	4.3539E-039	1.1836E-039
5	5	0	3	3	0	-456.658	1.3063E-038	3.5512E-039
6	4	3	4	2	3	-456.363	1.1331E-038	2.9609E-039
10	2	8	8	2	6	-455.057	9.1629E-040	3.8111E-041
14	4	10	13	4	10	-454.642	1.3999E-042	1.1875E-045
13	3	10	12	3	10	-452.218	3.6768E-041	1.0968E-043
12	2	11	11	0	11	-447.641	4.1461E-040	6.9517E-042
11	5	7	10	3	7	-447.636	3.6056E-041	3.4212E-043
12	1	11	11	1	11	-447.499	1.3824E-040	2.3186E-042
11	1	10	9	1	8	-445.768	1.6038E-039	5.2769E-041
11	2	10	9	2	8	-444.75	5.3059E-040	1.7444E-041
12	0	12	10	0	10	-443.312	4.3578E-040	1.3117E-041

12	1	12	10	1	10	-443.298	1.3072E-039	3.9347E-041
7	3	4	5	1	4	-442.899	1.3667E-038	2.8348E-039
15	5	10	14	5	10	-442.328	4.5192E-043	1.0509E-046
6	4	2	4	2	2	-442.001	4.2567E-039	1.1092E-039
9	3	6	7	3	4	-440.562	5.997E-039	3.7897E-040
10	3	8	8	3	6	-440.012	2.3115E-039	9.4049E-041
12	3	10	11	1	10	-437.659	2.5982E-040	2.6251E-042
10	5	6	9	3	6	-435.8	2.5762E-040	5.0242E-042
12	2	10	11	2	10	-435.072	8.6978E-041	8.8425E-043
6	6	1	5	4	1	-434.717	7.7972E-040	9.3603E-041
12	4	9	11	2	9	-434.287	1.2264E-040	7.9944E-043
9	4	5	7	4	3	-428.998	2.9578E-039	1.5173E-040
9	5	5	8	3	5	-424.823	1.8507E-040	6.9662E-042
6	3	4	4	1	4	-424.14	1.0701E-038	3.7395E-039
9	2	7	7	2	5	-419.512	7.6961E-039	6.0512E-040
9	5	4	7	5	2	-417.462	1.1218E-039	4.1963E-041
9	7	2	7	7	0	-415.775	5.2858E-041	8.0457E-043
9	7	3	7	7	1	-415.771	1.7619E-041	2.6819E-043
9	5	5	7	5	3	-415.334	3.7338E-040	1.4054E-041
9	6	3	7	6	1	-415.189	3.152E-040	7.7804E-042
9	6	4	7	6	2	-415.056	1.0506E-040	2.5942E-042
9	4	6	7	4	4	-413.141	9.6312E-040	5.2053E-041
8	5	4	7	3	4	-412.81	1.0924E-039	7.4396E-041
12	3	9	11	3	9	-410.8	4.351E-041	2.9861E-043
11	2	10	10	0	10	-410.604	4.1131E-040	1.3523E-041
11	1	10	10	1	10	-410.298	1.2345E-039	4.0618E-041
10	1	9	8	1	7	-410.128	1.3915E-039	8.5572E-041
15	15	1	14	13	1	-409.723	1.0455E-046	2.9108E-052
13	4	9	12	4	9	-408.843	1.7595E-041	3.8066E-044
10	2	9	8	2	7	-408.034	4.1053E-039	2.5204E-040
11	0	11	9	0	9	-406.941	3.3569E-039	1.8829E-040
11	1	11	9	1	9	-406.908	1.1187E-039	6.2748E-041
11	4	8	10	2	8	-405.061	1.232E-040	1.7182E-042
5	4	2	3	2	2	-403.813	6.4316E-039	2.496E-039
11	3	9	10	1	9	-402.051	2.6854E-040	5.5823E-042
9	3	7	7	3	5	-399.537	1.897E-039	1.435E-040
5	4	1	3	2	1	-398.185	1.9959E-038	7.741E-039
7	5	3	6	3	3	-398.098	6.4176E-040	7.4068E-041
11	2	9	10	2	9	-397.03	8.1272E-040	1.7096E-041
14	5	9	13	5	9	-396.851	7.7398E-043	4.9791E-046
15	14	1	14	14	1	-391.199	2.0661E-046	5.1735E-052
15	14	2	14	14	0	-391.199	6.8869E-047	1.7245E-052
8	3	5	6	3	3	-388.609	4.4816E-039	5.3065E-040
15	6	9	14	6	9	-387.986	2.9581E-043	5.0819E-047
6	3	3	4	1	3	-386.052	8.9355E-039	3.0185E-039
6	2	4	4	0	4	-380.721	5.9733E-039	2.3645E-039
8	2	6	6	2	4	-380.138	6.527E-039	9.2655E-040
6	5	2	5	3	2	-379.787	2.8527E-039	5.2229E-040
10	4	7	9	2	7	-379.414	9.5345E-040	2.6937E-041
9	1	8	7	1	6	-374.865	1.0011E-038	1.0964E-039
8	4	4	6	4	2	-373.995	1.9204E-039	1.8245E-040
10	2	9	9	0	9	-373.466	3.3665E-039	2.0668E-040

10	1	9	9	1	9	-372.808	1.1232E-039	6.9072E-041
9	2	8	7	2	6	-370.777	3.2146E-039	3.5083E-040
10	0	10	8	0	8	-370.469	2.6265E-039	2.6142E-040
10	1	10	8	1	8	-370.387	7.8748E-039	7.8374E-040
8	5	3	6	5	1	-367.279	6.1573E-040	4.1851E-041
11	3	8	10	3	8	-367.095	4.2424E-040	6.4119E-042
10	3	8	9	1	8	-367.049	2.2552E-039	9.1756E-041
8	6	2	6	6	0	-366.584	1.167E-040	5.2111E-042
8	5	4	6	5	2	-366.568	1.8456E-039	1.257E-040
8	6	3	6	6	1	-366.554	3.5009E-040	1.5634E-041
8	4	5	6	4	3	-365.984	5.681E-039	5.5309E-040
15	7	8	14	7	8	-364.676	1.8638E-043	2.1014E-047
12	4	8	11	4	8	-362.623	2.3117E-041	1.2121E-043
5	3	3	3	1	3	-361.69	6.6924E-039	3.4584E-039
15	8	7	14	8	7	-359.896	9.4758E-044	6.3049E-048
15	9	6	14	9	6	-359.222	4.0766E-044	1.5027E-048
15	8	8	14	8	6	-359.219	3.1534E-044	2.101E-048
15	9	7	14	9	5	-359.175	1.3587E-044	5.0089E-049
15	10	5	14	10	5	-358.918	1.5492E-044	3.0394E-049
15	10	6	14	10	4	-358.916	5.1638E-045	1.0131E-049
5	5	1	4	3	1	-358.231	9.9454E-040	2.7036E-040
9	4	6	8	2	6	-357.973	6.8918E-040	3.7248E-041
15	7	9	14	7	7	-357.617	6.0905E-044	6.9579E-048
10	2	8	9	2	8	-357.583	7.666E-040	3.1885E-041
8	3	6	6	3	4	-357.137	1.2236E-038	1.6316E-039
15	11	4	14	11	4	-355.093	5.4472E-045	5.6377E-050
15	11	5	14	11	3	-355.093	1.8157E-045	1.8792E-050
13	5	8	12	5	8	-353.955	1.1189E-041	1.8708E-044
14	6	8	13	6	8	-353.314	5.4172E-043	2.5346E-046
4	4	1	2	2	1	-353.206	2.9646E-038	1.599E-038
4	4	0	2	2	0	-351.97	9.9325E-039	5.3567E-039
14	13	2	13	13	0	-350.671	1.6016E-045	1.3466E-050
14	13	1	13	13	1	-350.671	5.3386E-046	4.4888E-051
15	12	3	14	12	3	-347.631	1.8796E-045	1.0667E-050
15	12	4	14	12	2	-347.631	6.2652E-046	3.5555E-051
15	6	10	14	6	8	-341.764	8.2608E-044	1.5373E-047
8	4	5	7	2	5	-340.299	3.7863E-039	3.6863E-040
8	1	7	6	1	5	-339.984	7.4149E-039	1.3786E-039
14	7	7	13	7	7	-339.396	3.2811E-043	9.8361E-047
14	11	3	13	11	3	-337.625	7.7918E-045	2.1018E-049
14	11	4	13	11	2	-337.625	2.3375E-044	6.3053E-049
14	10	5	13	10	3	-337.596	7.2639E-044	3.7529E-048
14	10	4	13	10	4	-337.596	2.4213E-044	1.251E-048
14	9	5	13	9	5	-337.158	6.6815E-044	6.4908E-048
14	9	6	13	9	4	-337.145	2.0044E-043	1.9472E-047
14	8	6	13	8	6	-337.123	1.6082E-043	2.8238E-047
14	8	7	13	8	5	-336.883	4.8216E-043	8.4704E-047
14	7	8	13	7	6	-336.363	9.7571E-043	2.9422E-046
9	2	8	8	0	8	-336.322	2.7991E-039	3.0547E-040
7	2	5	5	2	3	-335.899	4.3051E-038	1.0497E-038
5	3	2	3	1	2	-335.446	3.9259E-038	2.0024E-038
9	1	8	8	1	8	-334.917	8.4137E-039	9.2146E-040

9	0	9	7	0	7	-333.925	1.6877E-038	2.8377E-039
9	1	9	7	1	7	-333.731	5.6169E-039	9.4432E-040
7	3	4	5	3	2	-333.544	2.4124E-038	5.0036E-039
14	12	3	13	12	1	-333.432	6.7834E-045	9.8333E-050
14	12	2	13	12	2	-333.432	2.2611E-045	3.2778E-050
9	3	7	8	1	7	-333.341	1.8721E-039	1.4163E-040
8	2	7	6	2	5	-332.689	2.0477E-038	3.7795E-039
15	1	15	17	1	17	-332.231	1.3393E-052	4.652E-055
14	6	9	13	6	7	-328.423	1.4827E-042	7.2549E-046
7	4	4	6	2	4	-324.971	1.9979E-039	3.2913E-040
13	6	7	12	6	7	-322.604	7.985E-042	9.476E-045
13	12	1	12	12	1	-322.591	1.7738E-044	6.3212E-049
13	12	2	12	12	0	-322.591	5.9126E-045	2.1071E-049
10	3	7	9	3	7	-321.918	4.2595E-040	1.3521E-041
7	4	3	5	4	1	-320.896	8.7147E-039	1.4222E-039
7	5	2	5	5	0	-317.759	1.8943E-039	2.1852E-040
11	4	7	10	4	7	-317.672	2.5811E-040	3.0951E-042
7	4	4	5	4	2	-317.63	2.8837E-039	4.7505E-040
7	5	3	5	5	1	-317.574	6.3121E-040	7.2851E-041
13	11	3	12	11	1	-317.178	2.7903E-044	1.8713E-048
13	11	2	12	11	2	-317.178	8.3708E-044	5.614E-048
9	2	7	8	2	7	-316.321	5.8969E-039	4.6365E-040
13	10	4	12	10	2	-315.789	9.814E-044	1.2606E-047
13	10	3	12	10	3	-315.789	2.9442E-043	3.7817E-047
13	7	6	12	7	6	-315.118	4.6246E-042	3.4554E-045
12	5	7	11	5	7	-314.897	1.6594E-041	6.7332E-044
13	9	4	12	9	4	-314.769	8.6777E-043	2.0933E-046
13	9	5	12	9	3	-314.766	2.8925E-043	6.9777E-047
13	8	5	12	8	5	-314.252	2.1813E-042	9.5084E-046
13	8	6	12	8	4	-314.177	7.2694E-043	3.1693E-046
13	7	7	12	7	5	-313.95	1.5361E-042	1.1504E-045
7	3	5	5	3	3	-312.726	7.3912E-039	1.6429E-039
13	6	8	12	6	6	-310.597	2.5474E-042	3.0916E-045
6	4	3	5	2	3	-310.214	8.3531E-039	2.1828E-039
5	2	3	3	0	3	-309.749	4.2709E-038	2.5771E-038
7	1	6	5	1	4	-304.756	4.6206E-038	1.3912E-038
4	3	2	2	1	2	-303.02	3.1971E-038	2.2926E-038
8	3	6	7	1	6	-301.902	1.2133E-038	1.6179E-039
8	2	7	7	0	7	-299.357	1.9063E-038	3.5185E-039
8	0	8	6	0	6	-297.367	1.0971E-038	2.9664E-039
8	1	8	6	1	6	-296.91	3.2781E-038	8.8614E-039
12	11	2	11	11	0	-296.535	2.0871E-043	3.2935E-047
12	11	1	11	11	1	-296.535	6.9571E-044	1.0978E-047
8	1	7	7	1	7	-296.411	6.3834E-039	1.1869E-039
12	6	6	11	6	6	-294.901	1.1601E-041	3.2544E-044
5	4	2	4	2	2	-294.335	3.3616E-039	1.3046E-039
12	10	2	11	10	2	-293.576	3.2586E-043	9.8113E-047
12	10	3	11	10	1	-293.576	9.7757E-043	2.9434E-046
7	2	6	5	2	4	-293.399	1.2906E-038	3.8297E-039
12	9	4	11	9	2	-292.074	3.2329E-042	1.8231E-045
12	9	3	11	9	3	-292.074	1.0776E-042	6.0768E-046
12	7	5	11	7	5	-291.278	6.412E-042	1.1201E-044

12	8	4	11	8	4	-291.204	2.8873E-042	2.938E-045
12	8	5	11	8	3	-291.184	8.6613E-042	8.8138E-045
12	7	6	11	7	4	-290.882	1.9211E-041	3.3587E-044
12	6	7	11	6	5	-289.754	3.4137E-041	9.6724E-044
14	5	10	13	5	8	-288.921	1.2985E-042	9.958E-046
4	3	1	2	1	1	-288.666	1.5452E-038	1.1041E-038
6	2	4	4	2	2	-286.994	2.5726E-038	1.0184E-038
15	5	11	14	5	9	-286.167	6.4902E-044	1.9294E-047
13	5	9	12	5	7	-285.849	2.6037E-042	4.8861E-045
11	5	6	10	5	6	-280.276	2.0029E-040	1.834E-042
6	3	3	4	3	1	-277.706	1.1096E-038	3.7482E-039
9	3	6	8	3	6	-276.803	3.6153E-039	2.2846E-040
12	5	8	11	5	6	-276.378	4.0874E-041	1.7757E-043
4	4	1	3	2	1	-275.951	9.1714E-039	4.9466E-039
10	4	6	9	4	6	-275.568	3.004E-040	7.7198E-042
7	3	5	6	1	5	-273.789	7.3083E-039	1.6245E-039
8	2	6	7	2	6	-273.304	4.5889E-039	6.5144E-040
11	10	1	10	10	1	-271.05	2.2454E-042	1.4926E-045
11	10	2	10	10	0	-271.05	7.4845E-043	4.9753E-046
6	4	2	4	4	0	-269.646	2.7708E-039	7.2199E-040
11	9	2	10	9	2	-269.087	9.8443E-042	1.2206E-044
11	9	3	10	9	1	-269.087	3.2814E-042	4.0688E-045
11	6	5	10	6	5	-269.073	1.3386E-040	8.2874E-043
6	4	3	4	4	1	-268.617	8.2859E-039	2.1652E-039
11	8	3	10	8	3	-267.945	2.9571E-041	6.6007E-044
11	8	4	10	8	2	-267.94	9.8569E-042	2.2002E-044
11	7	4	10	7	4	-267.553	7.0166E-041	2.6887E-043
11	7	5	10	7	3	-267.437	2.3379E-041	8.961E-044
6	1	5	4	1	3	-267.409	2.9744E-038	1.3838E-038
11	6	6	10	6	4	-267.136	4.4276E-041	2.752E-043
6	3	4	4	3	2	-266.462	3.1574E-038	1.1034E-038
7	2	6	6	0	6	-262.911	1.302E-038	3.8633E-039
11	5	7	10	5	5	-261.08	6.0613E-041	5.7513E-043
7	0	7	5	0	5	-260.896	5.8301E-038	2.4131E-038
7	1	7	5	1	5	-259.854	1.923E-038	7.9543E-039
7	1	6	6	1	6	-256.962	3.9552E-038	1.1908E-038
6	2	5	4	2	3	-252.549	6.3337E-038	2.8681E-038
10	5	5	9	5	5	-249.725	2.3847E-040	4.5763E-042
6	3	4	5	1	4	-249.521	3.2116E-038	1.1223E-038
3	3	1	1	1	1	-248.082	1.4732E-038	1.3735E-038
10	9	2	9	9	0	-245.823	2.0729E-041	5.3118E-044
10	9	1	9	9	1	-245.823	6.9097E-042	1.7706E-044
4	2	2	2	0	2	-245.689	2.5684E-038	2.2051E-038
10	8	2	9	8	2	-244.467	2.7518E-041	1.2655E-043
10	8	3	9	8	1	-244.466	8.2554E-041	3.7965E-043
10	6	4	9	6	4	-244.217	1.5023E-040	1.9196E-042
10	7	3	9	7	3	-243.782	7.3345E-041	5.7839E-043
10	7	4	9	7	2	-243.754	2.2001E-040	1.7351E-042
10	6	5	9	6	3	-243.59	4.4948E-040	5.7509E-042
3	3	0	1	1	0	-243.047	5.0165E-038	4.6745E-038
10	5	6	9	5	4	-241.422	6.8549E-040	1.3369E-041
9	4	5	8	4	5	-237.527	2.8999E-039	1.4876E-040

5	2	3	3	2	1	-234.354	1.0426E-037	6.291E-038
8	3	5	7	3	5	-233.463	3.2184E-039	3.8108E-040
7	2	5	6	2	5	-229.498	2.9725E-038	7.2474E-039
5	3	3	4	1	3	-228.471	1.2661E-038	6.5428E-039
6	2	5	5	0	5	-227.563	7.1021E-038	3.2161E-038
11	4	8	10	4	6	-226.576	4.4133E-041	6.1548E-043
5	1	4	3	1	2	-226.092	1.5275E-037	1.0464E-037
12	4	9	11	4	7	-225.943	2.6093E-041	1.7009E-043
6	0	6	4	0	4	-224.644	3.1213E-038	1.8825E-038
5	3	2	3	3	0	-223.393	2.9573E-038	1.5084E-038
6	1	6	4	1	4	-222.414	9.1026E-038	5.4815E-038
9	5	4	8	5	4	-222.131	2.2381E-039	8.372E-041
10	4	7	9	4	5	-221.1	6.029E-040	1.7033E-041
9	8	1	8	8	1	-220.774	1.5973E-040	1.4205E-042
9	8	2	8	8	0	-220.774	5.3242E-041	4.735E-043
13	4	10	12	4	8	-220.544	1.6044E-042	4.6401E-045
9	7	2	8	7	2	-219.897	5.6527E-040	8.6043E-042
9	7	3	8	7	1	-219.892	1.8842E-040	2.8681E-042
9	6	3	8	6	3	-219.772	1.3051E-039	3.2216E-041
9	6	4	8	6	2	-219.604	4.3469E-040	1.0734E-041
9	5	5	8	5	3	-219.069	7.3361E-040	2.7613E-041
5	3	3	3	3	1	-218.749	9.6024E-039	4.9622E-039
6	1	5	5	1	5	-216.28	2.4644E-038	1.1465E-038
14	4	11	13	4	9	-212.23	8.5274E-043	1.0407E-045
5	2	4	3	2	2	-209.907	2.8052E-038	1.8368E-038
4	3	2	3	1	2	-209.151	3.6471E-038	2.6153E-038
9	4	6	8	4	4	-209.109	7.8371E-040	4.2356E-041
8	4	4	7	4	4	-204.032	2.7931E-039	2.6536E-040
15	4	12	14	4	10	-203.029	4.8804E-044	2.3942E-047
8	5	3	7	5	3	-196.265	2.0101E-039	1.3662E-040
8	7	1	7	7	1	-195.879	3.3691E-040	9.2812E-042
8	7	2	7	7	0	-195.878	1.0107E-039	2.7843E-041
8	6	2	7	6	2	-195.452	1.0352E-039	4.6227E-041
8	6	3	7	6	1	-195.417	3.1051E-039	1.3867E-040
8	5	4	7	5	2	-195.331	5.9961E-039	4.0837E-040
5	2	4	4	0	4	-194.156	3.6906E-038	2.4166E-038
7	3	4	6	3	4	-193.378	2.4145E-038	5.008E-039
8	4	5	7	4	3	-191.471	7.6197E-039	7.4184E-040
3	3	1	2	1	1	-190.043	8.7575E-039	8.165E-039
5	0	5	3	0	3	-188.586	1.3656E-037	1.1426E-037
3	2	1	1	0	1	-188.362	9.2853E-038	1.0543E-037
6	2	4	5	2	4	-186.565	2.0116E-038	7.963E-039
5	1	5	3	1	3	-184.347	4.2121E-038	3.5121E-038
4	1	3	2	1	1	-180.321	7.0719E-038	6.7686E-038
4	2	2	2	2	0	-179.616	2.9486E-038	2.5315E-038
5	1	4	4	1	4	-174.619	1.2621E-037	8.6463E-038
7	4	3	6	4	3	-174.512	2.1115E-038	3.4459E-039
7	5	2	6	5	2	-171.237	1.3417E-038	1.5478E-039
7	6	1	6	6	1	-171.137	5.1783E-039	3.9177E-040
7	6	2	6	6	0	-171.132	1.7261E-039	1.3059E-040
7	5	3	6	5	1	-171.014	4.4656E-039	5.1539E-040
7	4	4	6	4	2	-169.964	6.7817E-039	1.1172E-039

9	3	7	8	3	5	-166.074	3.8868E-040	2.9404E-041
4	2	3	2	2	1	-165.461	7.5057E-038	6.7177E-038
8	3	6	7	3	4	-163.759	4.5186E-039	6.0253E-040
4	2	3	3	0	3	-163.601	1.3947E-037	1.2483E-037
10	3	8	9	3	6	-163.209	2.8224E-040	1.1484E-041
6	3	3	5	3	3	-157.581	1.8396E-038	6.2144E-039
11	3	9	10	3	7	-156.919	2.2057E-041	4.5851E-043
7	3	5	6	3	3	-155.145	5.1859E-039	1.1527E-039
4	0	4	2	0	2	-151.962	6.056E-038	6.6952E-038
12	3	10	11	3	8	-149.283	1.5189E-041	1.5347E-043
6	4	2	5	4	2	-147.666	1.481E-038	3.8589E-039
6	5	1	5	5	1	-146.56	7.048E-039	1.2903E-039
6	5	2	5	5	0	-146.522	2.1138E-038	3.87E-039
6	4	3	5	4	1	-146.384	4.3901E-038	1.1472E-038
5	2	3	4	2	3	-146.148	1.1565E-037	6.9782E-038
4	1	4	2	1	2	-145.342	1.4737E-037	1.6171E-037
13	3	11	12	3	9	-142.196	1.1312E-042	5.2899E-045
6	3	4	5	3	2	-140.167	4.4616E-038	1.5592E-038
14	3	12	13	3	10	-136.758	7.2773E-043	1.5011E-045
3	2	2	2	0	2	-136.211	4.4356E-038	5.1166E-038
2	2	0	0	0	0	-136.164	2.432E-038	3.3898E-038
4	1	3	3	1	3	-133.219	6.7417E-038	6.4526E-038
15	3	13	14	3	11	-133.148	4.9269E-044	4.2738E-047
3	1	2	1	1	0	-130.994	2.0124E-037	2.537E-037
5	3	2	4	3	2	-126.295	1.097E-037	5.5951E-038
5	4	1	4	4	1	-122.233	6.7489E-038	2.6175E-038
5	4	2	4	4	0	-121.98	2.2433E-038	8.7057E-039
5	3	3	4	3	1	-120.126	3.3619E-038	1.7373E-038
3	0	3	1	0	1	-112.967	2.1368E-037	2.9734E-037
15	13	2	14	13	2	-111.845	4.4853E-046	2.7891E-051
15	13	3	14	13	1	-111.845	1.4951E-046	9.2968E-052
2	2	1	1	0	1	-111.107	9.3307E-038	1.305E-037
4	2	2	3	2	2	-109.478	6.8431E-038	5.8751E-038
7	2	6	6	2	4	-106.835	1.6419E-039	4.8718E-040
6	2	5	5	2	3	-106.401	1.5813E-038	7.1606E-039
3	1	3	1	1	1	-105.141	4.1233E-038	5.6531E-038
8	2	7	7	2	5	-103.19	1.506E-039	2.7796E-040
5	2	4	4	2	2	-100.429	1.5965E-038	1.0454E-038
4	3	1	3	3	1	-98.623	5.4857E-038	3.9197E-038
9	2	8	8	2	6	-97.474	1.527E-040	1.6665E-041
4	3	2	3	3	0	-97.098	1.6048E-037	1.1508E-037
3	1	2	2	1	2	-93.869	3.1527E-037	3.9746E-037
10	2	9	9	2	7	-91.712	1.3755E-040	8.4443E-042
4	2	3	3	2	1	-88.206	1.2676E-037	1.1345E-037
11	2	10	10	2	8	-87.167	1.3329E-041	4.3822E-043
12	2	11	11	2	9	-84.087	1.1052E-041	1.853E-043
13	2	12	12	2	10	-82.167	9.5544E-043	7.7822E-045
14	2	13	13	2	11	-81.03	6.9155E-043	2.6073E-045
15	2	14	14	2	12	-80.404	5.1445E-044	8.5562E-047
15	12	3	16	12	5	-79.846	2.6759E-049	1.5186E-054
15	12	4	16	12	4	-79.839	8.9201E-050	5.0622E-055
3	2	1	2	2	1	-77.255	3.0599E-037	3.4743E-037

15	10	5	16	10	7	-71.635	1.3627E-049	2.6736E-054
15	10	6	16	10	6	-70.418	5.0139E-050	9.8372E-055
3	2	2	2	2	0	-70.137	8.344E-038	9.625E-038
2	0	2	0	0	0	-70.091	6.1575E-038	1.0257E-037
2	1	1	1	1	1	-58.039	1.6705E-037	2.6005E-037
4	1	4	3	1	2	-51.473	1.9765E-038	2.1688E-038
5	1	5	4	1	3	-51.128	2.517E-039	2.0987E-039
6	1	6	5	1	4	-47.795	2.9731E-039	1.7904E-039
3	1	3	2	1	1	-47.103	1.7769E-038	2.4361E-038
7	1	7	6	1	5	-43.573	3.965E-040	1.6401E-040
8	1	8	7	1	6	-39.949	4.6979E-040	1.2699E-040
9	1	9	8	1	7	-37.32	5.9343E-041	9.9768E-042
2	1	2	1	1	0	-37.125	1.5086E-037	2.45E-037
10	1	10	9	1	8	-35.47	6.3442E-041	6.3141E-042
11	1	11	10	1	9	-34.1	6.9963E-042	3.9243E-043
12	1	12	11	1	10	-33	6.3945E-042	1.9248E-043
13	1	13	12	1	11	-32.056	5.9473E-043	9.1488E-045
14	1	14	13	1	12	-31.207	4.5393E-043	3.3994E-045
15	1	15	14	1	13	-30.424	3.4954E-044	1.2141E-046
15	1	14	16	1	16	29.694	2.47E-044	4.1082E-047
14	1	13	15	1	15	30.424	3.9562E-044	1.4917E-046
13	1	12	14	1	14	31.207	5.1542E-043	4.1989E-045
12	1	11	13	1	13	32.056	6.7762E-043	1.1366E-044
11	1	10	12	1	12	33	7.3138E-042	2.4064E-043
10	1	9	11	1	11	34.1	8.038E-042	4.943E-043
9	1	8	10	1	10	35.47	7.3297E-041	8.0274E-042
1	1	0	2	1	2	37.125	1.7547E-037	3.1498E-037
8	1	7	9	1	9	37.32	6.9079E-041	1.2844E-041
7	1	6	8	1	8	39.949	5.5274E-040	1.6642E-040
6	1	5	7	1	7	43.573	4.7345E-040	2.2026E-040
2	1	1	3	1	3	47.103	2.1524E-038	3.3508E-038
5	1	4	6	1	6	47.795	3.6116E-039	2.4742E-039
4	1	3	5	1	5	51.128	3.0994E-039	2.9665E-039
3	1	2	4	1	4	51.473	2.4372E-038	3.0726E-038
1	1	1	2	1	1	58.039	2.1156E-037	3.8517E-037
15	14	1	16	14	3	68.896	2.0093E-048	5.0313E-054
15	14	2	16	14	2	68.896	6.6975E-049	1.6771E-054
0	0	0	2	0	2	70.091	8.1904E-038	1.6483E-037
2	2	0	3	2	2	70.137	1.1101E-037	1.5473E-037
2	2	1	3	2	1	77.255	4.1905E-037	5.8608E-037
15	2	13	16	2	15	80.128	4.3976E-044	3.8178E-047
14	2	12	15	2	14	80.404	7.1364E-044	1.4744E-046
13	2	11	14	2	13	81.03	9.6176E-043	4.512E-045
12	2	10	13	2	12	82.167	1.3349E-042	1.3571E-044
11	2	9	12	2	11	84.087	1.5563E-041	3.2737E-043
10	2	8	11	2	10	87.167	1.9006E-041	7.9051E-043
3	2	1	4	2	3	88.206	1.8152E-037	2.0611E-037
9	2	7	10	2	9	91.712	1.9979E-040	1.5709E-041
2	1	2	3	1	2	93.869	4.6197E-037	7.5026E-037
3	3	0	4	3	2	97.098	2.3827E-037	2.2203E-037
8	2	6	9	2	8	97.474	2.2707E-040	3.2234E-041
3	3	1	4	3	1	98.623	8.1954E-038	7.6409E-038

4	2	2	5	2	4	100.429	2.4028E-038	2.0629E-038
7	2	5	8	2	7	103.19	2.2921E-039	5.5886E-040
1	1	1	3	1	3	105.141	6.3258E-038	1.1517E-037
5	2	3	6	2	5	106.401	2.4384E-038	1.4713E-038
6	2	4	7	2	6	106.835	2.5363E-039	1.004E-039
15	3	13	17	3	15	108.827	1.0617E-047	9.21E-051
3	2	2	4	2	2	109.478	1.0685E-037	1.2326E-037
1	0	1	2	2	1	111.107	1.4667E-037	2.7681E-037
14	13	2	15	13	2	111.845	7.0714E-046	5.9458E-051
14	13	1	15	13	3	111.845	2.3571E-046	1.9819E-051
1	0	1	3	0	3	112.967	3.3842E-037	6.3872E-037
4	3	1	5	3	3	120.126	5.482E-038	3.9171E-038
4	4	0	5	4	2	121.98	3.6856E-038	1.9877E-038
4	4	1	5	4	1	122.233	1.11E-037	5.9866E-038
4	3	2	5	3	2	126.295	1.8343E-037	1.3153E-037
1	1	0	3	1	2	130.994	3.4299E-037	6.157E-037
15	3	12	16	3	14	131.025	4.799E-044	2.3777E-047
14	3	11	15	3	13	133.148	8.4713E-044	1.0524E-046
3	1	3	4	1	3	133.219	1.1595E-037	1.5897E-037
0	0	0	2	2	0	136.164	4.2332E-038	8.5193E-038
2	0	2	3	2	2	136.211	7.7223E-038	1.2864E-037
13	3	10	14	3	12	136.758	1.2698E-042	3.7878E-045
5	3	2	6	3	4	140.167	7.8936E-038	4.0261E-038
12	3	9	13	3	11	142.196	2.0179E-042	1.3849E-044
2	1	2	4	1	4	145.342	2.6628E-037	4.3245E-037
4	2	3	5	2	3	146.148	2.0965E-037	1.8764E-037
5	4	1	6	4	3	146.384	7.9661E-038	3.0896E-038
5	5	0	6	5	2	146.522	3.8378E-038	1.0433E-038
5	5	1	6	5	1	146.56	1.2798E-038	3.4792E-039
5	4	2	6	4	2	147.666	2.7014E-038	1.0484E-038
11	3	8	12	3	10	149.283	2.7889E-041	4.2151E-043
2	0	2	4	0	4	151.962	1.1241E-037	1.8726E-037
6	3	3	7	3	5	155.145	9.752E-039	3.2943E-039
10	3	7	11	3	9	156.919	4.1778E-041	1.3261E-042
5	3	3	6	3	3	157.581	3.4938E-038	1.8055E-038
9	3	6	10	3	8	163.209	5.4846E-040	3.4659E-041
3	0	3	4	2	3	163.601	2.7144E-037	3.7773E-037
7	3	4	8	3	6	163.759	8.8003E-039	1.8253E-039
2	2	1	4	2	3	165.461	1.4719E-037	2.0586E-037
8	3	5	9	3	7	166.074	7.6415E-040	9.048E-041
6	4	2	7	4	4	169.964	1.3546E-038	3.5296E-039
6	5	1	7	5	3	171.014	8.9576E-039	1.6399E-039
6	6	0	7	6	2	171.132	3.464E-039	4.1584E-040
6	6	1	7	6	1	171.137	1.0393E-038	1.2476E-039
6	5	2	7	5	2	171.237	2.6939E-038	4.9321E-039
6	4	3	7	4	3	174.512	4.2963E-038	1.1227E-038
4	1	4	5	1	4	174.619	2.5691E-037	2.819E-037
2	2	0	4	2	2	179.616	6.1254E-038	8.5377E-038
2	1	1	4	1	3	180.321	1.4733E-037	2.2937E-037
3	1	3	5	1	5	184.347	8.9204E-038	1.223E-037
5	2	4	6	2	4	186.565	4.2989E-038	2.8149E-038
1	0	1	3	2	1	188.362	1.9988E-037	3.7725E-037

3	0	3	5	0	5	188.586	2.9425E-037	4.0947E-037
2	1	1	3	3	1	190.043	1.8982E-038	2.955E-038
7	4	3	8	4	5	191.471	1.6612E-038	2.7109E-039
6	3	4	7	3	4	193.378	5.305E-038	1.8539E-038
4	0	4	5	2	4	194.156	8.1344E-038	8.9929E-038
15	4	11	16	4	13	194.696	5.3591E-044	1.704E-047
7	5	2	8	5	4	195.331	1.3279E-038	1.5318E-039
7	6	1	8	6	3	195.417	6.879E-039	5.2044E-040
7	6	2	8	6	2	195.452	2.2938E-039	1.7354E-040
7	7	0	8	7	2	195.878	2.2434E-039	1.0483E-040
7	7	1	8	7	1	195.879	7.478E-040	3.4943E-041
7	5	3	8	5	3	196.265	4.4685E-039	5.1573E-040
14	4	10	15	4	12	203.029	1.1152E-043	9.4608E-047
7	4	4	8	4	4	204.032	6.4087E-039	1.0558E-039
8	4	4	9	4	6	209.109	1.8358E-039	1.7441E-040
3	1	2	4	3	2	209.151	8.5444E-038	1.0772E-037
3	2	2	5	2	4	209.907	6.5923E-038	7.6044E-038
15	3	12	17	3	14	210.985	4.0621E-048	2.0126E-051
13	4	9	14	4	11	212.23	2.023E-042	4.3767E-045
5	1	5	6	1	5	216.28	5.9437E-038	4.9558E-038
3	3	1	5	3	3	218.749	2.3393E-038	2.181E-038
8	5	3	9	5	5	219.069	1.7895E-039	1.2163E-040
8	6	2	9	6	4	219.604	1.0627E-039	4.7452E-041
8	6	3	9	6	3	219.772	3.1927E-039	1.4258E-040
8	7	1	9	7	3	219.892	4.6115E-040	1.2704E-041
8	7	2	9	7	2	219.897	1.3835E-039	3.8113E-041
12	4	8	13	4	10	220.544	3.9371E-042	2.0644E-044
8	8	1	9	8	1	220.774	3.9233E-040	6.3296E-042
8	8	0	9	8	2	220.774	1.3078E-040	2.1099E-042
9	4	5	10	4	7	221.1	1.4829E-039	7.6067E-041
8	5	4	9	5	4	222.131	5.528E-039	3.7649E-040
4	1	4	6	1	6	222.414	2.2508E-037	2.4698E-037
3	3	0	5	3	2	223.393	7.3419E-038	6.8414E-038
4	0	4	6	0	6	224.644	7.7886E-038	8.6106E-038
11	4	7	12	4	9	225.943	6.5455E-041	7.8489E-043
3	1	2	5	1	4	226.092	3.834E-037	4.8336E-037
10	4	6	11	4	8	226.576	1.1099E-040	2.8524E-042
5	0	5	6	2	5	227.563	1.7934E-037	1.5005E-037
4	1	3	5	3	3	228.471	3.2089E-038	3.0713E-038
6	2	5	7	2	5	229.498	7.5652E-038	3.4258E-038
7	3	5	8	3	5	233.463	8.3243E-039	1.8503E-039
3	2	1	5	2	3	234.354	2.7065E-037	3.0731E-037
8	4	5	9	4	5	237.527	7.6257E-039	7.4243E-040
9	5	4	10	5	6	241.422	1.8314E-039	6.8505E-041
1	1	0	3	3	0	243.047	1.3491E-037	2.4218E-037
9	6	3	10	6	5	243.59	1.2115E-039	2.9905E-041
9	7	2	10	7	4	243.754	5.934E-040	9.0324E-042
9	7	3	10	7	3	243.782	1.9784E-040	3.0115E-042
9	6	4	10	6	4	244.217	4.0596E-040	1.0024E-041
9	8	1	10	8	3	244.466	2.2331E-040	1.9859E-042
9	8	2	10	8	2	244.467	7.4435E-041	6.6198E-043
2	0	2	4	2	2	245.689	6.9821E-038	1.1631E-037

9	9	1	10	9	1	245.823	1.8794E-041	9.3473E-044
9	9	0	10	9	2	245.823	5.6382E-041	2.8042E-043
1	1	1	3	3	1	248.082	4.044E-038	7.3626E-038
5	1	4	6	3	4	249.521	8.868E-038	6.0751E-038
9	5	5	10	5	5	249.725	6.5901E-040	2.4805E-041
4	2	3	6	2	5	252.549	1.7705E-037	1.5847E-037
6	1	6	7	1	6	256.962	1.1257E-037	6.7789E-038
5	1	5	7	1	7	259.854	5.5379E-038	4.6175E-038
5	0	5	7	0	7	260.896	1.6861E-037	1.4107E-037
10	5	5	11	5	7	261.08	1.7543E-040	3.3665E-042
6	0	6	7	2	6	262.911	3.7964E-038	2.2896E-038
4	3	2	6	3	4	266.462	9.3404E-038	6.698E-038
10	6	4	11	6	6	267.136	1.3134E-040	1.6783E-042
4	1	3	6	1	5	267.409	8.8331E-038	8.4543E-038
10	7	3	11	7	5	267.437	6.9439E-041	5.4759E-043
10	7	4	11	7	4	267.553	2.085E-040	1.6443E-042
14	12	3	16	12	5	267.785	7.1548E-049	1.0372E-053
14	12	2	16	12	4	267.792	2.3848E-049	3.457E-054
10	8	2	11	8	4	267.94	2.9336E-041	1.3491E-043
10	8	3	11	8	3	267.945	8.801E-041	4.0475E-043
4	4	1	6	4	3	268.617	2.4728E-038	1.3337E-038
10	6	5	11	6	5	269.073	4.0022E-040	5.1206E-042
10	9	2	11	9	2	269.087	2.9436E-041	7.5428E-044
10	9	1	11	9	3	269.087	9.8118E-042	2.5143E-044
4	4	0	6	4	2	269.646	8.3039E-039	4.4784E-039
10	10	1	11	10	1	271.05	6.7677E-042	9.3466E-045
10	10	0	11	10	2	271.05	2.2559E-042	3.1155E-045
7	2	6	8	2	6	273.304	1.3959E-038	4.142E-039
6	1	5	7	3	5	273.789	2.2275E-038	1.0363E-038
9	4	6	10	4	6	275.568	9.2222E-040	4.9842E-041
3	2	1	4	4	1	275.951	2.82E-038	3.202E-038
11	5	6	12	5	8	276.378	1.259E-040	1.1528E-042
8	3	6	9	3	6	276.803	1.1155E-038	1.4875E-039
4	3	1	6	3	3	277.706	3.4362E-038	2.4553E-038
15	5	10	16	5	12	278.981	8.478E-044	1.9715E-047
10	5	6	11	5	6	280.276	6.268E-040	1.2224E-041
15	8	7	16	8	9	284.507	4.8625E-047	3.2353E-051
15	8	8	16	8	8	285.002	1.6E-047	1.066E-051
12	5	7	13	5	9	285.849	8.335E-042	3.382E-044
14	5	9	15	5	11	286.167	2.0804E-043	1.3383E-046
4	2	2	6	2	4	286.994	8.274E-038	7.1037E-038
14	10	5	16	10	7	287.283	2.72E-050	1.4053E-054
14	10	4	16	10	6	288.497	1.1097E-050	5.7334E-055
2	1	1	4	3	1	288.666	5.0036E-038	7.7894E-038
13	5	8	14	5	10	288.921	4.209E-042	7.0374E-045
11	6	5	12	6	7	289.754	1.1103E-040	6.8743E-043
11	7	4	12	7	6	290.882	6.2773E-041	2.4054E-043
11	8	3	12	8	5	291.184	2.8335E-041	6.3249E-044
11	8	4	12	8	4	291.204	9.4465E-042	2.1086E-044
11	7	5	12	7	5	291.278	2.0985E-041	8.0432E-044
11	9	3	12	9	3	292.074	3.5383E-042	4.3872E-045
11	9	2	12	9	4	292.074	1.0615E-041	1.3162E-044

5	2	4	7	2	6	293.399	4.2606E-038	2.7898E-038
11	10	1	12	10	3	293.576	3.2294E-042	2.1467E-045
11	10	2	12	10	2	293.576	1.0765E-042	7.1557E-046
4	2	2	5	4	2	294.335	1.1139E-038	9.5637E-039
11	6	6	12	6	6	294.901	3.8531E-041	2.3949E-043
7	1	7	8	1	7	296.411	2.1333E-038	8.8239E-039
11	11	0	12	11	2	296.535	6.9784E-043	2.4507E-046
11	11	1	12	11	1	296.535	2.3261E-043	8.1689E-047
6	1	6	8	1	8	296.91	1.0977E-037	6.6104E-038
6	0	6	8	0	8	297.367	3.6806E-038	2.2197E-038
15	5	11	17	5	13	297.698	2.9808E-047	8.861E-051
7	0	7	8	2	7	299.357	6.4474E-038	2.6685E-038
7	1	6	8	3	6	301.902	4.1464E-038	1.2484E-038
2	1	2	4	3	2	303.02	1.0976E-037	1.7825E-037
5	1	4	7	1	6	304.756	1.5975E-037	1.0944E-037
3	0	3	5	2	3	309.749	1.5069E-037	2.097E-037
5	2	3	6	4	3	310.214	2.9528E-038	1.7817E-038
12	6	6	13	6	8	310.597	9.0192E-042	2.5301E-044
15	11	5	17	11	7	311.929	2.0273E-049	2.0982E-054
15	11	4	17	11	6	312.203	6.0609E-049	6.2728E-054
5	3	3	7	3	5	312.726	2.6396E-038	1.364E-038
12	7	5	13	7	7	313.95	5.5132E-042	9.6309E-045
12	8	4	13	8	6	314.177	2.6115E-042	2.6574E-045
12	8	5	13	8	5	314.252	7.8385E-042	7.9764E-045
12	9	3	13	9	5	314.766	1.0416E-042	5.8738E-046
12	9	4	13	9	4	314.769	3.1249E-042	1.7622E-045
11	5	7	12	5	7	314.897	5.9788E-041	5.6731E-043
12	7	6	13	7	6	315.118	1.6677E-041	2.9157E-044
12	10	2	13	10	4	315.789	3.5488E-043	1.0685E-046
12	10	3	13	10	3	315.789	1.0646E-042	3.2056E-046
8	2	7	9	2	7	316.321	2.137E-038	3.9443E-039
12	11	1	13	11	3	317.178	1.0147E-043	1.6012E-047
12	11	2	13	11	2	317.178	3.0441E-043	4.8037E-047
5	5	1	7	5	3	317.574	2.2992E-039	6.2502E-040
5	4	2	7	4	4	317.63	1.0506E-038	4.0772E-039
10	4	7	11	4	7	317.672	9.4055E-040	2.6572E-041
5	5	0	7	5	2	317.759	6.9052E-039	1.8771E-039
5	4	1	7	4	3	320.896	3.2175E-038	1.2479E-038
15	12	4	17	12	6	321.425	9.1438E-051	5.1892E-056
15	12	3	17	12	5	321.446	2.7425E-050	1.5564E-055
9	3	7	10	3	7	321.918	1.5792E-039	1.1946E-040
12	12	1	13	12	1	322.591	6.5942E-044	5.6106E-048
12	12	0	13	12	2	322.591	2.1981E-044	1.8702E-048
12	6	7	13	6	7	322.604	2.9687E-041	8.4115E-044
6	2	4	7	4	4	324.971	7.4996E-039	2.9687E-039
13	6	7	14	6	9	328.423	5.6446E-042	6.6986E-045
15	10	6	17	10	8	331.743	8.2645E-051	1.6215E-055
6	2	5	8	2	7	332.689	7.9319E-038	3.5919E-038
8	1	7	9	3	7	333.341	7.2712E-039	1.3519E-039
13	12	1	14	12	3	333.432	2.6356E-044	9.3924E-049
13	12	2	14	12	2	333.432	8.7853E-045	3.1308E-049
5	3	2	7	3	4	333.544	9.3773E-038	4.7829E-038

7	1	7	9	1	9	333.731	2.185E-038	9.038E-039
7	0	7	9	0	9	333.925	6.5704E-038	2.7195E-038
15	10	5	17	10	7	334.463	3.1734E-050	6.2261E-055
8	1	8	9	1	8	334.917	3.2888E-038	8.8903E-039
3	1	2	5	3	2	335.446	1.5379E-037	1.9388E-037
5	2	3	7	2	5	335.899	1.6896E-037	1.0195E-037
8	0	8	9	2	8	336.322	1.1004E-038	2.9754E-039
13	7	6	14	7	8	336.363	3.8365E-042	2.8666E-045
13	8	5	14	8	7	336.883	1.8999E-042	8.2818E-046
13	8	6	14	8	6	337.123	6.3429E-043	2.7654E-046
13	9	4	14	9	6	337.145	7.9063E-043	1.9072E-046
13	9	5	14	9	5	337.158	2.6357E-043	6.358E-047
13	10	4	14	10	4	337.596	9.5685E-044	1.229E-047
13	10	3	14	10	5	337.596	2.8705E-043	3.6871E-047
13	11	2	14	11	4	337.625	9.2384E-044	6.1959E-048
13	11	3	14	11	3	337.625	3.0795E-044	2.0653E-048
13	7	7	14	7	7	339.396	1.3061E-042	9.782E-046
6	1	5	8	1	7	339.984	2.9588E-038	1.3765E-038
7	2	5	8	4	5	340.299	1.5128E-038	3.6885E-039
14	6	8	15	6	10	341.764	3.3203E-043	1.5535E-046
14	12	2	15	12	4	347.631	2.5791E-045	3.7386E-050
14	12	3	15	12	3	347.631	7.7372E-045	1.1216E-049
15	6	9	16	6	11	349.406	1.483E-043	2.5478E-047
13	13	0	14	13	2	350.671	6.675E-045	1.4454E-049
13	13	1	14	13	1	350.671	2.225E-045	4.8181E-050
2	2	0	4	4	0	351.97	4.1616E-038	5.8004E-038
2	2	1	4	4	1	353.206	1.2484E-037	1.746E-037
13	6	8	14	6	8	353.314	2.2822E-042	2.7697E-045
12	5	8	13	5	8	353.955	4.7261E-041	2.0532E-043
15	13	3	16	13	3	354.513	3.8085E-046	2.3682E-051
15	13	2	16	13	4	354.513	1.1426E-045	7.1047E-051
14	11	4	15	11	4	355.093	2.3115E-044	6.2351E-049
14	11	3	15	11	5	355.093	7.705E-045	2.0784E-049
6	3	4	8	3	6	357.137	5.2356E-038	1.8296E-038
9	2	8	10	2	8	357.583	3.2862E-039	3.5863E-040
14	7	7	15	7	9	357.617	2.6112E-043	7.8278E-047
8	2	6	9	4	6	357.973	2.959E-039	4.2006E-040
4	3	1	5	5	1	358.231	4.2745E-039	3.0543E-039
14	10	4	15	10	6	358.916	2.2256E-044	1.1499E-048
14	10	5	15	10	5	358.918	6.6769E-044	3.4496E-048
14	9	5	15	9	7	359.175	5.8623E-044	5.6949E-048
14	8	6	15	8	8	359.219	1.3608E-043	2.3895E-047
14	9	6	15	9	6	359.222	1.7592E-043	1.709E-047
14	8	7	15	8	7	359.896	4.1004E-043	7.2034E-047
3	1	3	5	3	3	361.69	2.9172E-038	3.9995E-038
11	4	8	12	4	8	362.623	1.0115E-040	1.4106E-042
14	7	8	15	7	8	364.676	8.2236E-043	2.4798E-046
15	9	7	17	9	9	365.666	1.0001E-048	3.6868E-053
6	4	3	8	4	5	365.984	2.52E-038	6.585E-039
6	6	1	8	6	3	366.554	1.5565E-039	1.8685E-040
6	5	2	8	5	4	366.568	8.2062E-039	1.5024E-039
6	6	0	8	6	2	366.584	5.1892E-040	6.2295E-041

9	1	8	10	3	8	367.049	1.0047E-038	1.1003E-039
10	3	8	11	3	8	367.095	1.8904E-039	7.6914E-041
6	5	1	8	5	3	367.279	2.7457E-039	5.0266E-040
15	11	4	16	11	6	367.322	5.1657E-045	5.3462E-050
15	11	5	16	11	5	367.323	1.7219E-045	1.7821E-050
8	1	8	10	1	10	370.387	3.5563E-038	9.6133E-039
8	0	8	10	0	10	370.469	1.1865E-038	3.2083E-039
7	2	6	9	2	8	370.777	1.4541E-038	4.3146E-039
15	12	3	16	14	3	372.183	1.8498E-045	1.0498E-050
9	1	9	10	1	9	372.808	5.1227E-039	8.6123E-040
9	0	9	10	2	9	373.466	1.5395E-038	2.5885E-039
6	4	2	8	4	4	373.995	8.8008E-039	2.2932E-039
7	1	6	9	1	8	374.865	4.6041E-038	1.3862E-038
15	7	8	16	7	10	376.911	1.4001E-043	1.5785E-047
9	2	7	10	4	7	379.414	4.467E-039	3.5122E-040
5	3	2	6	5	2	379.787	1.3385E-038	6.8271E-039
15	10	5	16	12	5	379.973	1.37E-044	2.6878E-049
6	2	4	8	2	6	380.138	3.0669E-038	1.214E-038
4	0	4	6	2	4	380.721	2.8134E-038	3.1104E-038
15	9	6	16	9	8	380.786	3.4824E-044	1.2837E-048
15	9	7	16	9	7	380.926	1.1618E-044	4.2829E-049
15	8	7	16	10	7	381.057	7.8067E-044	5.1943E-048
15	9	6	17	9	8	384.249	4.5128E-048	1.6635E-052
4	1	3	6	3	3	386.052	4.301E-038	4.1165E-038
14	6	9	15	6	9	387.986	1.4351E-042	7.0218E-046
6	3	3	8	3	5	388.609	2.1797E-038	7.3632E-039
14	14	0	15	14	2	391.199	3.3851E-046	2.4352E-051
14	14	1	15	14	1	391.199	1.0155E-045	7.3056E-051
15	7	9	16	7	9	391.799	5.17E-044	5.9063E-048
13	5	9	14	5	9	396.851	3.8928E-042	7.3053E-045
10	2	9	11	2	9	397.03	4.0907E-039	2.5114E-040
6	3	3	7	5	3	398.098	3.2442E-039	1.0959E-039
3	2	1	5	4	1	398.185	1.0093E-037	1.146E-037
7	3	5	9	3	7	399.537	9.6459E-039	2.1441E-039
10	1	9	11	3	9	402.051	1.3796E-039	8.4837E-041
15	7	9	17	7	11	403.497	4.9652E-047	5.6723E-051
3	2	2	5	4	2	403.813	3.3278E-038	3.8388E-038
10	2	8	11	4	8	405.061	6.4071E-040	2.6649E-041
9	1	9	11	1	11	406.908	5.8616E-039	9.8546E-040
9	0	9	11	0	11	406.941	1.7592E-038	2.9579E-039
8	2	7	10	2	9	408.034	2.161E-038	3.9885E-039
12	4	9	13	4	9	408.843	9.2922E-041	6.0572E-043
14	13	1	15	15	1	409.723	5.5415E-046	4.6594E-051
8	1	7	10	1	9	410.128	7.3874E-039	1.3735E-039
10	1	10	11	1	10	410.298	6.5583E-039	6.5272E-040
10	0	10	11	2	10	410.604	2.1879E-039	2.1776E-040
11	3	9	12	3	9	410.8	2.3162E-040	4.8149E-042
7	3	4	8	5	4	412.81	5.8629E-039	1.216E-039
7	4	4	9	4	6	413.141	5.1762E-039	8.5272E-040
7	6	2	9	6	4	415.056	5.6904E-040	4.3052E-041
7	6	1	9	6	3	415.189	1.7082E-039	1.2924E-040
7	5	3	9	5	5	415.334	2.0247E-039	2.3368E-040

7	7	1	9	7	3	415.771	9.5712E-041	4.4724E-042
7	7	0	9	7	2	415.775	2.8714E-040	1.3418E-041
7	5	2	9	5	4	417.462	6.1362E-039	7.0784E-040
7	2	5	9	2	7	419.512	4.2449E-038	1.035E-038
4	1	4	6	3	4	424.14	6.0144E-038	6.5995E-038
8	3	5	9	5	5	424.823	1.0431E-039	1.2351E-040
15	6	10	16	6	10	426.892	9.2548E-044	1.7223E-047
7	4	3	9	4	5	428.998	1.6957E-038	2.7672E-039
11	2	9	12	4	9	434.287	7.1836E-040	1.5111E-041
5	4	1	6	6	1	434.717	4.5752E-039	1.7745E-039
11	2	10	12	2	10	435.072	5.111E-040	1.6804E-041
9	3	6	10	5	6	435.8	1.5183E-039	9.5947E-041
15	14	1	16	16	1	436.566	2.5807E-046	6.4622E-052
11	1	10	12	3	10	437.659	1.5429E-039	5.0767E-041
8	3	6	10	3	8	440.012	1.3859E-038	1.848E-039
7	3	4	9	3	6	440.562	3.6036E-038	7.4743E-039
4	2	2	6	4	2	442.001	2.5729E-038	2.209E-038
14	5	10	15	5	10	442.328	2.7352E-042	2.0976E-045
5	1	4	7	3	4	442.899	8.2912E-038	5.68E-038
10	1	10	12	1	12	443.298	7.943E-039	7.9052E-040
10	0	10	12	0	12	443.312	2.6481E-039	2.6356E-040
9	2	8	11	2	10	444.75	3.2432E-039	3.5394E-040
9	1	8	11	1	10	445.768	9.8436E-039	1.0781E-039
15	15	1	16	15	1	447.086	1.0189E-046	2.8366E-052
15	15	0	16	15	2	447.086	3.0566E-046	8.5097E-052
11	1	11	12	1	11	447.499	8.5444E-040	4.7926E-041
10	3	7	11	5	7	447.636	2.2299E-040	7.0784E-042
11	0	11	12	2	11	447.641	2.5642E-039	1.4383E-040
15	5	10	17	5	12	450.362	1.12E-045	2.6044E-049
12	3	10	13	3	10	452.218	2.3168E-040	2.3407E-042
13	4	10	14	4	10	454.642	8.9079E-042	2.5763E-044
8	2	6	10	2	8	455.057	5.8406E-039	8.2913E-040
4	2	3	6	4	3	456.363	7.2611E-038	6.4988E-038
3	3	0	5	5	0	456.658	8.3811E-038	7.8098E-038
3	3	1	5	5	1	456.854	2.7957E-038	2.6065E-038
5	0	5	7	2	5	457.062	4.2287E-038	3.538E-038
6	4	2	7	6	2	458.41	1.4576E-039	3.798E-040
8	4	5	10	4	7	458.627	7.8913E-039	7.6829E-040
14	14	1	16	14	3	460.095	1.1353E-047	8.1675E-053
14	14	0	16	14	2	460.095	3.7845E-048	2.7225E-053
15	15	1	17	15	3	461.025	9.0283E-048	2.5135E-053
15	15	0	17	15	2	461.025	2.7085E-047	7.5405E-053
11	3	8	12	5	8	462.15	2.6364E-040	3.9845E-042
13	13	0	15	13	2	462.516	3.4714E-045	7.5171E-050
13	13	1	15	13	3	462.516	1.1571E-045	2.5057E-050
8	6	3	10	6	5	463.362	1.1571E-039	5.1675E-041
8	5	4	10	5	6	463.552	3.4557E-039	2.3536E-040
8	7	2	10	7	4	463.651	2.8829E-040	7.9418E-042
8	7	1	10	7	3	463.674	9.6107E-041	2.6475E-042
8	6	2	10	6	4	463.82	3.8648E-040	1.7258E-041
8	8	0	10	8	2	465.24	1.454E-041	2.3458E-043
8	8	1	10	8	3	465.24	4.3621E-041	7.0374E-043

12	2	10	13	4	10	465.989	7.9323E-041	8.0643E-043
14	13	1	16	13	3	466.358	1.1221E-046	9.4345E-052
14	13	2	16	13	4	466.358	3.3662E-046	2.8303E-051
8	5	3	10	5	5	468.794	1.1788E-039	8.0121E-041
15	14	2	17	14	4	471.453	9.1828E-049	2.2994E-054
15	14	1	17	14	3	471.453	2.7548E-048	6.8982E-054
12	2	11	13	2	11	472.134	5.2225E-040	8.7564E-042
12	1	11	13	3	11	473.448	1.7464E-040	2.9291E-042
9	3	7	11	3	9	478.837	1.9608E-039	1.4834E-040
11	1	11	13	1	13	479.554	1.0943E-039	6.1377E-041
11	0	11	13	0	13	479.56	3.283E-039	1.8415E-040
7	4	3	8	6	3	480.375	2.8699E-039	4.6835E-040
12	3	9	13	5	9	480.663	3.0471E-041	2.0912E-043
10	2	9	12	2	11	481.117	4.001E-039	2.4563E-040
10	1	9	12	1	11	481.598	1.3408E-039	8.2454E-041
12	1	12	13	1	12	484.463	9.1936E-040	2.7673E-041
12	0	12	13	2	12	484.53	3.065E-040	9.2259E-042
8	4	4	10	4	6	484.677	3.0113E-039	2.8609E-040
5	2	3	7	4	3	484.726	5.5043E-038	3.3213E-038
8	3	5	10	3	7	487.992	5.3481E-039	6.3324E-040
9	2	7	11	2	9	488.743	6.7131E-039	5.2783E-040
15	5	11	16	5	11	488.817	2.0252E-043	6.0203E-047
5	1	5	7	3	5	490.069	1.2029E-038	1.003E-038
13	3	11	14	3	11	491.367	2.3252E-041	1.0874E-043
14	4	11	15	4	11	498.589	7.1017E-042	8.6671E-045
13	2	11	14	4	11	499.14	7.0949E-041	3.3285E-043
8	4	4	9	6	4	499.471	5.0397E-040	4.7881E-041

VITA

Paul A.T. Haris was born in New York City, NY on 28 December 1967. He attended The Haverford School where he graduated in May, 1986. He obtained a Bachelor of Science degree in Electrical Engineering from The Pennsylvania State University, and was commissioned a Second Lieutenant in the United States Air Force on 5 January 1991. He was funded under a Class 1 College Scholarship from the U.S. Air Force, was sent to the Strategic Defense Initiative Office at the Pentagon under the Advanced Training Program, graduated as a Distinguished Graduate of his ROTC Detachment, and was nominated for a Regular Commission. In 1991, Paul was awarded The Aerospace Education Foundation Dr. Theodore von Karman Graduate Scholarship. During his studies in the Master Degree program, he participated in the Latitudinal Distribution of Middle Atmospheric Structure Campaign which took him to the Andoy Rocket Range, Norway and to Antarctica on board the German research vessel RV Polarstern. In January 1993 Paul received his Masters of Science in Electrical Engineering from The Pennsylvania State University. He immediately enrolled in the Ph. D. program. He was awarded Second place in the Eighth Annual Graduate Research Exhibition in 1993 and participated in the VOCAR campaign at Pt. Mugu Naval Air Weapons Test Facility, California to test lidar capabilities to measure atmospheric refractivity. Paul was promoted to First Lieutenant in the U.S. Air Force in 1994, and was conferred as a Doctor of Philosophy in Electrical Engineering from The Pennsylvania State University in August 1995. He was funded throughout his graduate studies by a Research Assistantship under the Exploratory and Educational Grant from the Applied Research Laboratory and the Office of Naval Research. He is a member of Sigma Xi Scientific Research Society, Eta Kappa Nu Electrical Engineering Honor Society, and Tau Betta Pi National Engineering Society. He has authored and co-authored a number of scientific papers. He has been assigned to the Air Force Operational Test and Evaluation Center, Kirtland AFB, NM.